

**Investigation of Kinetic Processes of Gas-Solid-Ionic-Conductor-
Interfaces with Respect to Potential Application in Chemical Sensors**

Dissertation

zur Erlangung des akademischen Grades

Doktor der Ingenieurwissenschaften

(Dr.-Ing.)

der Technischen Fakultät

der Christian-Albrechts-Universität zu Kiel

Evangelos D. Tsagarakis

Kiel

2004

1. Gutachter: Prof. W. Weppner
2. Gutachter: Prof. G. Popkirov
3. Gutachter: Prof. K.A. Thoma

Datum der mündlichen Prüfung: 29.03.2004

Acknowledgements

The author would like to express his sincere appreciation to the following for their contribution to this thesis.

I would foremost like to thank my thesis advisor Professor W. Weppner for his constant guidance, support and readiness for stimulating scientific discussions during accomplishment of this work. His analytical approach to scientific problems has been essential to make this thesis possible.

I am also grateful to Professor R.A. Huggins for fruitful discussions and beneficial suggestions throughout this work. His pioneering vision has been very useful during this work.

I would like to express my sincere gratitude to a great teacher, Professor K.A. Thoma who introduced me to the field of Solid State Ionics and gave me the opportunity to participate in a student exchange program at the University of Kiel.

I would like to thank Professor R. Veyhl for creating sputtering films.

I express special thanks to Dr W.F. Chu for his assistance in preparing NASICON, useful discussions, and sharing his valuable experience on experimental aspects. I gratefully acknowledge his suggestions on the manuscript.

I am also grateful to Dr. V. Thangadurai for creating constructive environment, encouragement and useful suggestions on the manuscript.

I would also like to thank T. Metzger for providing the TZP discs and technical assistance, and S. Wulff for her assistance in ICP.

I thank M. Schwitzke for her assistance with the SEM and EDAX investigations.

I would like to acknowledge J. Schwenzel for his help on the production of thin films by thermal evaporation method.

I would also like to thank the members of the Sensors and Solid State Ionics group for an excellent atmosphere, and the library team for being always helpful.

Thanks to my grandparents, Elpiniki and Evangelos Tsagarakis for their encouragement and support during this work.

I thank my parents Irini and Dimitrios Tsagarakis for their continuous moral support and encouragement throughout my studies.

LIST OF SYMBOLS

The following principal symbols have been used throughout in this work.

a_i	Activity of species i
A_i, B_i	Constant phase angle impedance coefficients
A_x, A'_x, B_x, B'_x	Specific constants
A	Electrode area
c_e	Concentration of electrons
c_i	Concentration of species i
c_k	Complex Fourier coefficient of k -order
C	Capacitance
C_{dl}	Overall double layer capacitance
C_D	Diffuse layer capacitance
C_g	Geometric capacitance
C_H	Helmholtz layer capacitance
d	Determinant of stoichiometric numbers, thickness
d_{ij}	Minor of determinant d
D_i	Diffusion coefficient of species i
\tilde{D}_i	Chemical diffusion coefficient of species i
D_i^T	Tracer diffusion coefficient of species i
E	Electromotive force (emf)
\vec{E}	Electrical field
E_F	Fermi energy
f_j	Correlation factor
$f(t)$	Function of variable t
F	Faraday's constant, degrees of freedom
G	Gibbs energy
ΔG_f^0	Standard Gibbs energy of formation
ΔH	Change in enthalpy

I	Electrical current
I_{\max}	Maximum current
J	Electrical current density
J_0	Exchange current density
J_i	Flux density of particle i
K	Ratio of adsorption to desorption specific rate constants
k	Boltzmann's constant
k_{ad}	Adsorption specific rate constant
k_{des}	Desorption specific rate constant
L	Diffusion length, inductance
L_{Deb}	Debye length
m_i	Mass of species i
M_i	Molecular weight of species i
n_i	Number of species i
P_i	Partial gas pressure of the component i
q	Electron charge
Q	Charge to form a monolayer of adsorbed intermediates
R	Gas constant, electrical resistance
S	Entropy
t	Time
T	Absolute temperature, period
t_i	Transference number of species i
u_i	Electrical mobility of species i
U	Applied voltage
U_0	Amplitude of applied voltage
\bar{v}_i	Mean velocity of particle i
V	Volume
W	Enhancement factor
x	Distance coordinate
\bar{Y}	Complex admittance

z_i	Charge number of species i
\bar{Z}	Complex impedance
Z'	Real part of complex impedance
Z''	Imaginary part of complex impedance
\bar{Z}_w	Complex Warburg impedance
α	Transfer coefficient
α_k, b_k	Fourier coefficients of k-order
ε	Dielectric constant
ε_0	Permittivity of vacuum
η_i	Electrochemical potential of species i
θ	Surface coverage due to adsorption
μ_{e^-, h^+}	Chemical potential of electrons and holes, respectively
μ_i	Chemical potential of species i
μ_i^0	Chemical potential of species i in the standard state
ρ	Charge density
σ	electrical conductivity
σ_i	Partial electrical conductivity of species i
τ	Relaxation time
v_{ad}, v_{des}	Adsorption - desorption rates
φ	Phase shift between input voltage and output current
ϕ	Electrostatic potential
ω	Angular frequency

ABBREVIATIONS

DTA	Differential thermal analysis
EDAX	Energy – dispersive X-ray microanalysis
IAQ	Indoor air quality
ICP	Inductively coupled plasma
MAK	Maximale Arbeitsplatzkonzentration
MFC	Mass flow controller
SAW	Surface acoustic wave
SEM	Scanning electron microscope
TGA	Thermogravimetric analysis
TPB	Triple phase boundary
TWA	Time-weighted average
TZP	Tetragonal zirconia polycrystals
YSZ	Yttria stabilized zirconia
XRD	X-ray diffraction

CONTENTS

1	Introduction	1
1.1	<i>Solid state ionic materials and sensor devices</i>	1
1.2	<i>Objective of the work</i>	8
2	Background of the work and present state of the art	12
3	Fundamental theoretical aspects	23
3.1	<i>Classification of electrochemical gas sensors</i>	23
3.1.1	<i>Potentiometric sensors</i>	24
3.1.1.1	<i>Type I sensors</i>	24
3.1.1.2	<i>Type II sensors</i>	25
3.1.1.3	<i>Type III sensors</i>	28
3.1.2	<i>Amperometric sensors</i>	30
3.2	<i>Ionic transport in the solid state</i>	31
3.3	<i>General aspects on interfaces</i>	35
3.3.1	<i>Double layer structure</i>	35
3.3.2	<i>Polarization at the interfaces</i>	39
3.3.3	<i>Fundamental aspects on electrolyte – electrode interface</i>	40
3.4	<i>Electrode kinetics</i>	45
3.4.1	<i>Adsorption</i>	46
3.4.2	<i>Charge transfer</i>	47
3.4.3	<i>Diffusion</i>	49
3.5	<i>Impedance spectroscopy</i>	51
3.6	<i>Fundamental aspects on electrochemical CO₂ sensor</i>	58
3.7	<i>Phase diagrams</i>	61
3.8	<i>Components of CO₂ sensor</i>	65
3.8.1	<i>Na₂CO₃ as gas sensitive compound</i>	65
3.8.2	<i>Na_xCoO₂ as reference electrode</i>	67
3.9	<i>Analysis of the kinetic method</i>	68

4	Experimental aspects	75
4.1	<i>Measuring apparatus (Kiel cell)</i>	75
4.2	<i>Preparation of cells and experimental setup</i>	76
4.3	<i>Experimental methods</i>	85
5	Results and discussion	89
5.1	<i>Response of O₂ sensors based on ZrO₂</i>	89
5.1.1	<i>Results</i>	89
5.1.2	<i>Discussion</i>	94
5.2	<i>Potentiometric CO₂ sensor</i>	99
5.2.1	<i>Cell with glassy reference and complex auxiliary compound</i>	99
5.2.1.1	<i>Results</i>	99
5.2.1.2	<i>Discussion</i>	106
5.2.2	<i>Cell with Na_xCoO₂ reference and Na₂CO₃ auxiliary compound</i>	108
5.2.2.1	<i>Results</i>	108
5.2.2.2	<i>Discussion</i>	111
5.2.3	<i>Investigation of the reference side</i>	112
5.2.3.1	<i>Results</i>	112
5.2.3.2	<i>Discussion</i>	114
5.2.4	<i>Investigation of the measuring side</i>	115
5.2.4.1	<i>Results</i>	115
5.2.4.2	<i>Discussion</i>	120
5.3	<i>Kinetic measurements</i>	124
5.3.1	<i>Results</i>	124
5.3.2	<i>Discussion</i>	130
6	Summary and Outlook	138

CHAPTER 1

Introduction

1.1 Solid state ionic materials and sensor devices

The phenomenon of ionic transport in solids has been subject of scientific research over many years. At the end of 19th century Warburg and Tegetmeier [1] carried out transference measurements, showing the validity of Faraday's law for solid ionic conductors also called solid electrolytes. Ionic motion in solids raised interest in scientific studies on the understanding of the mechanisms of ion transport in solid materials, but also for technological applications of solid electrolytes in galvanic cells. Several ionic conductors have been discovered with electrical conductivity at elevated temperatures comparable to those of liquid electrolytes. The first application of solid electrolytes demonstrated by Nernst [2] making use of zirconium dioxide in a device known as "Nernst Glower" whereas at high temperatures the resistance decreased and current could be passed through the material. Due to the passage of current, heat is produced causing a further decrease in the resistance and light is emitted. However, it took long time until the detailed aspects of ionic motion in solids was well understood. The combination of knowledge emanating from many scientific fields in order to study the physics and chemistry of materials with ionic motion resulted to the interdisciplinary field of solid state ionics. Solid electrolytes such as AgI, RbAg₄I₅ were found to exhibit significant electrical conductivity drawing much attention to this scientific field, studying thermodynamic and kinetic properties of those materials and possible applications of those in electrochemical cells, as well.

The discovery of beta - alumina in Ford Motor Company at Dearborn, Michigan by Yao and Kummer [3] in 1967 as a fast ionic conducting ceramic material constituted an important group of materials with appreciable ionic motion. Sodium beta - alumina which has the nominal formula Na₂O·11Al₂O₃, belongs to a family of complex oxides with the general formula A₂O·nM₂O₃ in which A is commonly a monovalent cation and M is Fe, Ga, or Al. Sodium beta"- alumina with the nominal formula Na₂O·5.33Al₂O₃ is a stabilized phase by the addition of specific monovalent or divalent ions such as Li⁺ or Mg⁺². The ionic transport in both beta and beta"- alumina

is two - dimensional. The unit cell of sodium beta'' - alumina [4] is schematically represented in figure 1.1. Both beta and beta'' - alumina have hexagonal layer - type structure consisting of regions of closely packed Al-O known as spinel blocks, separated by loosely packed layers containing the mobile cations, known as conduction planes or bridging layers. Beta - alumina can be prepared typically in its sodium form and could be readily ion-exchanged with K^+ , Li^+ , Ag^+ , Rb^+ , NH_4^+ , H_3O^+ and H^+ providing solid electrolytes for other ions [5]. The conductivity is higher in the sodium form making sodium beta - alumina an attractive material for potential use in electrochemical cells. Because of its high ionic conductivity, the material family of sodium beta and beta'' - alumina has been extensively used as solid electrolytes for investigations in the so - called sodium - sulfur cell for energy – storage applications [4, 6, 7].

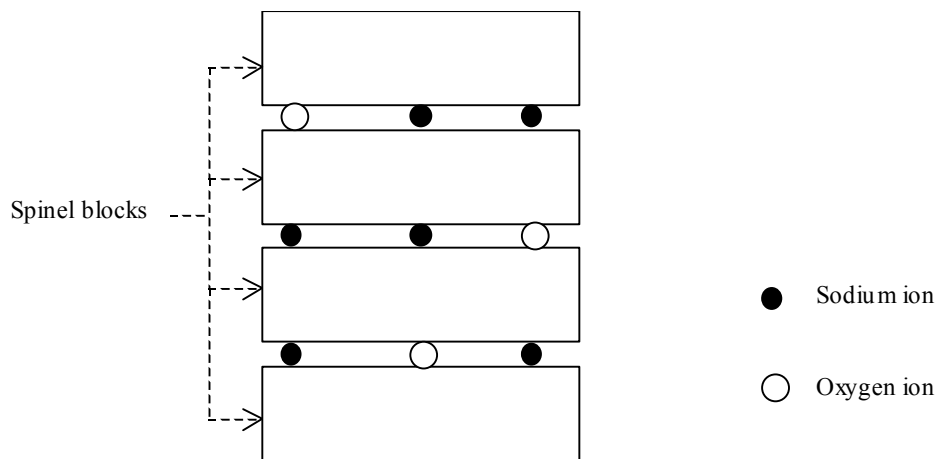


Figure 1.1: Schematic representation of the structure of sodium β'' -alumina showing close - packed spinel blocks separated by bridging layer where sodium ions can move.

Significant improvement has been given to the development of solid electrolytes by the discovery of NASICON (**Na Super Ionic Conductor**) by Hong, Goodenough and Kafalas [8, 9]. Its chemical composition is given by the formula $Na_{1+x}Zr_2P_{3-x}Si_xO_{12}$, where x may vary from zero to three. The structure of NASICON

has a rhombohedral symmetry except in the interval $1.8 < x < 2$ where a small distortion to monoclinic symmetry takes place. The crystalline framework of the Nasicon structure, which is schematically shown in figure 1.2 is constituted by $\text{SiO}_4 / \text{PO}_4$ tetrahedra with filled octahedral cavities ZrO_6 . In this three dimensional rigid network mobile sodium ions can move in the interstitial space.

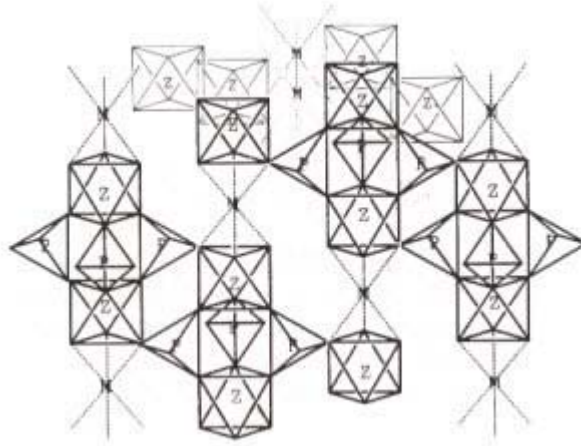


Figure 1.2: View of crystal structure of NASICON according to [8].

The discovery of materials in which ionic species are appreciably mobile and electronic species sufficiently immobile stimulated the interest for scientific investigation of the phenomena and mechanisms of ion motion in the solid state. Employment of solid electrolytes in galvanic cells and utilization of appropriate electrochemical techniques turned on the possibility to investigate a variety of thermodynamic and kinetic properties of solid materials such as chemical potential, partial gas pressure, energy of formation, phase equilibria, electrical conductivity, diffusion coefficient, mobility and reaction rate constant. Furthermore, solid electrolytes became potential candidates for use as components of electrochemical devices, since there are several advantages in comparison to devices based on liquid electrolytes. In solid ionic conducting materials commonly only one type of ionic species is mobile. Solids are compact materials with mechanical stability and several geometrical shapes of them can be easily maintained. Therefore handling and

manufacturing of a device based on solid materials is easier. Additionally, this allows the possibility of miniaturization both with regard to the thickness and lateral dimension and integration into microelectronic circuits, which in the field of gas sensors would result in much lower electrical consumption of the device. In sensors, cells based on solid electrolytes and solid electrodes are also advantageous because they can be applied within wide range of temperatures and pressures. Furthermore, low fabrication cost and possibility of mass production are other advantages that should be considered. The use of solid materials in an electrochemical cell under the restriction that only solid phases are present constitutes a so - called all – solid - state electrochemical cell. Devices based on all – solid - state electrochemical cells are accordingly named all – solid - state devices. The increased knowledge and understanding of materials properties, as well as the discovery of several solid electrolytes with high electrical conductivity provided the opportunity to use those materials in several applications. The major ones comprise sensors for measurement of gas partial pressures, energy storage systems such as rechargeable batteries, direct energy converters such as fuel cells, electrochromic windows and displays, chemotronic devices and thermoelectrical converters [10].

In those devices, fast ionic motion in the solid electrolyte is a requirement, but not a sufficient criterion for successful performance of the device. Rather, combination of materials with a variety of electrical properties is required e.g. solid electrolytes with high ionic conductivities and electrodes with mixed ionic and electronic conduction. The formation of junctions between materials with different electrical properties is a key aspect for the successful performance of the electrochemical devices. Interfaces are in solid ionic galvanic cells the important regions where the voltage drop occurs while typically the materials bulk is commonly free of internal electrical fields. In this view, the performance of the total cell is dependent and may governed by the interfacial processes in a narrow region at the junction electrolyte-electrode. Since at the interface electrolyte-electrode there are various physicochemical phenomena involved, the electrode kinetics is a significant parameter for the overall behavior of the system under real operating conditions. Thus, the electrical performance of electrochemical devices is directly related to appropriate fabrication of junctions between solid electrolytes and electrodes. In equilibrium gas sensors where potential differences are measured, any change of the gas partial pressure requires new

equilibration at the interface electrode-electrolyte, which is commonly dominated by the kinetics of the interface, which is therefore critical for the response time of the sensor. While the sensing properties of the system in equilibrium are given by thermodynamic laws, the transition to another equilibrium state (e.g. by changing the gas partial pressure) is determined by kinetic effects. It is thus of major importance both with regard to scientific interest but also from an application point of view to understand and describe in an adequate way the kinetics of solid-gas interface which is the critical region determining the sensing characteristics of the system. Furthermore, investigating the electrode kinetics provides the possibility to recognize the essential variables on manufacturing appropriate solid-gas interfaces for gas sensing based on all - solid - state electrochemical cells.

Gas analysis with electrochemical sensors is a research area of increasing interest. Sensors find large applicability areas such as automotive, indoor air quality (IAQ), medical, military, aerospace, and agriculture. Overview of the application fields and markets for electrochemical gas sensors are given in [11, 12]. Especially after the attack at the World Trade Center in New York on September 11th 2001, it became evident that sensors detecting toxic gases are of increasing importance for homeland security. Controlling air pollution, industrial safety and medical applications are also areas where gas sensor usage benefits the human society. The continuous concentration increase of “greenhouse gases” such as carbon dioxide made CO₂ an important target gas. The atmospheric CO₂ concentration has risen since the industrialization about 30% of its pre-industrial value, and continues to increase even nowadays, enhancing the natural greenhouse effect. European Union has set attention and alarm levels with regard to air pollution monitoring in indoor as well as in outdoor environments. In Germany, the maximum allowable concentration of gases in indoor working environments is given by the index MAK (Maximale Arbeitsplatzkonzentration) which for CO₂ has the value of 5×10^3 ppm [13]. In the United States of America the most commonly used index for indoor air quality in working places is TWA (Time-Weighted Average) which is calculated by weighting various concentrations throughout the workday.

The general principle of electrochemical gas sensors is the direct conversion of chemical energy of the reaction involving species from the galvanic cell and the gaseous species under detection, into electrical energy. Or vice versa, by the

application of electrical energy to a galvanic cell forcing the chemical reaction to occur. In both cases, chemical information is directly transduced into electrical information e.g. easily measurable electrical quantities, voltages or currents. The performance of gas sensors is determined by several characteristic variables. Consideration of those variables is essential because it reveals the optimum operating conditions and applicability of the device. In the following, the most considerable variables as the sensitivity, speed of response, selectivity and choice of electrode material are briefly presented.

Sensitivity to a specific gas is the change of the sensor signal over the change of the concentration, upon a variation in concentration of these gaseous species. If the sensor output varies linearly with the concentration of the species under detection, the sensitivity can be calculated from the slope of this line. For potentiometric sensors where typically the voltage varies with the logarithm of the gas partial pressure, it is useful to refer the sensitivity to the change of the gas partial pressure by one order of magnitude, thus having units [mV/dec].

The speed of response also is a considerable variable since it may determine or limit the applicability of the sensor device. In potentiometric devices where the output voltage obeys Nernst law, rapid change in the partial pressure of gas under detection should provide a new voltage value consistent to Nernst's law in thermodynamic equilibrium. However, in reality a time delay is observed until the final steady state equilibrium voltage is reached. The response time is a measure of how quick the sensor may respond to changes in the partial pressure of the detecting gas. The equilibration at the sensing electrode is commonly not rapid and there are several processes involved with the rate determining one to determine the response time of the device. A frequently used parameter is the response time t_{90} , which is defined as the time taken to achieve 90% of the final change in the sensor signal upon a variation in the gas partial pressure. From a practical point of view it is very useful since complete equilibration may require very long times over quite small signal changes.

A variable indicating ability of the sensor to respond or not on various gaseous species is the selectivity. In many cases it is desirable that the sensor resists to poisoning with other gases, thus remaining sensitive only to the gaseous species under detection. Since electrochemical gas sensors may show cross sensitivities to gases other than those under detection, it is useful to identify how selective is the response

of the device to various gaseous species. On the other hand, there are other situations where by taking advantage of kinetic principles, discrimination of different types of gases may be achieved [14, 15].

The selection of electrode material may be essential in many cases because the sensor performance may be improved by choosing appropriate electrode material. The electrode material and morphology should in general be considered at electrochemical gas sensors, since the electrode reaction determines the sensing characteristics of such a device. Parameters such as composition, microstructure, porosity, particle size and inhomogeneities may lead to localization of the electrode reaction or affect the kinetic behavior of the system.

In a sensor device the variation of output signal with the concentration of the measured species may be described by mathematical equations. The window within those equations are valid is the measurement range of the device. It is typically dependent on the sensing principle and the specific system under investigation, but also on most of the above mentioned variables.

Beside electrochemical sensors there are also other techniques providing the possibility of gas detection such as infrared analysis, semiconducting oxide sensors and surface acoustic wave sensors. These principles are summarized below.

An alternative method for monitoring gas concentrations is by infrared gas analysis (IR sensors) based on the ability of certain gas molecules to absorb infrared radiation at wavelengths that are characteristic of the chemical structure of the molecule. This method may require complicated electronic systems with often calibrations and is sensitive to small temperature changes.

Semiconducting oxide sensors are based on another method in which electronic properties such as the resistance of a metal oxide semiconductor material, changes when it is exposed to the target gas. However in this method, the sensor performance depends strongly on the presence of trace impurities and is limited to specific gases.

Surface acoustic wave sensors (SAW), for monitoring atmospheric gases have been also investigated. The principle of operation of SAW sensors based on the transmission of a periodic deformation across the surface of a piezoelectric material, typically quartz. Changes in frequency of the transmitted wave are monitored as a function of the gas concentration. Disadvantage of this method is the commonly short device lifetime.

The above techniques require in general complicated manufacturing processes in comparison to the electrochemical sensors and are limited to a number of detectable gases. In contrast, electrochemical techniques can be applied in a variety of extreme experimental conditions thus advantageous for a wide range of applications. Furthermore, electrochemical gas sensors provide directly electrical quantities, which may be easily measured.

1.2 Objective of the work

Application of solid electrolytes as membranes selectively transporting one ionic species in electrochemical gas sensor devices is accompanied by the utilization of appropriate electrodes forming junctions in contact with the electrolyte. The kinetics of the interface electrolyte - electrode is of complex nature involving several processes and is of significance regarding the overall behavior of the sensor device, leading in many cases to sluggish response times or deviations from thermodynamic equilibrium.

Goal of the work is the investigation of the kinetics of the interface gas-solid in electrochemical gas sensors by systematic studies on systems involving one or two gas species applying potentiometric and kinetic principles. The characterization of interfacial kinetics in systems type I and type III should reveal the critical parameters responsible for the electrode kinetics. Furthermore it should be investigated if dynamic measurements combined with a model for the interfacial processes involved may allow to reveal information for the electrical performance of the interface solid-gas in the presence of two gaseous species.

In the ZrO_2 based potentiometric oxygen sensors operated at elevated temperatures, the voltage output as a function of the oxygen partial pressure in thermodynamic equilibrium is given by Nernst's law. Rapid change of the oxygen partial pressure leads to a new thermodynamic equilibrium state, however only after a certain time delay. The steady state thermodynamic voltage is given by Nernst's law, but the transient change from one to the other equilibrium state is a matter of the system kinetics. In this work it is to be investigated if the interface ZrO_2 - Pt - gas is responsible for the delay in the response time. Since both with regard to applications, where fast response times are required, and fundamental understanding of the

mechanisms of the response in electrochemical sensors, and guiding from the experimental results a model for the response time behavior should be proposed.

While type I electrochemical gas sensors based on electronic junctions at metal-solid electrolyte interface, more advanced potentiometric techniques for the detection of complex gases require ionic junctions with exchange of both electrons and ions across interfaces between solid ionic conductors and mixed ionic-electronically conducting electrodes. These techniques may allow to expand the applicability and overcome limitations of type I or type II gas sensors since gases may become detectable even if those species are not mobile or present in the solid electrolyte employed. The objective is to investigate the kinetics of the interface electrode-electrolyte in type III all-solid state electrochemical cell based on Na^+ conducting electrolytes, under the presence of carbon dioxide in the gas phase. The structure of the sensor is complex involving solid-solid and solid-gas interfaces. The gaseous species equilibrate with the electrolyte through an intermediate layer so - called gas sensitive layer [16], which forms a solid-solid interface in contact with the electrolyte. Thus, it should be studied if the morphology and selection of electrode material as gas sensitive layer is essential for the kinetics of the sensing interface. Additionally, a solid reference electrode is establishing a constant reference potential forming another solid-solid interface at the reference side of the electrochemical type III cell. To investigate and characterize properly the kinetic behavior of that system, the interfacial properties should be investigated carefully with separate experiments. Additionally, it should be investigated if kinetic processes at the interfaces are responsible for controversies in the results and deviations from thermodynamic equilibrium reported on type III structures for potential detection of carbon dioxide.

A major problem of the potentiometric principles is commonly the cross sensitivities to species other than the detectable ones. A way of overcoming this problem may be by employing appropriate solid-gas junctions and intelligent techniques taking advantage of the interfacial kinetics. The kinetics of the solid-gas interface in monolithic electrochemical cells should be studied employing dynamic techniques under the simultaneous presence of two gaseous species. From a fundamental point of view it is necessary to analyze the kinetic method and to identify and model the various kinetic processes occurring at the interface solid-gas when a periodical perturbation is applied to the system. The model must be correlated to the

physical system through the experimental results formulating the interfacial kinetic behavior of the system when this is subjected to a periodical perturbation.

Finally, it should be examined by comparison of the results involving different types of interfaces but also different sensing principles which are the critical parameters dominating the kinetic behavior of the interface solid-gas with respect to gas sensing method.

As a guide for the structure of the work presented in the following, a short outline of the next chapters comes next.

Chapter 2 contains the present state of the art on research contributions reported in literature. The scientific knowledge gained for far before this work has started is reported.

In chapter 3, the theoretical background for the fundamental aspects of interfacial kinetics and transport processes in solid materials and sensor devices are presented. The dynamic method for the investigation of the interface solid-gas under the presence of multiple gas species is analyzed in terms of a mathematical approach based on the Fourier coefficients.

Chapter 4 comprise the experimental aspects and details on the preparation of materials and electrochemical cells. The measurement apparatus and experimental techniques used in this work for the investigation of the kinetics of the solid-gas interface are also discussed as well.

Chapter 5 presents the results of this work in three sections. First those for the response time of potentiometric oxygen sensor based on stabilized zirconia electrolytes, followed up by those for the kinetics of Na^+ conductor based electrochemical CO_2 sensor. Finally the results on investigation of the solid-gas interface in monolithic electrochemical cell employing dynamic technique will be given.

Chapter 6 contains summary and outlook of the most important results and accomplishments of this work.

References to chapter 1:

- 1) E. Warburg, *Wiedemann Ann. Phys.* **21**, 622 (1884); E. Warburg, F. Tegetmeier, *Wiedemann Ann. Phys.* **32**, 455 (1888)
- 2) W. Nernst, *Z. Elektrochem.* **6**, 41 (1900)
- 3) Y. F. Y. Yao and J. T. Kummer, *J. Inorg. Nucl. Chem.* **29**, 2453-2475 (1967)
- 4) J.L. Sudworth, P. Barrow, W. Dong, B. Dunn, G.C. Farrington, and J.O. Thomas, *Mat. Res. Bull.*, 22-26, March 2000
- 5) J. T. Kummer, *Prog. Solid State Chem.* **7** (1972) 141-175
- 6) N.K. Gupta and R.P. Tischer, *J. Electrochem. Soc.* **119** [8], 1033-1037 (1972)
- 7) F.A. Elrefaie and W.W. Smeltzer, *Solid State Ionics* **12**, 517-524 (1984)
- 8) J. B. Goodenough, H. Y-P. Hong and J. A. Kafalas, *Mat. Res. Bull.* **11**, 203-220, (1976)
- 9) H. Y-P. Hong, *Mat. Res. Bull.* **11**, 173-182 (1976)
- 10) H. Rickert, "Electrochemistry of Solids", Springer-Verlag, Berlin-Heidelberg-New York (1982)
- 11) M.J. Madou, S.R. Morrison, "Chemical Sensing with Solid State Devices", Academic Press Inc., San Diego, London (1989)
- 12) J.R. Stetter, W.R. Penrose, and S. Yao, *J. Electrochem. Soc.* **150** [2], S11-S16 (2003)
- 13) "MAK-und BAT-Werte-Liste 1997", Deutsche Forschungsgemeinschaft, Wiley-VCH (1997)
- 14) J. Liu and W. Weppner, *Appl. Phys. A* **55**, 250-257 (1992)
- 15) M. Schmah, Ph.D. Thesis, Max-Planck Institut für Festkörperforschung Stuttgart (1999)
- 16) W. Weppner, German Patent DE 2926172 C2 (1979), US Patent 4.352.068 (1980)

CHAPTER 2

Background of the work and present state of the art

This chapter includes the present state of the art regarding scientific investigations reported in literature for the system $ZrO_2 - Pt - O_2$, electrochemical type III cells for the possibility of CO_2 detection and cells where kinetic principles have been employed.

i) Electrodes of the type oxygen, noble metal / oxide ion conductor

It is known since long time [1] that zirconia doped with alkaline or rare earth oxides exhibits significant ionic conductivity at elevated temperatures due to oxygen ion movement via oxygen vacancies. Pure zirconiumdioxide exists in three modifications, monoclinic up to 1167 °C, tetragonal up to 2367 °C and cubic modification up to 2677 °C [2]. By the addition of a certain amount of lower valence oxides a stabilized cubic phase is observed which remains free of phase transitions within a wide temperatures range, thus making the material favorable for a variety of applications. Stabilized ZrO_2 has the cubic fluorite structure in which the cations have eightfold coordination. Zirconia based ceramics have been extensively investigated both with regard to materials properties but also for application in electrochemical cells for the detection of oxygen gas. At the temperature and oxygen partial pressure range where the cell is operated as oxygen gauge, the ionic conductivity is large compared to the electronic conductivity [3], which may practically be regarded as negligible. Several investigations of the electronic properties of minority charge carriers are known [3-8]. Among those, the application of voltage relaxation techniques on galvanic cells with zirconia electrolytes by Weppner [6] resulted to very useful knowledge for the transport properties of electronic minority species. The mobility of electrons and holes at 900 °C determined to be $2.4 \times 10^{-2} \text{ cm}^2/\text{Vsec}$ and $1.6 \times 10^{-4} \text{ cm}^2/\text{Vsec}$, respectively. Moreover, the activation enthalpy evaluated to be 0.55 eV for electrons and 1.4 eV for holes.

A number of studies on electrochemical cells with stabilized zirconia electrolytes for use as high temperature oxygen sensors have been conducted. Driving force was the fundamental scientific interest on the various phenomena involved in this system

but also from a practical point of view the optimization of cell performance. Most of those studies performed so far are due to polarization measurements far away from equilibrium conditions, indicating that the reaction mechanism may depend on several parameters such as temperature, oxygen partial pressure, electrode material and morphology. That seems to be the origin of the disagreement observed in some cases, thus for an appropriate analysis and interpretation of those polarization measurements all the experimental parameters should be taken into consideration. Studies of the polarization behavior of yttria stabilized zirconia cells has been performed earlier by Bauerle [9] with platinum electrodes and later by Matsui [10, 11] with platinum, gold and silver electrodes. Wang et al. [12] investigated the polarization phenomena of several doped ceria electrolytes with platinum paste electrodes, concluding that at high oxygen partial pressures a charge transfer or activation mechanism whereas at low oxygen partial pressures diffusion or dissociation are rate determining. Robertson et al. [13], investigated the oxygen exchange kinetics of YSZ electrolytes with porous platinum electrodes using polarization techniques at the temperature region 600-800 °C, deduced that a mechanism involving surface diffusion of oxygen is responsible for the limitation in oxygen exchange. Other studies dealing with the polarization characteristics of zirconia electrolytes doped with Yb_2O_3 , CaO and Sc_2O_3 have been also reported [14-22]. Gur et al. [22] sustained that electrode material and morphology play an important role with regard to the interfacial behavior. They carried out investigations on the steady state D.C. polarization characteristics of Sc_2O_3 doped zirconia electrolytes with platinum electrodes proposing two alternative mechanisms involving a diffusion process of either atomic oxygen or an electronic species as limiting for the behavior they observed. Pizzini [23] pointed out the significance of electrode kinetics and electrode-electrolyte configurations, and analyzed in a comprehensive description possible routes to understand kinetics hindrances of the electrode reaction under polarization conditions. He anticipated that the complexity of the I-V characteristics of such a system originated from the electrode porosity and morphology.

Badwal et al. [24] investigated the electrode kinetics of the interface stabilized zirconia-palladium at high temperatures by means of impedance spectroscopy. The kinetics of the interface oxygen ion conductor - electronic conductor, oxygen containing medium have been subject of studies by Schwandt et al. [25] using

platinum and gold as electrode materials. For platinum the results derived applying impedance spectroscopy indicate a mechanism involving a sort of surface diffusion of dissociatively adsorbed oxygen, while for gold a more complex mechanism should be considered. It should be emphasized that while there are a lot of investigations on material properties of stabilized zirconia electrolytes, and polarization studies in electrochemical cells commonly far away from equilibrium, there are no systematic studies of the interface $\text{ZrO}_2\text{-Pt-O}_2$ medium with respect to response time behavior.

ii) Electrochemical cells for possibility of CO₂ detection

The cell assembly of the zirconia based oxygen sensors consists of a solid ionic conducting material sandwiched between two metallic electrodes, thus on the formation of two electronic junctions. The situation is however more complicated in chemical sensors for the detection of multicomponent gases, involving more advanced cell structures where materials combination is required. In view of this complexity, the reported investigations on electrochemical systems under carbon dioxide atmospheres utilizing potentiometric techniques are categorized into smaller groups. Common characteristic of all is the application of type III electrochemical cell structures, which will be in detail analyzed in section 3.1.1.3. Investigations on potentiometric cells for possibility of CO₂ detection are thus distinguished into those utilizing solid reference electrode which contains the electrolyte mobile species, those utilizing gas reference electrode different than the gas under detection and those based on so-called open structures. In open structure cells neither a solid reference electrode containing the mobile species of the electrolyte is present nor a reference gas other than the gas under detection is used. This distinction is not only based upon the specific cell assembly but it also reflects the applicability of the sensor. While cells with gas reference electrode are not directly to be used for most of the applications e.g. for indoor air quality, electrochemical cells with solid reference electrode may be directly applicable to the gas under detection. Another fundamental difference is that cells with gas reference electrode or open structures reduce the number of solid - solid interfaces by one, as compared to cells utilizing solid reference electrode.

Several studies report the utilization of solid reference electrode. Bredikhin et al. [26] employed Na_xCoO_2 as solid reference electrode and SnO_2 doped with Sb, V as surface modification in cells with NASICON electrolytes. They investigated the performance of the junction solid ionic conductor-semiconductor with respect to CO₂

sensing, proposing that several electrode reactions might occur simultaneously producing voltage shifts and changes to the cell sensitivity. Zhang et al. [27] employed Li_2CO_3 - Li_3PO_4 - LiAlO_2 solid electrolytes for lithium ions, in contact with two phase LiCoO_2 - Co_3O_4 or one phase pure LiCoO_2 solid reference electrodes. The electromotive force of such cells found to vary logarithmically with the CO_2 partial pressure in CO_2 - O_2 gas mixtures at temperatures between 350 - 400 °C, with response times in the order of 1 min at 400 °C. The cell voltage reported to decrease with time during long-term experiments when pure LiCoO_2 used as reference. Brüser et al. [28] utilized alkali ion conductors in combination with SiO_2 - $\text{Na}_2\text{Si}_2\text{O}_5$ - Au mixtures as reference electrode studying the sensing characteristics in CO_2 - O_2 mixtures at temperatures above 550 °C. Investigations on galvanic cells of type: Au, CO_2 , O_2 | M_xCO_3 | M^{i+} - β'' -alumina | $\text{M}_x\text{Si}_2\text{O}_5$, SiO_2 carried out by Widmer et al. [29] with $\text{M}^{i+} = \text{Na}^+$, Li^+ , Ca^{+2} , Sr^{+2} . They observed a gradual increase in the response time of the investigated cells with time evolution, suggesting the formation of a reactive layer between the solid electrolyte and one of the electrodes. Bhoga et al. [30] investigated cells with alkali glassy electrolyte and Na_2ZrO_3 - ZrO_2 mixture as reference electrode. Kim et al. [31] investigated the characteristics of electrochemical cell with Li_2CO_3 - Li_3PO_4 - Al_2O_3 electrolytes and LiMn_2O_4 solid reference electrode. The cell sensitivity to CO_2 found to be in agreement to the calculated one in the carbon dioxide range from 10^2 - 10^4 ppm above 350 °C, and a small effect in the sensing behavior when water vapor was present in the gas phase was observed.

Several authors report studies on potential CO_2 sensors with gas reference electrode. The first investigations on electrochemical cells for possibility of CO_2 detection with gas reference electrode, were performed by Maruyama and Saito [32, 33]. They employed NASICON solid electrolytes in combination with Na_2CO_3 sensing electrode reporting the sensing characteristics of electrochemical cells under CO - CO_2 - O_2 , with oxygen gas reference electrode, at elevated temperatures. Miura et al. [34, 35] reported later investigations on NASICON electrolyte based cells coated with binary carbonate electrodes (BaCO_3 - Na_2CO_3 , SrCO_3 - Na_2CO_3 , CaCO_3 - Na_2CO_3 , Li_2CO_3 - BaCO_3) exposed to CO_2 at the sensing side. As reference separately from the target gas, oxygen contained gas has been used. The cell response time t_{90} reported to be in dry target gas shorter than 8 sec at 550 °C for the BaCO_3 - Na_2CO_3 mixture as sensing electrode. The sensitivity was in coincidence with

the theoretical one, however the reproducibility of the open circuit voltage of this cell fabrication at fixed CO₂ partial pressure and constant temperature found to be low. The voltage found to differ considerably from one cell to another, attributed to possible changes in the activity of sodium in the sensing electrode when BaCO₃ - Na₂CO₃ has been used. Later on, they reported investigations on MgO - stabilized zirconia electrolytes coated with Li₂CO₃ auxiliary phase in the temperature range 400-600 °C [36]. Schäfer [37] utilized alkali-ion conducting glasses as solid electrolytes in electrochemical systems with the corresponding alkali metal carbonates as auxiliary sensing electrodes. He found long term drifts of the cell voltage and showed the formation of a crystalline reaction layer in the contact zone between the electrolyte and the auxiliary phase. Other studies in electrochemical cells with gas reference electrodes carried out by Obata et al. [38] using NASICON electrolytes, at room temperatures demonstrating a strong influence of the cell electrical characteristics by the presence of humidity.

Moreover, devices based on open structures have been also investigated. Imanaka et al. [39] investigated the sensing characteristics of electrochemical cells combining lithium and oxygen ion conductors at 650 °C whereas the observed response times were in the order of minutes. Other experimental works involve experiments on open structure cells utilizing sodium and lithium ion conductors [40- 42] for CO₂ detection are also reported.

The application of other techniques for the detection of CO₂ incorporate studies on systems based on amperometric electrochemical techniques [43], changes of the resistance [44], capacitance changes [45], or conductivity changes [46, 47] with the CO₂ partial pressure.

A number of investigations have been conducted on the kinetics of electrochemical sensors under CO₂ atmospheres. Most studies deal with complete cells thus with the overall behavior of the electrochemical cell under the presence of the detectable gaseous species. From this point of view, the various processes taking place at the sensing and the reference electrode are not separated, therefore only limited conclusions for the sensing electrode kinetics can be derived. Dubbe et al. [48, 49] studied the kinetics of electrochemical cell based on Na₂CO₃ - BaCO₃ solid electrolytes with silver electrodes by means of impedance spectroscopy, considering a

combination of reaction processes as limiting for the electrode kinetics. They assumed that the electrode reaction is of complex nature proceeding in consecutive steps. Schäfer [50, 51], concluded that a metastable phase is formed at the reference side of electrochemical cells with Li^+ conducting ceramics as electrolytes and Li_2CO_3 as sensitive auxiliary electrode. The reproducibility of the cell signal employing different solid electrolyte glasses found to be within 30 mV at 600 °C. The sensing mechanism of NASICON based electrochemical cells with metal carbonate auxiliary phase studied by Yamazoe et al. [52] showing that the interface between the electrolyte and the sensing electrode dominates the cell sensing characteristics under carbon dioxide atmospheres. Currie et al. [53] performed potentiometric measurements on miniaturized cells with $\text{Na}_2\text{CO}_3 - \text{BaCO}_3 - \text{Ag}_2\text{SO}_4$ electrolytes suggesting the formation of Na_2O or Na_2O_2 compounds at the sensing electrode, at intermediate or low temperatures and under the presence of oxygen and carbon dioxide in the gas phase. The partial formation of sodium oxide or peroxide proposed also by Jiu et al. [54] at lower temperatures, in electrochemical cells with in situ formation of Na_2CO_3 , whereas aging in the open circuit voltage has been observed during the first days of exposure of the cell to $\text{CO}_2 - \text{O}_2$ mixtures. The response times upon changes in the CO_2 partial pressure found to be 3 - 4 hours at 150 °C. Miura et al. [36, 40] have studied the electrode reaction in electrochemical cells with MSZ electrolytes coated with pre-molten Li_2CO_3 auxiliary phase. The authors considered the possible formation of an intermediate layer at the sensing interface acting as an ionic bridge. Näge [55] carried out experiments with YSZ electrolytes and various alkali carbonate electrodes, presenting several possibilities for the electrode reaction. He also analyzed the thermodynamic conditions at the interface between sodium-beta alumina and stabilized zirconia in bi-electrolyte galvanic cells [41, 56]. The interface NASICON-Au- Na_2CO_3 investigated by Salam et al. [57] by means of impedance spectroscopy in symmetrical cells showing an increase of the total cell resistivity with time during aging of the electrochemical cell at elevated temperatures. However, the role of kinetics at electrolyte - sensing electrode interface in Na^+ conductor based cells for potential use as CO_2 sensors has not been extensively studied with regard to the commonly observed deviations from thermodynamic equilibrium.

iii) Kinetic studies for gas detection

Kinetic studies by the application of transient electrochemical techniques may be divided into two categories. Those where large modulations typically triangular in shape are applied, thus far away from the equilibrium, and those incorporating smaller modulations where the system is not extremely far away from equilibrium. Nevertheless, in both categories the system is not in thermodynamic equilibrium and kinetics is dominant. High amplitude cyclic voltammetry for the investigation of solid - gas interfaces in electrochemical cells, has been the subject of investigations by several authors [58-64]. Kinetic measurements in electrochemical systems involving solid electrolytes by the application of smaller modulations have been also performed. Liu and Weppner [65], described the concept of θ - sensor applying sinusoidal voltage perturbation in monolithic cells exposed to CO₂ atmospheres. Based on the kinetics of controlled chemical reactions of the gas with the electroactive species of the solid ionic conductor this principle demonstrated to the detection of CO₂ partial pressures whereas the applied electrical perturbation voltage or current, is periodical with time. The shape of the observed current voltage relationship is dependent on the gas concentration and under CO₂ - O₂ mixtures has the shape of the Greek letter θ (theta). Thus, in analogy to the λ - sensor named after the shape of voltage versus air to fuel ratio curve, the device based on this principle called θ - sensor. The sensing characteristics depend upon a variety of parameters such as shape of applied perturbation and the electrochemical kinetics of the system under investigation. The primary characteristics considered for CO₂ exposure was the maximum current and the phase shift between voltage perturbation and current response. Dynamic measurements on all - solid state electrochemical systems with reference electrodes reported by Steudel [66] in CO₂ atmospheres, and Schmäh [67] in chlorine and hydrogen sulfide atmospheres. In the later one work, the shape of derived current-voltage curves found to be dependent on the specific gas present, and a mathematical process for gas pattern recognition under the limitation of charge transfer control has been proposed. However, the fundamental background of the kinetics of the solid-gas interface under dynamic conditions when one or two gas species are present has not been so far comprehensively analyzed in terms of the possible rate determining steps.

Literature to chapter 2

- 1) T.H.Etsell and S.N. Flengas, *Chemical Reviews* **70** [3], 339-376 (1970)
- 2) C. Schwandt, Ph.D. Thesis, Max-Planck Institute für Festkörperforschung Stuttgart (1995)
- 3) B. C. H. Steele, *Journal of Power Sources* **49**, 1-14 (1994)
- 4) W. Weppner, *Journal of Solid State Chemistry* **20**, 305-314 (1977)
- 5) W. Weppner, *Z. Naturforsch.* **31a**, 1336-1343 (1976)
- 6) W. Weppner, *Electrochimica Acta* **22**, 721-727 (1977)
- 7) L. D. Burke, H. Rickert, and R. Steiner, *Z. Physik. Chem. N.F.* **74**, 146 (1971)
- 8) H. Schmalzried, *Z. Phys. Chem. N. F.* **38**, 87 (1963)
- 9) J. E. Bauerle, *J. Phys. Chem. Solids* **30**, 2657-2670 (1969)
- 10) N. Matsui, *Solid State Ionics* **3/4**, 525-529 (1981)
- 11) N. Matsui, *Surface Science* **86**, 353-358 (1979)
- 12) D. Y. Wang and A. S. Nowick, *J. Electrochem. Soc.* **126** [7], 1155-1165 (1979)
- 13) N. L. Robertson and J. N. Michaels, *J. Electrochem. Soc.* **137** [1], 129-135 (1990)
- 14) H. Tannenberger, Paper presented at the 154th Meeting of the American Chemical Society, Chicago (1967)
- 15) M. Kleitz, Ph.D. Thesis, University of Grenoble (1968)
- 16) H. Yanagida, R. J. Brook, and F. A. Kröger, *J. Electrochem. Soc.* **117** [5], 593 (1970)
- 17) T. H. Etsell and S. N. Flengas, *J. Electrochem. Soc.* **118**, 1890 (1971)
- 18) R. J. Brook, W. L. Pelzmann, and F. A. Kröger, *J. Electrochem. Soc.* **118**, 185 (1971)
- 19) R. J. Brook and T. L. Markin, in "Fast Ion Transport in Solids", W. van Gool, Editor, North-Holland Publishing Co., Amsterdam (1973)

- 20) S. V. Karpachev and Y. M. Ovcchinikov, *Sov. Electrochem.* **5**, 181 (1969)
- 21) S. Pancharatnam, Ph.D. Thesis, Stanford University (1974)
- 22) T. M. Gür, I. D. Raistrick, and R. A. Huggins, *J. Electrochem. Soc.* **127** [12], 2620-2628
- 23) S. Pizzini, Proceedings of the NATO sponsored Advanced study Institute on Fast Ion Transport in Solids, "Fast ion transport in solids": Solid State batteries and devices, pp. 461-476, Belgirate, Italy 5-15 September 1972
- 24) S. P. S. Badwal, and H. J. De Bruin, *J. Electrochem. Soc.* **129** [9], 1921-1928 (1982)
- 25) C. Schwandt, W. Weppner, *J. Electrochem. Soc.* **144** [11], 3728-3738 (1977)
- 26) S. Bredikhin, J. Liu, W. Weppner, *Appl. Phys. A* **57**, 37-43 (1993)
- 27) Y. Zhang, H. Tagawa, S. Asakura, J. Mizusaki, H. Narita, *J. Electrochem. Soc.* **144** [12], 4345-4350
- 28) V. Brüser, W. Klingner, H. H. Möbius, U. Guth, Sensor 97 Kongreßband III, A.739, pp. 209-214
- 29) T. Widmer, V. Brüser, O. Schäf and U. Guth, *Ionics* **5**, 86-90 (1999)
- 30) S. S. Bhoga, K. Singh, *J. Solid State Electrochem.* **3**, 258-263 (1999)
- 31) D. Kim, J. Yoon, H. Park, K. Kim, *Sensors and Actuators B* **76**, 594-599 (2001)
- 32) T. Maruyama, X. Ye and Y. Saito, *Solid State Ionics* **23**, 113-117 (1987)
- 33) Y. Saito and T. Maruyama, *Solid State Ionics* **28/30**, 1644-1647 (1988)
- 34) N. Miura, S. Yao, Y. Shimizu, and N. Yamazoe, *J. Electrochem. Soc.* **139** [5], 1384-1388 (1992)
- 35) S. Yao, Y. Shimizu, N. Miura, Y. Yamazoe, *Appl. Phys. A* **57**, 25-29 (1993)
- 36) N. Miura, Y. Yan, M. Sato, S. Yao, Y. Shimizu, and N. Yamazoe, *Chemistry Letters*, 393-396 (1994)
- 37) O. Schäf, *Ionics* **2**, 266-272 (1996)

- 38) K. Obata, S. Kumazawa, K. Shimanoe, N. Miura, N. Yamazoe, *Sensors and Actuators B* **76**, 639-643 (2001)
- 39) N. Imanaka, Y. Hirota, G. Adachi, *Sensors and Actuators B* **24/25**, 380-382 (1995)
- 40) N. Miura, Y. Yan, S. Nonaka and N. Yamazoe, *J. Mater. Chem.* **5** [9], 1391-1394 (1995)
- 41) H. Näfe, F. Aldinger, *Sensors and Actuators B* **69**, 46-50 (2000)
- 42) N. Imanaka, T. Kawasato, and G. Adachi, *Chemistry Letters*, 497-500 (1990)
- 43) M. Takahashi, T. Ishiji, N. Kawashima, *Sensors and Actuators B* **77**, 237-243 (2001)
- 44) U. Hofer, G. Kuehner, W. Schweizer, G. Sulz, K. Steiner, *Sensors and Actuators B* **22**, 115-119 (1994)
- 45) T. Ishihara, K. Kometani, M. Hashida, and Y. Takita, *J. Electrochem. Soc.* **138** [1], 173-176 (1991)
- 46) A. Haeusler, J. Meyer, *Sensors and Actuators B* **34**, 388-395 (1996)
- 47) K. Ogura, H. Shiigi, T. Oho, and T. Tonosaki, *J. Electrochem. Soc.* **147** [11], 4351-4355 (2000)
- 48) A. Dubbe, H. D. Wiemhoefer, Y. Sadaoka, W. Goepel, *Sensors and Actuators B* **24/25**, 600-602 (1995)
- 49) A. Dubbe, H. D. Wiemhoefer, and Y. Sadaoka, *J. Electrochem. Soc.* **144** [3], 943-947 (1997)
- 50) O. Schäf, G. Schäfer, J. Arndt, "Materialien für die Sensorik mit Festkörpern" Habilitationsschrift (1999)
- 51) O. Schaef, *Ionics* **2**, 274-281 (1996)
- 52) N. Yamazoe, S. Hosohara, T. Fukuda, K. Isono, N. Miura, *Sensors and Actuators B* **34**, 361-366 (1996)
- 53) J. F. Currie, A. Essalik, J. Marusic, *Sensors and Actuators B* **59** 235-241 (1999)
- 54) J. Liu and W. Weppner, *Solid State Communications* **76** [3], 311-313 (1990)

- 55) H. Näfe, *J. Electrochem. Soc.* **144** [3], 915-922 (1997)
- 56) H. Näfe, *Solid State Ionics* **93**, 117-123 (1997)
- 57) F. Salam, S. Bredikhin, P. Birke, W. Weppner, *Solid State Ionics* **110**, 319-325 (1998)
- 58) H. V. Venkatesetty, Proc. of the 2nd int. Meeting on chemical sensors, Bordeaux 1986, pp. 293-297
- 59) Z. Zhou, W. Liu, C. Liu, *Sensors and Actuators B* **52** 219-225 (1998)
- 60) Y. Yang, C. Liu, *Sensors and Actuators B* **62**, 30-34 (2000)
- 61) P. Jasinski, A. Nowakowski and W. Weppner, *Sensors and Materials* **12**, [2] 89-97 (2000)
- 62) P. Jasinski, A. Nowakowski, W. Weppner, Proceedings of the Society of Photo- Optical Instrumentation Engineers, Bellingham, Wash., pp. 103-106 (1999)
- 63) P. Jasinski and A. Nowakowski, *Ionics* **6**, 230-234 (2000)
- 64) N. Spataru, T. Rao, D. Tryk, and A. Fujishima, *J. Electrochem. Soc.* **148** [3] E112-117 (2001)
- 65) J. Liu and W. Weppner, *Appl. Phys. A* **55**, 250-257 (1992)
- 66) E. Steudel and W. Weppner, *Ionics* **2**, 107-112 (1996)
- 67) M. Schmah, Ph.D. Thesis, Max-Planck-Institut für Festkörperforschung Stuttgart (1995)

CHAPTER 3

Fundamental theoretical aspects

3.1 Classification of electrochemical gas sensors

Electrochemical gas sensors translate chemical into electrical information or vice versa. This is accomplished due to direct conversion of chemical energy from reaction between species from the gas and the electrochemical cell into electrical energy, or vice versa by the application of electrical energy to force a chemical reaction to occur. It is thus a common feature of all-solid-state electrochemical sensors that the measuring quantities are of electrical nature, voltages or currents. However, the specific characteristics of each one of those vary with the sensor structure and sensing principle. It is therefore necessary to distinguish them into smaller groups with common characteristics. They may primary be divided into potentiometric devices operated under open circuit voltage conditions and amperometric devices where current is flowing through the cell. The various branches of electrochemical gas sensors are schematically shown in figure 3.1.

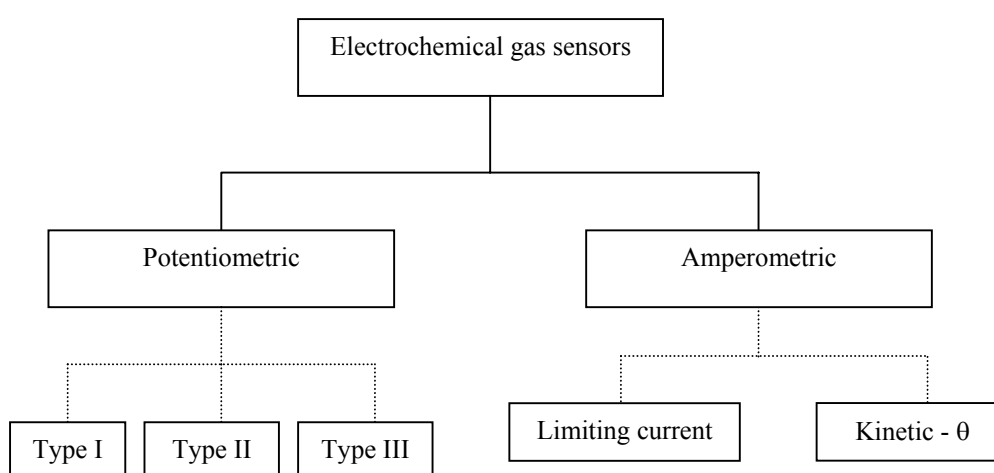


Figure 3.1: Schematic representation of the classification of electrochemical gas sensors.

3.1.1 Potentiometric sensors

The fundamental classification of potentiometric electrochemical gas sensors into three categories was carried out by Weppner [1]. Depending on the type of interfaces employed for sensing these can be separated into type I, type II and type III sensors. In potentiometric sensors of any of these types, an equilibrium potential drop at the electrode - electrolyte interfaces is being related to the activity or partial pressure of species under detection. The sensor output voltage is proportional to the logarithm of partial pressure of gas to be detected. The essential aspects of type I, type II and type III sensors will be analyzed in the following sections.

3.1.1.1 Type I sensors

Main characteristic of type I sensors is that they make use of a solid ionic conductor for the species that should be detected. In this way mobile and species under detection are the same. The most well known example of type I gas sensors is the " λ - probe" that is used as a ceramic oxygen sensor for automobile exhaust control. The name " λ - sensor" originates from the shape of the voltage versus fuel to air ratio, in a Nernst electrochemical cell where the reference electrode exposed to ambient air and the measuring electrode to the exhaust gas of a gasoline engine [2]. Sensors of this type take advantage of the equilibration of the gas with the ionic conductor that conducts ions of the neutral species to be measured. The potential difference between the two electrodes is given by Nernst law:

$$E = \frac{kT}{zq} \ln \left(\frac{P_A^{(l)}}{P_A^{(r)}} \right) \quad (3.1)$$

Where $P_A^{(l)}$ and $P_A^{(r)}$ the partial pressure of the gaseous species under detection at the left and right hand side, respectively. k is Boltzmann's constant, T the absolute temperature, z the charge number of the mobile ions A and q the elementary charge. According to equation (3.1) if the reference gas partial pressure is kept constant the sensor output quantity (voltage) is proportional to the logarithm of partial pressure of

the gas to be measured. The structure of type I gas sensors is schematically shown in figure 3.2.

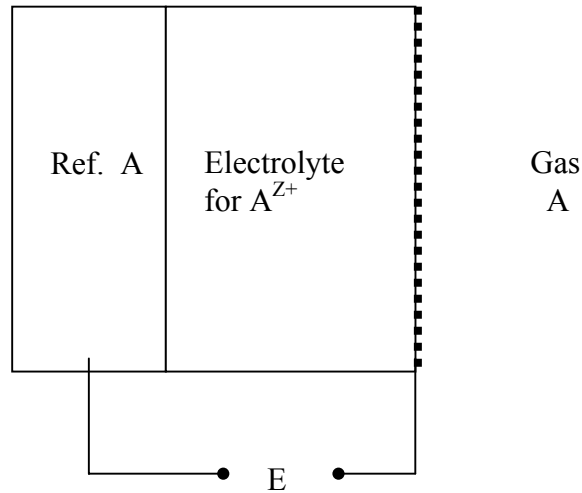


Figure 3.2: Schematic arrangement of a type I gas sensor for measurement the partial pressure of gas A.

The gas equilibrates with the electrolyte, and the chemical potential of electrons is measured at an inert metallic probe on the surface of the electrolyte, since only electrons may be exchanged across the interface. The exchange of electrons across the interface between the solid electrolyte and the electrode is similar to the semiconductor-metal junction. Beside the lambda probe, other examples of type I sensors are gauges for hydrogen [3-5], for Cl₂ [6] and for NO sensing [7].

3.1.1.2 Type II sensors

In type II electrochemical gas sensors, the gas equilibrates with a component of the electrolyte that is different from the predominantly mobile species. That is the

principal characteristic of type II sensors, and main difference to type I electrochemical gas sensors. An advantage in comparison with the type I sensors is that it avoids the problem that for detecting species A_i an electrolyte conducting those species has to be known and employed. Thus, it expands the applicability of solid electrolytes to the possibility of detection of complex gases. Across the interface between the electrode and the electrolyte only electrons are exchanged establishing thermodynamic equilibrium. The cell assembly of a type II gas sensor employing an electrolyte conducting A^{Z+} for the measurement of partial pressure of gas B is shown in figure 3.3. The gas equilibrates with the immobile species of the electrolyte and the chemical potential of electrons is measured at an inert metal on the surface of the electrolyte. Since what is measured is the chemical potential of electrons at the interface between the electrolyte and the electrode, it is not relevant which type of ions is mobile within the ionic conductor.

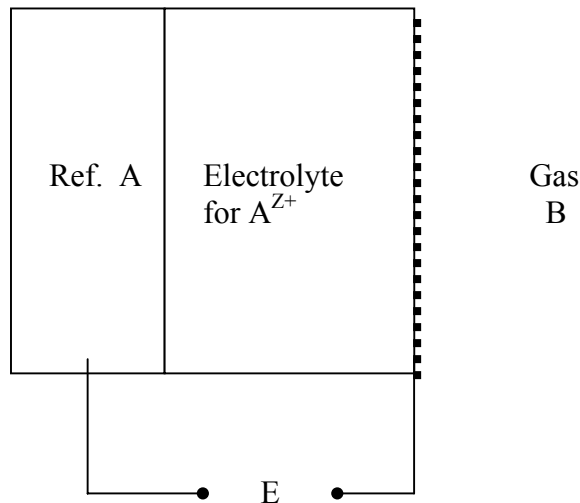


Figure 3.3: Measurement of the partial pressure of gas B employing a type II gas sensor.

Rather, an additional equilibrium is established between the measured immobile and mobile component according to the Duhem-Margules relationship:

$$SdT - VdP + \sum_i n_i d\mu_i = 0 \quad (3.2)$$

Where S , T , V , P , n_i and μ_i are the entropy, temperature, volume, total pressure, number of species i and chemical potential of the neutral component i , respectively. At typical experimental conditions of constant total pressure and temperature equation (3.2) reduces to the following:

$$\sum_i n_i d\mu_i = 0 \quad (3.3)$$

Relationship (3.3) includes all chemical components of the electrolyte. The absolute values of the chemical potentials of all neutral components i are related by Duhem-Gibbs equation through the Gibbs energy G of the electrolyte.

$$G = \sum_i n_i \mu_i \quad (3.4)$$

Assuming an electrolyte with N independent components, that requires equilibration with $N-1$ gases. The relationship between the gas partial pressures and the open circuit voltage is obtained by solving Duhem - Gibbs equation for the standard Gibbs energy of formation of the electrolyte from the pure elements ($a_j = 1$), for the measurable activity of the electroactive component i . Inserting this expression into Nernst's law for a reference electrode of defined activity a_i^{ref} of the mobile component, provides:

$$\Delta G_f^0 = kT \sum_j n_j \ln a_j \quad (3.5)$$

$$E = -\frac{kT}{n_i z_i q} \left[\frac{\Delta G_f^0}{kT} - \sum_{j \neq i} n_j \ln a_j - n_i \ln a_i^{\text{ref}} \right] \quad (3.6)$$

An example of type II sensors is the application of AgBr solid ionic conductor for silver ions to the detection of Br₂ gas [8] where according to what discussed above, bromine gas equilibrates with the immobile component of the electrolyte. Other investigations in type II electrochemical gas sensors involve studies for O₂ [9], SO₂ [10-12], SO_x [13-17], Cl₂ [19] and CO₂ [20] sensing.

3.1.1.3 Type III sensors

Limitations of type I or type II gas sensors because materials with specific electrical properties at the desired operating temperatures have to be employed, may be overcome by the concept of type III gas sensors [21]. In this approach, the gas is being equilibrated with the solid electrolyte through an auxiliary phase on top of the electrolyte. The auxiliary phase should preferably be a mixed ionic-electronic conductor and must contain both the mobile species of the solid electrolyte and the species to be detected. This layer is being used instead of a metallic contact with the electrolyte and forms an ionic junction with the solid ionic conductor allowing the equilibration of both mobile ions and electrons across the interface. Thus, in contrast to type I and II sensors, both ions and electrons are exchanged across the electrode-electrolyte interface in type III sensors.

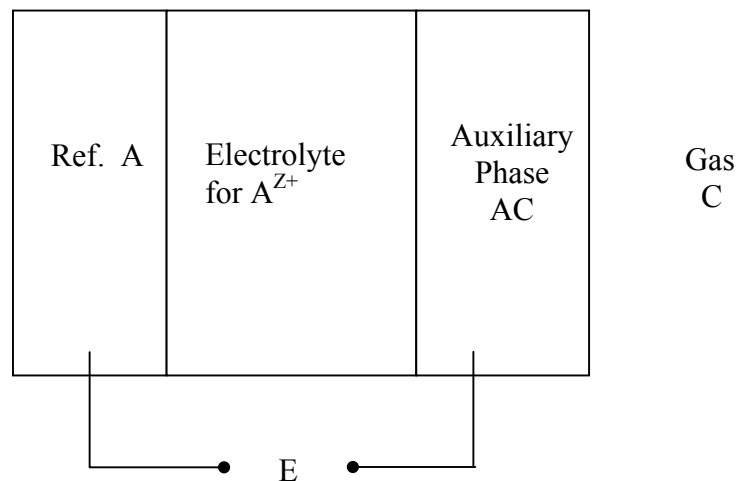


Figure 3.4: Schematic arrangement of a type III gas sensor for the measurement of partial pressure of gas C.

The formation of ionic junction is the main feature of type III gas sensors allowing to expand the number of gaseous species that may be detected with type I or type II sensors. Gas species may be detected with a type III electrochemical gas sensor even if they are not included as either mobile or immobile components of an electrolyte. Figure 3.4 shows schematically the arrangement of a type III gas sensor where the gas C equilibrates with an additional auxiliary phase AC containing the mobile species of the electrolyte. The gas C may in general be also a complex one composed of more than one atomic constituent. The chemical potential of species A is measured at the auxiliary phase whereas the chemical potential of the same electroactive species at the reference electrode remains constant. Application of Duhem-Gibbs equation and Nernst's law for the mobile component results in the following relation for response to gas C in the case of an electrolyte for the mobile electroactive component A [22]:

$$E = \frac{kT}{zqd} \ln p_C^g \sum_{p=1}^{k-1} (-1)^{p+1} n_{pC} d_{pA} - \frac{1}{zqd} \sum_{p=1}^{k-1} (-1)^{p+1} \Delta G_{f,p}^0 d_{pA} + \frac{kT}{zq} \ln a_A^r \quad (3.7)$$

Where the sum runs over all $k-1$ solid phases p . The determinant formed by the stoichiometric numbers n_{ij} of the i th phase and the j th component excluding those stoichiometries of the gaseous species B denoted as d . The minor formed by eliminating the column of the stoichiometries of the mobile component A and the p th row of the determinant d , denoted as d_{pA} .

$$d = \begin{vmatrix} X_{11} & X_{12} & \dots & X_{1k} \\ X_{21} & X_{22} & \dots & X_{2k} \\ \dots & \dots & \dots & \dots \\ X_{(k-1)1} & X_{(k-1)2} & \dots & X_{(k-1)k} \end{vmatrix}, d_{pA} = \begin{vmatrix} X_{11} & X_{12} & \dots & X_{1k} \\ X_{21} & X_{22} & \dots & X_{2k} \\ \dots & \dots & \dots & \dots \\ X_{p1} & X_{p2} & \dots & X_{pk} \\ \dots & \dots & \dots & \dots \\ X_{(k-1)1} & X_{(k-1)2} & \dots & X_{(k-1)k} \end{vmatrix}$$

An example of type III sensors is the measurement of oxygen partial pressure at significantly lower temperatures than conventionally required by type I oxygen sensors [23]. Other investigations on type III sensors involve studies for the possibility of detection of complex gases such as NO₂ [23, 24], Cl₂ [24-26], CO₂ [27-36] and SO₂ [37, 38].

3.1.2 Amperometric sensors

Instead of measuring potential differences under open circuit conditions, partial gas pressures may be also determined by measuring currents under the application of appropriate voltages in electrochemical cells, or vice versa by voltage measurements under the passage of suitable currents through an electrochemical cell. Amperometric electrochemical gas sensors can be mainly divided into limiting-current and kinetic θ -sensors.

An example of the limiting-current principle is the application of tetragonal zirconia polycrystal electrolytes to the detection of oxygen gas [39]. An additional ceramic disc with a small hole in it, limits the access of oxygen to the solid electrolyte and the current is controlled by gas diffusion through the barrier of the diffusion hole. Accordingly, the current is linearly related to the oxygen partial pressure within the limiting current plateau regime. Other example is the measurement of chlorine partial pressure employing this principle on electrochemical cells with Ag- β'' -alumina electrolytes [40]. Limiting current sensors may be operated under lower temperatures but generally have smaller detection ranges than the potentiometric ones. Amperometric sensing principles for ceramic electrochemical gas sensors are described by Ullmann [41].

The θ -sensor concept [42] for the detection of gas species, based on kinetic principles and utilizes a periodical with time electrical perturbation applied to the electrochemical system. This method may allow to overcome several problems of the potentiometric sensors such as cross sensitivities to species other than those under detection. The advantages of this technique in comparison to other sensing principles will be discussed in section 3.9.

3.2 Ionic transport in the solid state

The phenomenon of electrical charge transport by the translation of ions in solid materials has been observed over 100 years ago. Ionic species are able to move through the lattice in solid materials when macroscopic forces are present. These may be concentration or activity gradients, electrical and magnetic fields, temperature gradients, hydrostatic potential gradients, gravitational gradients etc. In practical situations at non-metallic solids commonly activity or concentration gradients as well as electrical fields are typically the driving forces for the motion of ions. The motion of ions in solid state materials occurs because of imperfections of the crystalline lattice, so called crystal defects. In real conditions, all ordered crystalline compounds exhibit irregularities from the ideal crystal structure. Lattice defects may be point defects also called zero-dimensional defects, edge or screw dislocations also called one-dimensional defects, grain boundaries or surfaces also called two-dimensional defects, and cavities also called three-dimensional defects. The formation of thermally activated point defects in ionic crystals is mainly accomplished via the Schottky and the Frenkel mechanisms. In the first one mechanism, ionic motion occurs by the motion of vacancies (Schottky defects) which are missing particles from lattice positions. Example of this mechanism can be found in the alkali halides with NaCl structure where Schottky defects are the dominant thermal defects. In the second mechanism, electrical charge is transported by the motion of interstitial species (Frenkel defects) which are particles additional to the ideal crystal. Examples where Frenkel defects are dominant thermal defects can be found in AgCl (cation defect) and CaF₂ (anion defect). The electrical conductivity of a material is one of its characteristic and most important properties. The electrical conductivity σ_i of species i is related to the electrical mobility of the same species:

$$\sigma_i = c_i |z_i| F u_i \quad (3.8)$$

Where the electrical mobility is defined as the magnitude of the particle velocity over the magnitude of the electrical field:

$$u_i = \frac{|\bar{v}_i|}{|\bar{E}|} \quad (3.9)$$

In solid materials with more than one mobile species, the total electrical conductivity σ is given by the sum of the partial conductivities σ_i of the various ionic and electronic charge carriers, if these are transported independently:

$$\sigma = \sum_i \sigma_i = \sum_i c_i |z_i| F u_i \quad (3.10)$$

Where i denotes ions, electrons and holes. Assuming that charge and mass are transported by the same mobile species, the electrical conductivity is related to the component diffusion coefficient through Nernst-Einstein equation:

$$D_i = \frac{\sigma_i kT}{n_i z_i^2 q^2} \quad (3.11)$$

For a thermally activated diffusion process, the ionic conductivity of a solid electrolyte with one mobile ion follows an Arrhenius relationship with temperature:

$$\sigma = \frac{\sigma_0}{T} \exp\left(-\frac{\Delta H}{kT}\right) \quad (3.12)$$

The activation enthalpy is obtained from the slope of the straight line in a $\log(\sigma T)$ versus $1/T$ plot and σ_0 is the value of the intercept at $T^{-1}=0$. The electrical conductivity in a solid electrolyte may be determined by utilizing AC impedance spectroscopy over a wide frequency range. In an electrolyte with more than one mobile species it is important to know in what way each one of the charge carriers contributes to the total conductivity. The contribution of individual species to transport charge in solid materials is given by the transference number, which is the fraction of the partial conductivity of one type of particle to the total conductivity:

$$t_i = \frac{\sigma_i}{\sum_i \sigma_i} \quad (3.13)$$

For good solid electrolytes the transference number for a single mobile ionic species $t_i \rightarrow 1$, while for the electronic species $t_e \rightarrow 0$. The significance of transference number can be understood by looking at the general expression for the open circuit voltage of an electrochemical cell with an oxide ion conductor in between two reversible metallic electrodes. Assuming that only one type of ionic species i is mobile through the ionic conductor i.e. oxide ions, this expression may be written [43] as:

$$E = \frac{1}{z_i F} \int_{\mu'_{O_2}}^{\mu''_{O_2}} t_i d\mu_{O_2} \quad (3.14)$$

Thus if t_i equals to unity relation (3.14) reduces to the familiar Nernst equation, while if t_i different to unity the open circuit voltage is a function of the transference number. In electrochemical sensors based on galvanic cells of a solid electrolyte sandwiched between two reversible electrodes it is generally desirable to have one ionic mobile species within the electrolyte, that is the transference number for the electrons should vanish. However in other applications such as sensor electrodes, Li^+ rechargeable batteries electrodes or solid oxide fuel cell electrodes, it is essential to have mixed ionic-electronic conduction. In type III gas sensors, the solid electrolyte must have a transference number equal to unity, whereas the gas sensitive layer must allow mixed ionic electronic conduction [21]. It is thus seen that the nature of the transference number of a material is an important criterion for its applicability as electrolyte or electrode in a galvanic cell. Experimental methods for the determination of the transference number of individual species are comprehensively illustrated by Huggins [44].

The electrochemical potential η_i of species i is composed of two terms, one containing the chemical potential μ_i or the activity a_i for ideal solutions, and the other the local electrostatic potential ϕ :

$$\eta_i = \mu_i + z_i q \phi = \mu_i^0 + kT \ln a_i + z_i q \phi \quad (3.15)$$

where μ_i^0 is the chemical potential of species i in the standard state. For the case that one species is predominant mobile, the mass change $|\Delta m|$ of either one of the electrodes per unit time and unit current, in a galvanic cell is given by Faraday's law:

$$\frac{|\Delta m_A|}{\int_{t_1}^{t_2} I dt} = \frac{M_A}{|z|F} \quad (3.16)$$

where the atomic weight M_A of the particles transferred through the electrolyte over the charge number z of the mobile particles can be calculated according to (3.16), thus the mobile species may be identified. Tubandt [45] employed Faraday's law in combination with D.C. measurements to evaluate the identity of the mobile species in

solid materials. Equation (3.16) is also useful evaluating the thickness of in-situ formed gas sensitive layers on the surface of an electrolyte for one mobile ions in type III electrochemical gas sensors, in the absence of electrode polarization effects.

In many practical situations two types of species, either two different ionic or one ionic and one electronic ones (electrons or holes) are mobile within a solid material. In such cases it is advantageous for the microscopic description of kinetic parameters of the system [46] to use the chemical diffusion coefficients. For a system with two mobile species the chemical diffusion coefficients of the mobile species are equal each other. In general, the chemical diffusion coefficient includes the influence of the motion of all other species $i \neq j$ as well as the effect of the internal electric fields on the motion of species j . The chemical diffusion coefficient \tilde{D}_j with reference to the crystal lattice, is related to the diffusivity D_j of the species j , and the self or tracer diffusion coefficient D_j^T through the enhancement factor W_j , also called the Wagner factor:

$$\tilde{D}_j = W_j D_j = \frac{W_j}{f_j} D_j^T \quad (3.17)$$

Where f_j denotes the correlation factor. The Wagner factor describes in which degree the effective motion of ions is enhanced ($W_j > 1$) or reduced ($W_j < 1$) by the coupled motion of the other species. It is defined as [47]:

$$W = \left[(1 - t_i) \frac{\partial \ln a_i}{\partial \ln c_i} - \sum_{j \neq i, e, h} t_j \frac{z_i}{z_j} \frac{\partial \ln a_j}{\partial \ln c_j} \right] \quad (3.18)$$

Where e, h, i, j represent electrons, holes and neutral species i, j respectively. Two limiting cases can be distinguished for the enhancement factor. For a predominantly electronic conductor ($t_e \rightarrow 1$) the enhancement factor is:

$$W = \frac{\partial \ln a_i}{\partial \ln c_i} \quad (3.19)$$

While, for a predominantly ionic conductor the enhancement factor becomes:

$$W = \frac{c_e D_e}{z_i^2 c_i D_i} \frac{\partial \ln a_i}{\partial \ln c_i} \quad (3.20)$$

Where c_e, c_i, D_e, D_i are the concentrations and diffusivities of electrons and ions i respectively.

3.3 General aspects on interfaces

The technology in ionic devices requires, as seen in paragraph 3.1 for electrochemical gas sensors, the formation of junctions between materials with different electrical properties, mostly ionic and electronic conductors. When materials with different Fermi levels are brought into contact, species will move towards the interface to compensate this difference. While in semiconductors space charge regions result typically from the motion of only electronic species, in ionic junctions often electronic and ionic charge carriers have to cross interfaces between electrolytes and electrodes in order to achieve thermodynamic equilibrium. The potential drop is typically within a narrow interfacial region resulting in high electrical fields at the interfaces [8]. The electrical performance of the total device is based on the manufacturing of appropriate junctions whereas both ions and electrons have to be taken into consideration. That makes the situation more complex than in the case of semiconductors. It is therefore of both fundamental and practical interest with respect to the system performance to understand the phenomena dominating that region since the kinetics of the whole device may be dependent on the interfacial equilibration. In the following sections the double layer structure, polarization at the interface and the fundamental aspects on equilibration at the electrolyte - electrode interface will be analyzed.

3.3.1 Double layer structure

Description of the double layer structure from an electrostatic point of view is essential on understanding capacitive effects within the interfacial regions. According to Stern [48] the electrostatic model for the double layer consists of two contributions, one so called Helmholtz and the other so - called Gouy-Chapman. The overall double layer is due to a combination of these two contributions, composed by a compact inner layer of ions next to the electrode (Helmholtz layer) followed by a dispersed diffuse layer beyond (diffuse double layer).

The Helmholtz model corresponding to the compact layer of the interface is comparable to the classic problem of a parallel plate capacitor. The capacitance in this case is given by:

$$C_H = \frac{\varepsilon\varepsilon_0}{d} A \quad (3.21)$$

Where ε the dielectric constant of the material between the plates, ε_0 the permittivity of free space, d the distance between the plates, namely the thickness of Helmholtz layer, and A the electrode surface area. The parallel plate model assumes ordering of positive and negative charges in a rigid way on the two sides of the interface. The potential drop in between the Helmholtz layer is linear, resulting to a capacity which is independent from the potential.

The Gouy-Chapman model corresponding to the diffuse double layer region considers that the double layer capacity C_H is dependent on the potential and the concentration of charge carrier in the electrolyte. It is therefore not compact as in the case of Helmholtz description for the rigid layer region, but of variable thickness. In this model the distribution of species with the distance from the electrode is given by Boltzmann's law. Additionally point charges and a uniform dielectric constant are assumed while screening effects are neglected. The concentration of mobile ionic species i is therefore:

$$c_i = c_i^0 \exp\left[-\frac{z_i q \phi}{kT}\right] \quad (3.22)$$

where c_i^0 is the concentration of the mobile charged species in the electrolyte bulk.

Considering equation (3.22), the charge density is:

$$\rho(x) = \sum_i c_i z_i q = \sum_i c_i^0 z_i q \exp\left[-\frac{z_i q \phi}{kT}\right] \quad (3.23)$$

The potential varies with the charge distribution according to Poisson equation:

$$\frac{\partial^2 \phi}{\partial x^2} = -\frac{\rho(x)}{\varepsilon\varepsilon_0} \quad (3.24)$$

Combination of relationship (3.23) and (3.24) yields the solution for the diffuse double layer capacitance [49]:

$$C_D = \left[\frac{2z_i^2 q^2 \varepsilon\varepsilon_0 c_i^0}{kT} \right]^{1/2} \cosh\left(\frac{z_i q \phi}{2kT}\right) \quad (3.25)$$

The perturbation in concentration due to the electric field extends over a distance on the order of the Debye length L_{Deb} within the electrolyte, which is the length over which the potential drops at 1/e of its initial value:

$$L_{\text{Deb}} = \left[\frac{kT\epsilon\epsilon_0}{2z_i^2 q^2 c_i} \right]^{1/2} \quad (3.26)$$

Therefore, the Debye length may be regarded as the region where the electrical field practically occurs whereas out of this region solid electrolytes are under open circuit conditions practically free of internal field.

The electrical equivalence of the interface consists of two capacitors in series, as shown in figure 3.5 where the potential drop within the double layer region is also illustrated.

$$\frac{1}{C_{\text{dl}}} = \frac{1}{C_{\text{H}}} + \frac{1}{C_{\text{D}}} \quad (3.27)$$

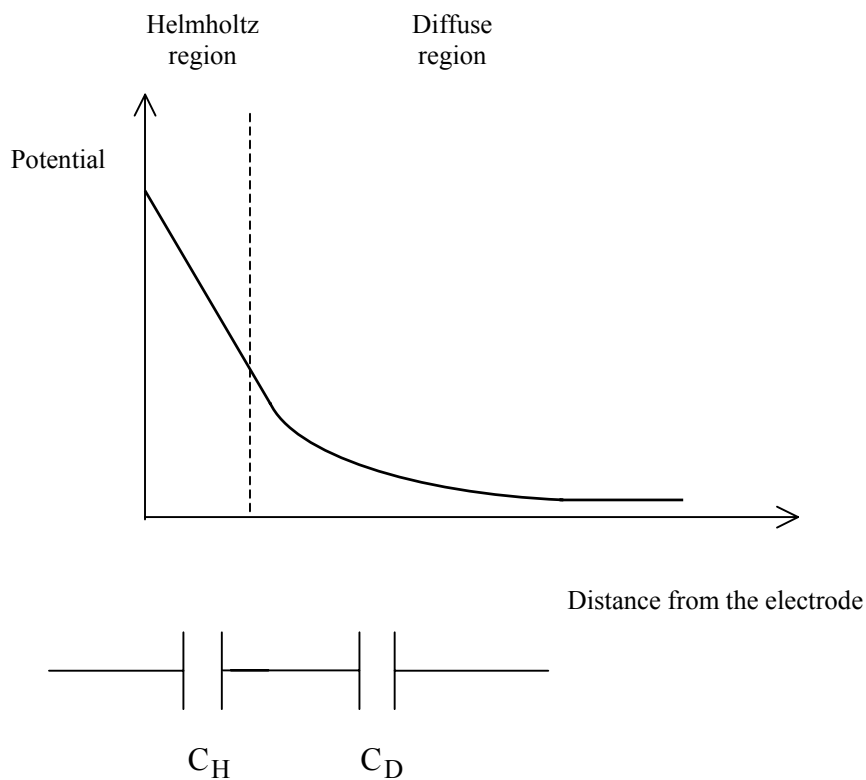


Figure 3.5: Potential drop throughout the double layer and the corresponding capacitances for the Helmholtz and diffuse regions.

In equation (3.27) C_H is the capacitance for the rigid compact layer, and C_D the diffuse double layer capacitance. According to this relationship, the total interfacial capacitance C_{dl} is determined by the smaller of the two individual capacitances C_H and C_D . Therefore, two limiting situations can be distinguished:

$$a) C_H \gg C_D \text{ Then } \frac{1}{C_{dl}} \approx \frac{1}{C_D} \quad (3.28)$$

$$b) C_D \gg C_H \text{ Then: } \frac{1}{C_{dl}} \approx \frac{1}{C_H} \quad (3.29)$$

For solid electrolytes where the mobile carrier concentration is high, equation (3.26) predicts a very small value for the Debye length, in comparison with typical semiconductors whereas because of smaller concentrations of electronic charge carriers the Debye length extends towards a larger region. Thus, for typical solid electrolytes the Helmholtz region is the most significant one contributing to the overall double layer.

As mentioned above the value of L_{Deb} for solid ionic conductors is typically very small. However since it is the penetration depth of the electrical field into the solid electrolyte it is useful to get estimation for its value. For $Na-\beta''-Al_2O_3$ with charge carrier concentration $9.31 \times 10^{-3} \text{ mole/cm}^3$, and assuming $\epsilon = 5$ at $500^\circ C$, the value for the Debye length evaluated from equation (3.26) is 0.4 \AA . It is thus smaller than the Na^+ radius [50], which determines the Helmholtz layer. The situation is similar to most ionic conductors since the charge carrier concentration is commonly not significantly different. From a physical point of view, very small value for the Debye length indicates that the penetration region of the electrolyte from the electrical field is small. In such cases, the Helmholtz contribution is dominant for the overall double layer structure. Assuming an electrode area of 1 cm^2 , we can get an estimation for the capacitances. For the Helmholtz layer capacitance equation (3.21) provides the value of $44 \text{ }\mu F$. For the diffuse layer capacitance, the factor which is independent on the potential is $110 \text{ }\mu F$. Thus, from equation (3.25) we get an estimation of the diffuse layer capacitance for two limiting cases 0.1 V and 1 V to be $142 \text{ }\mu F$ and $99 \times 10^3 \text{ }\mu F$ respectively. The smaller of the two capacitances, namely the Helmholtz layer capacitance is according to (3.27) the most significant one with respect to the electrical equivalence of the interface.

3.3.2 Polarization at the interfaces

Usually the passage of electrical current through an interface electrolyte - electrode causes changes in the electrode potential from its equilibrium value. This phenomenon is called polarization. Polarization is commonly due to concentration gradients caused e.g. by current flow or by accumulation of species in the vicinity of the electrode. Since in electrochemical systems potentials and fluxes are commonly measured or defined at junctions between ionically and electronically conducting phases, it is of interest to know how much current can be passed through an interface between a solid electrolyte and the electrode. In general [51] we can distinguish two types of interfaces in the two extremes:

- a) Non - polarizable (or reversible) interfaces.
- b) Polarizable (or non - reversible) interfaces.

A non - polarizable interface acts reversibly to the species under consideration, thus both ionic and electronic species may cross the interface electrolyte - electrode unhindered. The electrode potential changes only slightly when current flows through the electrode and if there is no external voltage applied, the electrochemical potentials or activities of the electroactive species under consideration across a reversible interface are equal. An example of a thermodynamically reversible electrode would be metallic sodium in contact with a sodium ion conductor:



The sodium ions are coming from the electrolyte and the electrons from the electrode.

The second type of an interface is the polarizable one, which acts as blocking to the species under consideration allowing no faradaic current to be passed through it. There is no equilibrium between an ideally polarizable electrode and the electrolyte because there is no common component capable of being transferred between the two phases, electrode and electrolyte. This kind of interface behaves in a first approximation as a capacitor. An example of blocking electrode would be the interface sodium ion conductor - Pt inert metal where no reversible reactions would occur if the interface remains unaffected by deposition of film at the electrode.

In reality however, no interface is ideally non - polarizable or ideally polarizable. Real interfaces between electrolytes and electrodes are in between those two extremes. The earlier ones do change to some extent their potential and the later ones

do resist to such changes, to some extent. That suggests that the upper distinction should be rather seen as a relative one. The reversibility of an interface is an important factor in ionic devices, especially in electrochemical gas sensors. An interface which serves as sensing electrode in a potentiometric electrochemical gas sensor should be reversible allowing all common electrochemical species to cross the interface on both directions, back and forth, thus establishing equilibrium sufficiently fast.

3.3.3. Fundamental aspects on electrolyte - electrode interface

For an appropriate description of the fundamental aspects on interfaces between solid ionic conductors and solid electrodes, both electrons and ions are taken into consideration. It is assumed in the following analysis that two types of charge carriers i.e. mobile ions and electrons or holes equilibrate across the interface. All other components except the electroactive ones are assumed to be sufficiently immobile so that they can be neglected in the following discussion, situation which often holds in most solid electrolytes within reasonable large periods of time. The electrochemical cell under consideration consists of an oxide ion conductor sandwiched between two reversible metallic electrodes under two different oxygen partial pressures denoted as $P_{O_2}^{(l)}$ and $P_{O_2}^{(r)}$, in thermodynamic equilibrium. That is chosen as an example to reveal and analyze the fundamental relationships, which hold between the electrical properties of the various species involved in the system. Isothermal conditions are assumed, with any temperature gradients between the two electrodes of the electrochemical cell to be omitted. It is furthermore presumed that the electrons are sufficiently immobile so that they do not move through the electrolyte, but rather in the external circuit. Therefore oxide ions are the single mobile ionic species in the solid electrolyte. Additionally, the total input impedance of the measuring unit employed for the voltage measurements at the two electrodes regarded to be high enough to ensure that practically no current is flowing through the cell. In other words, open circuit voltage conditions are assumed. An additional requirement is that the solid ionic conductor has to be chemically stable at the activities imposed by the contact with the electrodes, and the electroneutrality condition is maintained in every volume element. The electrochemical cell is:

$$P_{O_2}^{(l)} \text{ Reversible} \left| \text{Solid electrolyte for } O^{2-} \right| \text{ Reversible} \text{ , } P_{O_2}^{(r)} \text{ electrode} \quad (3.31)$$

For the electrochemical cells appeared in this work, the Stockholm convention [52] has been adopted if otherwise no other convention is indicated. Figure (3.6) bellow shows chemical potential profiles of the electroactive species as well as the electrochemical potential of oxide ions and the electrostatic potential ϕ , across an anionic O^{2-} conductor sandwiched between two reversible, inert metallic electrodes. For simplicity in figure (3.6) the potential drop within the interfacial regions is shown as linear, and the interfacial microstructure is omitted. Each of the phases in the schematic figure is a good electrical conductor, either for electrons (electrodes) or ions (electrolyte). Within the electrolyte there is practically no electrical field as a result of the high conductivity of ionic charge carriers. Within the electrodes the electrical field is also negligible because of the high electronic conductivity of those phases. The major electrical field occurs thus at the two interfaces electrolyte - electrode, in accordance to the discussion in section 3.3.1, generating the open circuit voltage of the electrochemical cell (3.31). Since the potential drop at the interfaces is within a narrow region, the electrical field within this region is very high (typically of the order of 10^7 V/cm).

The diffusional flux of species, electrons from the electrode toward the electrolyte and ions from the electrolyte toward the electrode, is being accompanied by a generated electrical field at the electrolyte - electrode interface. Driving force for the generation of the electrical field is the compensation of the difference in concentration of ionic and electronic charge carriers between the two phases. The concentrations of ionic and electronic charge carriers will accordingly change between both materials in order to fulfill this requirement and establish a thermodynamic equilibrium. The charge neutrality condition under open circuit conditions may be written as:

$$\sum_i J_i = J_{D,i} + J_{E,i} = 0 \quad (3.32)$$

Where i are ionic and electronic species, and J_i the flux of species i . Considering Fick's first law for the one-dimensional diffusional flux in a concentration gradient and an electrical field, provides:

$$-D_i \frac{\partial c_i}{\partial x} - \frac{\sigma_i}{z_i q} \frac{\partial \phi}{\partial x} = 0 \quad (3.33)$$

Where D_i and σ_i are the diffusion coefficient and electrical conductivity of species i , respectively. The chemical potential of species i is related to the concentration of those species, in case of ideal behavior by:

$$\mu_i = \mu_i^0 + KT \ln c_i \Rightarrow \frac{\partial \mu_i}{\partial x} = \frac{KT}{c} \frac{\partial c_i}{\partial x} \quad (3.34)$$

Taking into account (3.34), equation (3.33) yields:

$$\frac{D_i c_i}{KT} \frac{\partial \mu_i}{\partial x} + \frac{\sigma_i}{z_i q} \frac{\partial \phi}{\partial x} = 0 \quad (3.35)$$

The electrochemical potential of species i is superimposed by the chemical potential μ_i and the electrostatic energy $z_i q \phi$ as:

$$\eta_i = \mu_i + z_i q \phi \quad (3.36)$$

If no current flows through the cell, as it has been assumed, there is no gradient in the electrochemical potential of the mobile species (oxide ions) through the electrolyte because of the high oxide ion conductivity of the electrolyte:

$$\frac{d\eta_{O^{2-}}}{dx} = 0 \quad (3.37)$$

The electromotive force of the galvanic cell (3.31) is given by the difference in Fermi levels of the electrons in both sides of the cell:

$$E = \frac{1}{q} [E_F^{(l)} - E_F^{(r)}] = \frac{1}{q} [\eta_{e^-}^{(l)} - \eta_{e^-}^{(r)}] \quad (3.38)$$

Where superscripts (l) and (r) denote Fermi level of the electrons and electrochemical potential at the left and right hand side, respectively. Assuming thermodynamic equilibrium for the process of dissociation of the neutral component O into 2-fold charged ions O^{2-} and electrons e^- :



In view of (3.39) we may write:

$$\mu_O = \eta_{O^{2-}} - 2\eta_{e^-} \quad (3.40)$$

And for the chemical potentials of species involved in (3.39):

$$\mu_O = \mu_{O^{2-}} - 2\mu_{e^-} \Rightarrow \mu_{e^-} = \frac{1}{2} \mu_{O^{2-}} - \frac{1}{2} \mu_O \quad (3.41)$$

$$O_2 = 2O \quad (3.42)$$

Thus for the chemical potentials of molecular and atomic oxygen holds:

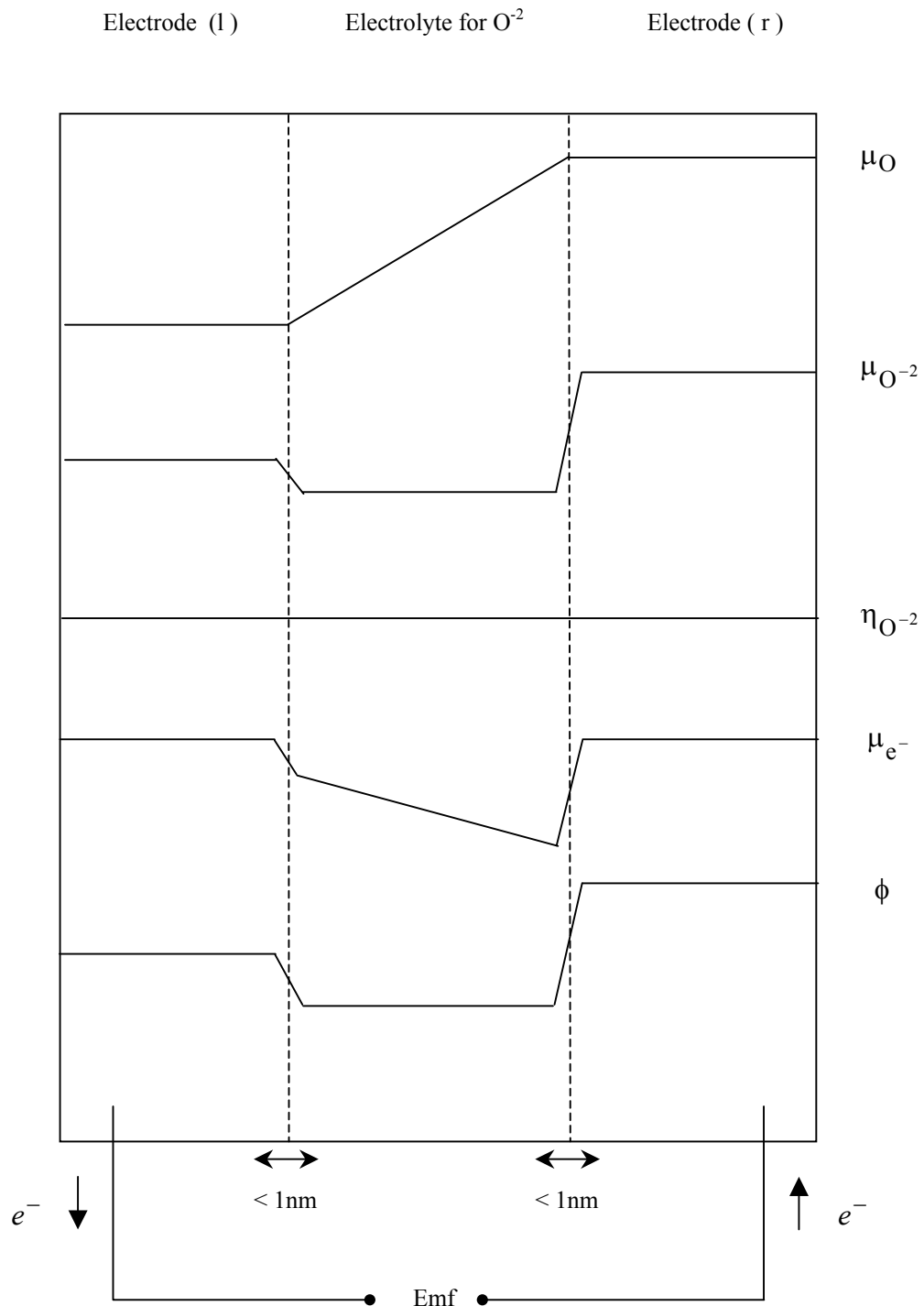


Figure 3.6: Spatial variations of the chemical potential of oxide ions, neutral oxygen and electrons in the case of an oxygen ion conductor sandwiched between two metallic electrodes. The electrochemical potential of oxide ions and the electrostatic potential are also shown.

$$\mu_{O_2} = 2\mu_O \Rightarrow \mu_O = \frac{1}{2}\mu_{O_2} \quad (3.43)$$

By differentiating (3.43) we get:

$$\frac{d\mu_O}{dx} = \frac{1}{2} \frac{d\mu_{O_2}}{dx} \quad (3.44)$$

Solving (3.40) for the electrochemical potential of electrons yields:

$$\eta_{e^-} = \frac{\eta_{O^{2-}} - \mu_O}{2} \quad (3.45)$$

Equation (3.45) relates the electrochemical potential of electrons to the chemical potential of neutral oxygen and the electrochemical potential of oxide ions, at each point in the electrochemical cell. Rewriting expression (3.45) for the two boundaries at the left and right hand side of the electrolyte and feeding into expression (3.38) for the open circuit voltage yields by considering equation (3.37):

$$E = \frac{1}{4q} \left[\mu_{O_2}^{(r)} - \mu_{O_2}^{(l)} \right] \quad (3.46)$$

Combination of (3.41) and (3.43) provides:

$$\mu_{e^-} = \frac{1}{2}\mu_{O^{2-}} - \frac{1}{4}\mu_{O_2} \quad (3.47)$$

Any variations in the oxygen partial pressure result to negligible change in the concentration of oxygen vacancies, because of the high degree of disorder [43]. Therefore, the concentration of oxygen vacancies is regarded to be constant throughout the solid electrolyte over a wide range of oxygen partial pressures. As a result, the chemical potential of the oxide ions is constant:

$$\frac{d\mu_{O^{2-}}}{dx} = 0 \quad (3.48)$$

Differentiation of equation (3.47) over the electrolyte and considering (3.48) provides the relationship for the chemical potential gradients of electrons and neutral molecular or atomic oxygen inside the solid electrolyte:

$$\frac{d\mu_{e^-}}{dx} = -\frac{1}{4} \frac{d\mu_{O_2}}{dx} = -\frac{1}{2} \frac{d\mu_O}{dx} \quad (3.49)$$

The chemical potential of electrons within the two electrodes is constant in view of the high electronic concentration of electronic charge carriers at the electrodes and the variation of chemical potential of electrons through the electrolyte is compatible with

equation (3.49). The electronic species, electrons and holes are in equilibrium between each other:

$$h^{\cdot} + e' = 0 \quad (3.50)$$

Where superscripts point and prime denote positive and negative charge respectively. According to the intrinsic electronic defect equilibrium (3.50) we may write for the chemical potentials of holes and electrons:

$$\mu_h + \mu_e = 0 \Rightarrow \mu_h = -\mu_e \quad (3.51)$$

For the above discussion a solid oxygen ion conductor sandwiched between two reversible electrodes has been considered and the conjunctive relations between the chemical potentials of ionic and electronic species in thermodynamic equilibrium portrayed. It should be emphasized that kinetic effects at the interfaces were not taken here into consideration. Rather a steady state view for the system has been analyzed. Thus the above analysis for this electrochemical system may apply in thermodynamic equilibrium conditions. Kinetic effects at the interface electrolyte-electrode will be separately discussed in section 3.4.

3.4 Electrode kinetics

From a microscopic point of view, there are several kinetic processes occurring at the electrolyte - electrode interface. Of great importance for electrochemical gas sensors are the processes occurring at the solid - gas interface where interaction of species from the gas and the solid phases is taking place. Therefore, the kinetic properties of this interface in an electrochemical cell for gas detection will depend on the presence of the specific gas on the surrounding. Specific adsorption of gas at the electrode surface, surface or bulk diffusion and charge transfer across the interface are kinetic processes involved in the sensing mechanism in an all - solid - state sensor. Fast electrode kinetics may accelerate the equilibration process on the sensing electrode but on the other hand slow kinetics may have the opposite effect, namely hindering the electrode reaction thus slowing down the equilibration of the gas with the solid. A comprehensive analysis of the various processes involved is therefore essential on understanding the kinetics of the solid - gas interface. These processes may be described in a phenomenological way by governing equations and therefore allowing evaluation of the kinetic parameters for the interface under investigation.

This may also permit the identification of the possible kinetic rate determining steps at the interface solid - gas in electrochemical gas sensors.

3.4.1 Adsorption

Adsorption is the process of particle attachment to a surface, which may be generally regarded as a reaction process between the free sites at the electrode surface and the adsorbed gaseous species. It can be accomplished in two ways [53], by physisorption and chemisorption. The first one associated with weak long range Van der Waals dipole-dipole interaction forces between the adsorbate and the adsorbent. In the second one, the molecules or atoms stick to the surface by forming a strong chemical bond. The reverse process of adsorption may also occur, known as desorption. The fundamental phenomenological problem of adsorption has been treated by Langmuir [54] and Wagner [55].

There are various adsorption isotherms depending on the assumptions being made. The most common used one is the so called Langmuir adsorption where all surface sites are assumed to be equivalent between each other composing a uniform surface. The equilibrium between the bulk and the surface established by the formation of one monolayer, thus the adsorption can not proceed beyond monolayer surface coverage. Additionally, in Langmuir adsorption the interactions between the adsorbed particles are neglected. A useful parameter is the fraction of the surface covered by the adsorbate, denoted as θ . For a completely covered surface θ equals to unity while for a completely uncovered surface θ is zero. The surface fraction which is free from adsorbate is therefore $(1 - \theta)$. The rate of reaction in adsorption, namely the rate of change of the surface coverage can be written in absolute rate theory in the case of non dissociative adsorption, and considering the adsorption of one type of species:

$$v_{ad} = \frac{d\theta}{dt} = k_{ad}c(1 - \theta) \quad (3.52)$$

Analogously for the rate of desorption we may write:

$$v_{des} = -\frac{d\theta}{dt} = k_{des}\theta \quad (3.53)$$

In equilibrium, the adsorption and desorption rates in equations (3.52) and (3.53) are the same, yielding for the equilibrium coverage:

$$\frac{\theta_0}{1-\theta_0} = Kc \quad (3.54)$$

$$\text{Whereas: } K = \frac{k_{ad}}{k_{des}} \quad (3.55)$$

Complex gas molecules may dissociate into their fragments. For dissociative adsorption of a diatomic molecule the rates of adsorption and desorption are:

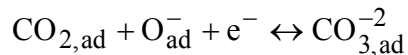
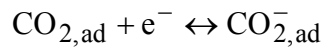
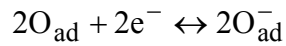
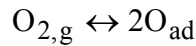
$$v_{ad} = \frac{d\theta}{dt} = k_{ad}c(1-\theta)^2 \quad (3.56)$$

$$v_{des} = -\frac{d\theta}{dt} = k_{des}\theta^2 \quad (3.57)$$

The equilibrium coverage results by equalizing adsorption and desorption rates:

$$\frac{\theta_0^2}{(1-\theta_0)^2} = Kc \quad (3.58)$$

The adsorption process is generally of importance with respect to the performance of electrochemical gas sensors. It may commonly involve several individual steps as the adsorption of carbon dioxide and oxygen on the surface of a type III electrochemical carbon dioxide sensor:



3.4.2 Charge transfer

In a reversible interface and under thermodynamic equilibrium equal number of ions are neutralized and formed at unit surface area per unit time. These two processes are in dynamic equilibrium between each other establishing thermodynamic equilibrium at the interface. When an interface is not at equilibrium e.g. with current flowing through it, the potential of the electrode is induced. Species that have to cross an interface have to overcome the energy barrier at the interfacial region resulting

from the presence of an electrical field. The activation energy barrier at the interface depends on the potential difference across the interface, which is generally different from the equilibrium one. Under conditions of charge transfer control, the current density as a function of the electrode potential is given by the Butler-Volmer equation [56] which for both anodic and cathodic reaction currents involved, takes the form:

$$J = J_0 \left[\exp\left(\frac{\alpha zF\eta}{RT}\right) - \exp\left(-\frac{(1-\alpha)zF\eta}{RT}\right) \right] \quad (3.60)$$

where J_0 is the exchange current density, α the transfer coefficient ($0 < \alpha < 1$), and η the charge transfer overpotential. Two limiting cases of the equation (3.60) can be distinguished, a low overpotential and a high overpotential limit. For low overpotentials $|\eta| \ll \frac{RT}{zF}$, equation (3.60) can be expanded using the Taylor-

MacClaurin expansion, therefore in this case holds:

$$J = J_0 \frac{zF}{RT} \eta \quad (3.61)$$

It is seen from this relationship that the current density varies linearly with the overpotential, similarly to the Ohm's law and is independent from the transfer coefficient. In this view, the proportionality constant in (3.61) is defined as the charge transfer resistance:

$$R_{\text{ch-tr}} = \frac{d\eta}{dJ} = \frac{RT}{J_0 zF} \quad (3.62)$$

On the other limit, for high cathodic overpotentials, $|\eta| \gg \frac{RT}{zF}$ holds:

$$J = -J_0 \exp\left(\frac{(1-\alpha)zF\eta}{RT}\right) \quad (3.63)$$

Taking the logarithm in this relationship we get:

$$\ln J = -\ln J_0 + \frac{(1-\alpha)zF\eta}{RT} \quad (3.64)$$

This relationship indicates that plotting $\ln J$ against the overpotential η provides in the high overpotential limit a straight line with slope of $\frac{(1-\alpha)zF}{RT}$ which is called Tafel slope.

3.4.3 Diffusion

This paragraph presents the phenomenological description concerning the flow of particles through crystalline solids upon the existence of concentration or activity gradients i.e. the process of diffusion. The first treatment of a flux of particles in a concentration gradient has been carried out empirically by Fick in 1855 [57] proposing that the particle flux is proportional to the concentration gradient. For an isotropic diffusion coefficient D_i that may be expressed as:

$$\vec{J}_i = -D_i \text{grad}c_i \quad (3.65)$$

where \vec{J}_i is the number of particles i crossing a unit area perpendicular to the direction of \vec{J}_i in unit time, and c_i the number of particles i in unit volume. The negative sign indicates that the flux is in opposite direction to the concentration gradient. In solid systems commonly the flux is within one dimension, thus equation (3.65) may be written for a particle flux over the x-axis:

$$J_x = -D \frac{\partial c}{\partial x} \quad (3.66)$$

Equation (3.66) is useful evaluating the current flowing through the interface electrolyte-electrode in electrochemical systems with diffusion as dominant. When current is flowing through an electrochemical cell, diffusion processes occurring at the electrode-electrolyte interface correspond to the motion of mobile species within the electrode just inside the phase boundary with the electrolyte ($x = 0$), thus creating concentration gradient. According to (3.66) the current is:

$$I = zFAD \left(\frac{\partial c}{\partial x} \right)_{x=0} \quad (3.67)$$

where A is the area of the electrolyte - electrode interface.

While equation (3.65) known as Fick's first law provides information for the spatial variation of the particle concentration, the variation of particle concentration with time is given by Fick's second law. For one dimensional diffusion with concentration independent diffusion coefficient D this can be written as:

$$\frac{\partial c(x, t)}{\partial t} = D \frac{\partial^2 c(x, t)}{\partial x^2} \quad (3.68)$$

where time t and distance x are independent variables. Equation (3.68) may therefore be utilized to describe particle concentration changes with time and distance within an

electrochemical cell. It is a partial differential equation involving first order partial derivative with respect to time and second order partial derivative with respect to distance. Solution of this equation requires therefore one initial and two boundary conditions for the concentration $c = c(x, t)$. Depending on how suitable these conditions are, solution of (3.68) may be relative simple, but it can also be rather complicated requiring the application of numerical methods. Solutions of this equation for a variety of initial and boundary conditions are given by Crank [58]. A statistical approach for the diffusion problem incorporating the concept of particle mean square displacement in the so called random walk model is discussed by [43, 59]. In a type III sensor the equilibration process includes the diffusion of electroactive species within the modifying compound [21].

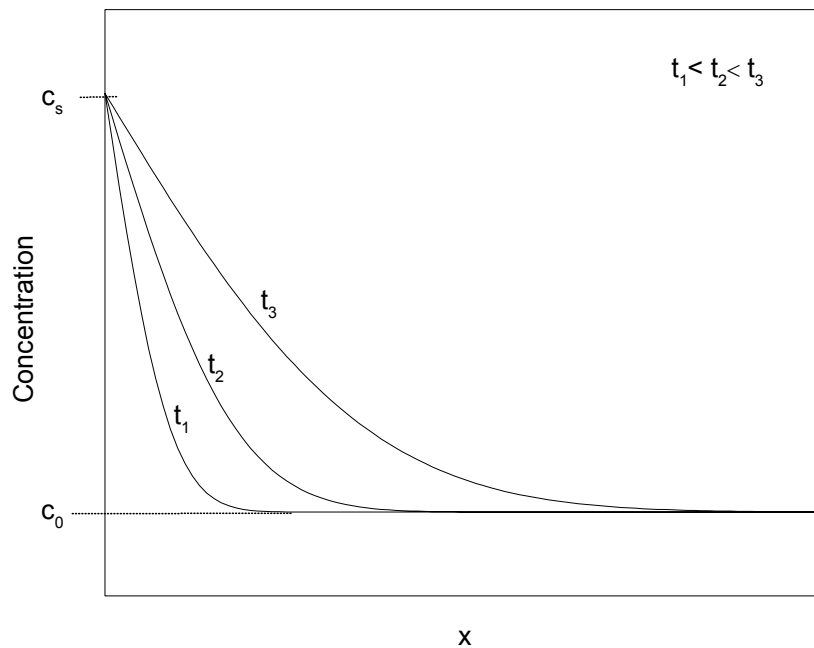


Figure 3.7: Concentration profiles according to the solution of diffusion equation subjected to the conditions (3.69) – (3.71).

Ignoring backward diffusion effects, the diffusion of one electroactive species within the modifying compound may be mathematically described by the diffusion equation (3.68) under the following conditions:

Initial condition:

$$t = 0, x \geq 0 : c = c_0 \quad (3.69)$$

Boundary conditions:

$$t > 0, x = 0 : c = c_s \quad (3.70)$$

$$t > 0, x \rightarrow \infty : c = c_0 \quad (3.71)$$

Solution of the diffusion equation satisfying the conditions (3.69)-(3.71) can be obtained by application of the Laplace transformation [58]:

$$\frac{c - c_0}{c_s - c_0} = \operatorname{erfc}\left(\frac{x}{2\sqrt{Dt}}\right) \quad (3.72)$$

where $\operatorname{erfc}\left(\frac{x}{2\sqrt{Dt}}\right)$ is the complementary error function of $x/2\sqrt{Dt}$. Figure 3.7

shows concentration profiles of the electroactive component at different times, according to solution (3.72).

3.5 Impedance spectroscopy

Impedance spectroscopy is a useful tool for evaluation of many electrical properties of materials and interfaces. This method involves the application of a small periodical voltage perturbation, typically sinusoidal, whereas the magnitude and phase shift of the corresponding current are registered over a wide range of frequencies. Historically, the first application of this technique to solid electrochemical systems goes back to the work of Bauerle [60] at 1969 studying the polarization behavior of zirconia-yttria solid electrolytes with various Pt electrodes. He presented a general equivalent circuit to explain electrical properties of ceramic polycrystalline electrolytes, consisting of a series combination of RC branches corresponding to grain interiors, grain boundaries, and electrode polarization. In view of this approach, the application of impedance spectroscopy offers the possibility to separate several physicochemical processes involved in an all - solid - state electrochemical system. The overall electrical behavior is a result of several contributions:

- a) Bulk electrolyte and grain boundary impedance.
- b) Electrode-electrolyte interfacial impedance.
- c) Measuring lead impedance.

A survey of the measurement method principles is given in [48, 61-63]. For the following analysis it is assumed that the electrical system under investigation is linear, that is the impedance is independent of the perturbation magnitude. Impedance spectroscopy utilizes a potential function that is harmonically periodic with time, namely monochromatic. For a sinusoidal varying voltage perturbation of the form:

$$\vec{V}(t) = V_0 \exp(i\omega t) \quad (3.73)$$

where the symbol \vec{V} represents a vector quantity. The resulting current response has in general the form :

$$\vec{I}(t) = I_0 \exp(i\omega t - i\varphi) \quad (3.74)$$

The complex admittance \vec{Y} is defined as the ratio of complex current $\vec{I}(t)$ over the complex voltage perturbation $\vec{V}(t)$ applied to the system, and the complex impedance \vec{Z} as the reciprocal of the complex admittance. Thus considering relations (3.73) and (3.74):

$$\vec{Y} = \frac{\vec{I}(t)}{\vec{V}(t)} \quad (3.75)$$

$$\vec{Z} = (\vec{Y})^{-1} = \frac{\vec{V}(t)}{\vec{I}(t)} = \frac{V_0}{I_0} \exp(i\varphi) \quad (3.76)$$

Therefore complex admittance and impedance are time independent. Since the impedance is a complex quantity it may be written in terms of a real and an imaginary part:

$$\vec{Z} = Z' + iZ'' \quad (3.77)$$

In the complex plane plot shown in figure 3.8 the admittance and impedance vectors are well defined if the real and imaginary parts of admittance and impedance respectively are known. Alternatively the admittance and impedance vectors are also well defined if the phase angle and modulus are known. The real and imaginary parts of impedance \vec{Z} are:

$$\text{Re}(\vec{Z}) = Z' = |\vec{Z}| \cos \varphi \quad (3.78)$$

$$\text{Im}(\vec{Z}) = Z'' = |\vec{Z}| \sin \varphi \quad (3.79)$$

And the phase angle and modulus are:

$$\varphi = \tan^{-1}\left(\frac{Z''}{Z'}\right) \quad (3.80)$$

$$|\vec{Z}| = \sqrt{(Z')^2 + (Z'')^2} \quad (3.81)$$

If we consider a series combination of k complex impedances the overall impedance is given by the sum of the individual impedances Z_1, Z_2, \dots, Z_k , whereas for a parallel connection the corresponding overall admittance is equal to the sum of the individual admittances Y_1, Y_2, \dots, Y_k .

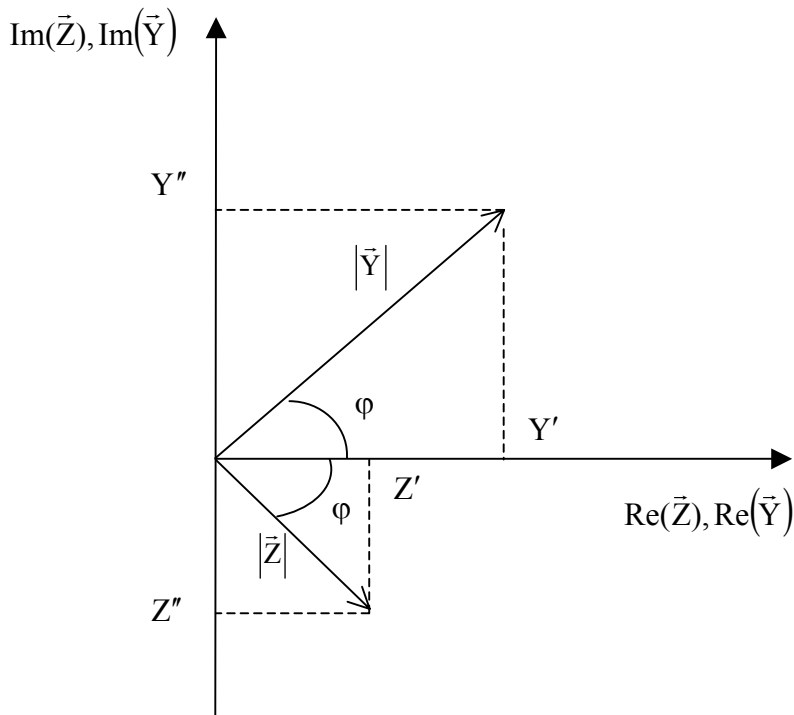


Figure 3.8: Complex plane representations of impedance and admittance vectors.

Impedance is according to (3.76) in general a complex quantity and is only real when $\varphi = 0$, that is for purely resistive behavior. In that case it is also frequency independent. Table 3.1 summarizes typical electrical components for equivalent circuit and the corresponding impedance including pure resistive, capacitive, inductive and RC elements.


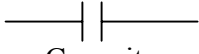

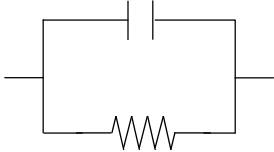
Circuit element	Admittance	Impedance
 Ohmic resistance	$\frac{1}{R}$	R
 Capacity	$i\omega C$	$-\frac{i}{\omega C}$
 Inductivity	$-\frac{i}{\omega L}$	$i\omega L$
 RC	$\frac{1}{R} + i\omega C$	$\frac{R}{1 + \omega^2 C^2 R^2} - \frac{i\omega CR^2}{1 + \omega^2 C^2 R^2}$

Table 3.1: Basic electrical elements of equivalent circuit representation.

As discussed in section 3.3.1 from space charge theory the interface electrolyte - electrode can be as a first approximation modeled as a parallel plate capacitor. The rate of charging this capacitor is determined by the bulk ionic resistance of the electrolyte. In solid electrochemical systems where an ionic conductor is sandwiched between two electrodes, two equivalent circuits are commonly used to describe the frequency dispersion of the cell, dependent on the type of electrodes employed. Figure 3.9 shows the equivalent circuit and the corresponding complex plane impedance plots for an electrochemical cell consisting of a solid electrolyte in between two (a) reversible electrodes and (b) blocking electrodes. Circuit (b) has been used to describe the frequency response of linear systems with a single time constant, known as Debye equivalent circuit [48]. The electrical resistance of the sample

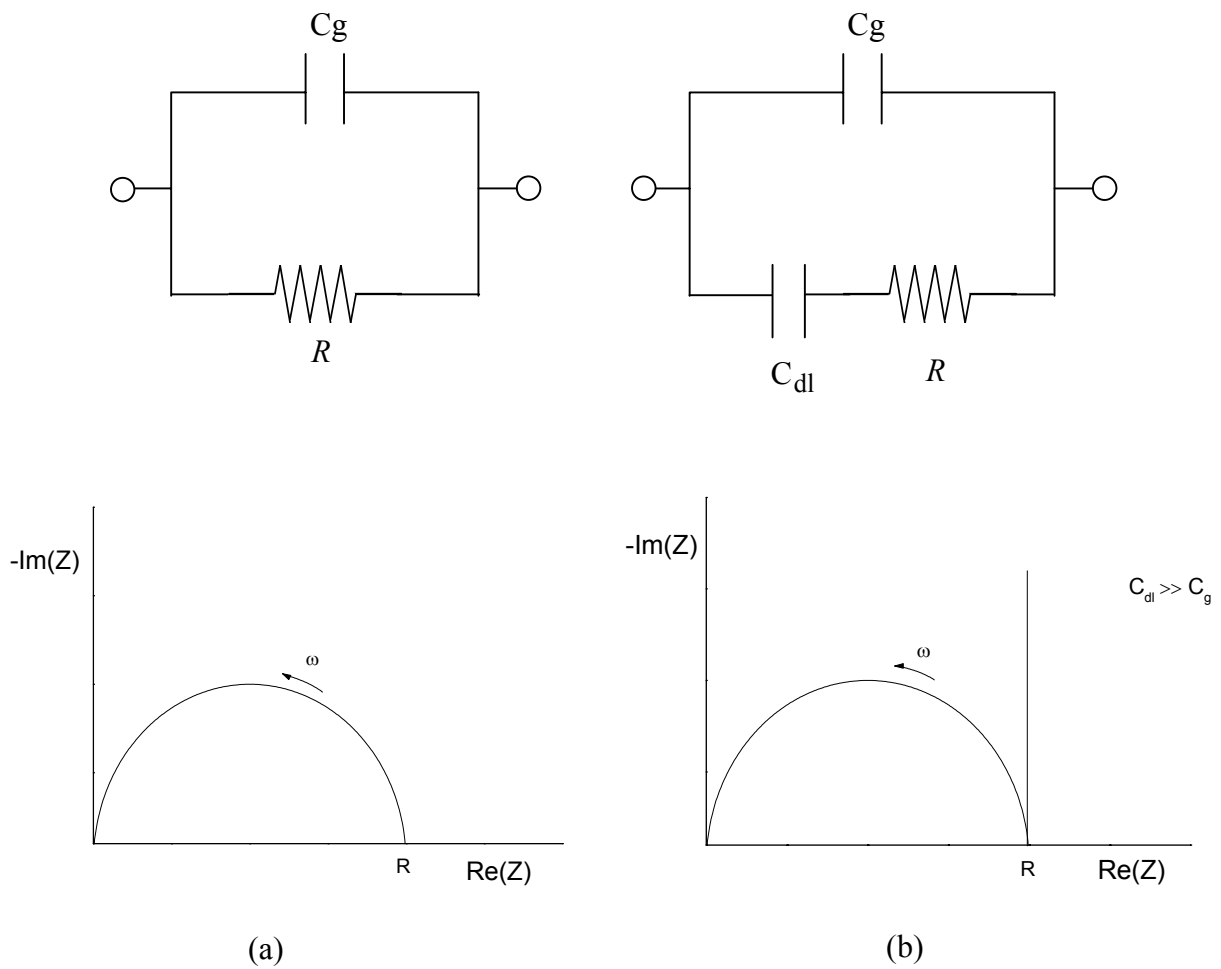


Figure 3.9: Equivalent circuits for the frequency dispersion of a solid ionic conductor with single time constant in between a) reversible (left hand-side) and b) blocking electrodes (right hand-side).

denoted as R , C_g is the geometric capacitance of the sample between two parallel electrodes and C_{dl} the double layer capacitance. The point where the semicircle touches the real axis provides the electrolyte ohmic resistance. The geometrical capacitance can be calculated in a complex plane plot from the point where $-Z''$ reaches its maximum value. At that point holds:

$$\omega RC_g = 1 \quad (3.82)$$

The geometrical capacitance C_g is typically in the order of pico-Farad. The double layer capacitance can be evaluated from the variation of $|\bar{Z}|$ with frequency in a Bode plot format whereas $|\bar{Z}|$ is plotted against frequency in a log-log plot. Typical values for the double layer capacitance are in the order of micro-Farad. The equivalent circuits shown in figure 3.9 may be also expand to describe the frequency dependence of the impedance in systems involving polycrystalline solid electrolytes with either reversible or blocking electrodes [9].

The equivalent circuit representing from an electrical point of view the interfacial electrolyte-electrode impedance is shown in figure 3.10. This equivalent circuit has been proposed by Randles [64] and applied to solid electrochemical systems by Ho et al. [65] and Franceschetti et al. [66] to describe the a.c. frequency response. It includes the uncompensated ohmic resistance of the electrolyte and electrode R_1 , the double layer capacitance of the electrode-electrolyte interface C_{dl} , the charge transfer resistance R_{CT} and the Warburg complex impedance \bar{Z}_w arising from the diffusion of the electroactive species towards or from the electrode-electrolyte interface. The complex impedance plane plot corresponding to Randles equivalent circuit is also shown in figure 3.10. Solution of the diffusion equation (3.68) under appropriate initial and boundary conditions combined with the Butler –Volmer equation for the small overpotential limit provides the complex Warburg impedance [48]:

$$\bar{Z}_w = \frac{RT}{z^2 F^2 A c^0 \sqrt{2D\omega}} \frac{1-i}{\sqrt{2}} \quad (3.83)$$

Thus imaginary and real parts are identical. In the complex plane plot Warburg impedance is represented by a straight line inclined 45° between the real and imaginary parts as shown in figure 3.10. Typically however in real systems the straight line may not incline exactly 45° to the real axis. This common experimental observation has been attributed to surface roughness [67] or because the conditions for this specific solution may not be in reality exactly fulfilled. Under these circumstances the frequency dispersion of the complex Warburg impedance obeying the Kramers-Kronig transformation is:

$$\bar{Z}_i = A_1 \omega^{-a} - iB_1 \omega^{-a} \quad (3.84)$$

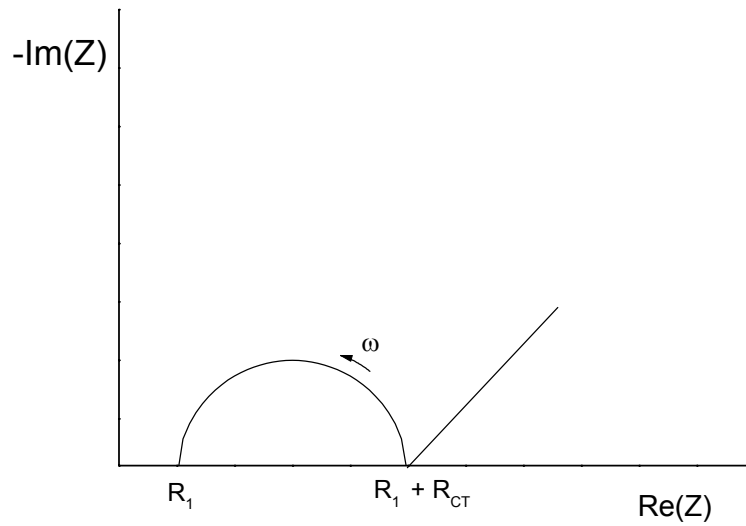
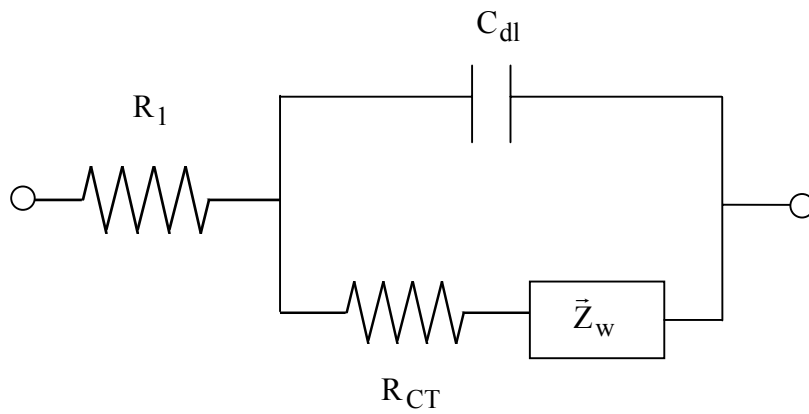


Figure 3.10: Complex plane representation of the impedance of the Randles equivalent circuit for the electrochemical interface.

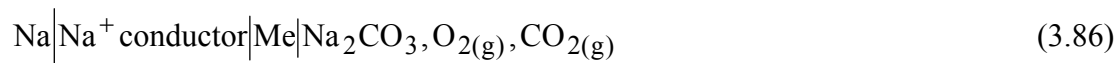
$$\text{Where } \frac{A_i}{B_i} = \tan\left(\frac{a\pi}{2}\right) \quad (3.85)$$

with A_i , B_i and a to be constants for constant temperature and independent of frequency.

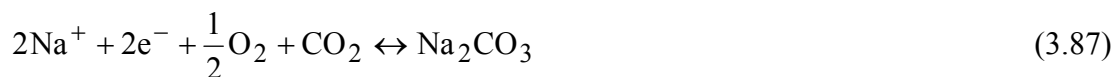
3.6 Fundamental aspects on electrochemical CO₂ sensor

The fundamental thermodynamic relationships of electrochemical type III cell based on sodium ion conductor for the detection of CO₂, under equilibrium conditions will be analyzed in this paragraph.

Describing thermodynamic properties of an electrochemical system consisting of a solid ionic conductor sandwiched between two electrodes is commonly complicated especially if there are interactions between species from the electrochemical system and the surrounding gas, as in the electrochemical gas sensors. Under several simplifying assumptions however, thermodynamic relationships for the most important properties of the system under investigation may be derived. It should be underlined that the following treatment is valid only under the assumptions been made. We consider the following electrochemical cell:



where Me is an inert metal, typically Pt, or Au. The electrodes are assumed to act reversibly to the species under consideration and the electrolyte capable to transport only one type of species, namely sodium ions. This condition may be expressed in terms of transference numbers ($t_{\text{Na}^+} \rightarrow 1, t_{\text{e}^-} \rightarrow 0$). The sensing electrode reaction involving the mobile species from the electrolyte, electrons from the metal and species from the gas phase may be written as:



At the reference side, the electrode reaction is:



If sodium carbonate is already present on the surface of the solid sodium ionic conductor as a gas sensitive compound, an additional equilibrium should be considered:



Summing up reaction (3.87) and (3.88) leads to the overall cell reaction:



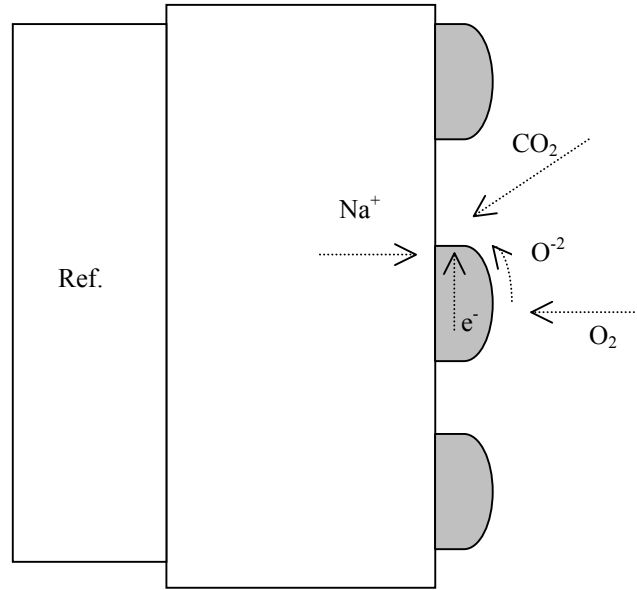


Figure 3.11: Schematic representation of the galvanic cell reaction on the triple phase boundaries (TPB) gas-solid-metal, for the formation of Na_2CO_3 in a CO_2 sensor.

In the three component system $\text{Na} - \text{C} - \text{O}$ the activities of all components are fixed at the sensing electrode at given CO_2 and O_2 partial pressures, if the total pressure and temperature are kept constant. The sodium activity in sodium carbonate is then fixed according to Gibbs-Duhem relationship:

$$2\mu_{\text{Na}(\text{mes})} + \frac{3}{2}\mu_{\text{O}_2} + \mu_{\text{C}} = \Delta G_f^0(\text{Na}_2\text{CO}_3) \quad (3.91)$$

The chemical potential μ_i of species i is related to the activity a_i or pressure p_i for ideal diluted systems as:

$$\mu_i = \mu_i^0 + \text{KT} \ln a_i = \mu_i^0 + \text{KT} \ln P_i \quad (3.92)$$

Where $i = \text{O}_2, \text{CO}_2, \text{Na}$ and μ_i^0 the chemical potential at standard state.

$$\text{And: } \mu_i^0 = \Delta G_{f,i}^0 \quad (3.93)$$

Where i is $\text{CO}_2, \text{O}_2, \text{Na}$

Considering that:



We may write for the chemical potentials of species shown in (3.94):

$$\mu_C + \mu_{O_2} = \mu_{CO_2} \Rightarrow \mu_C = \mu_{CO_2} - \mu_{O_2} \quad (3.95)$$

Replacing μ_C in the expression (3.91) and solving for the chemical potential of sodium in sodium carbonate $\mu_{Na(mes)}$ we get:

$$\mu_{Na(mes)} = \frac{1}{2} \left[\Delta G_f^0(Na_2CO_3) - \frac{1}{2} \mu_{O_2} - \mu_{CO_2} \right] \quad (3.96)$$

Assuming furthermore that Joule's heating and other irreversible energy losses are negligible, the galvanic cell voltage is related to the Gibbs energy of the galvanic cell reaction:

$$\Delta G_r = -2qE \quad (3.97)$$

The galvanic cell voltage may be expressed by the difference in the chemical potential of the neutral electroactive species at both electrodes, according to Nernst's law:

$$E = -\frac{1}{q} \left[\mu_{Na(mes)} - \mu_{Na(ref)} \right] \quad (3.98)$$

Where $\mu_{Na(mes)}$ and $\mu_{Na(ref)}$ denotes chemical potential of sodium at the sensing and reference electrode, respectively. Considering relations (3.92), (3.93), (3.96) and (3.98) and that $\Delta G_{O_2}^0 = 0$ [68] we get an expression for the variation of the open circuit voltage of the galvanic cell (3.86) with CO_2 partial pressure:

$$E = -\frac{1}{2q} \left[\Delta G_f^0(Na_2CO_3) - \Delta G_f^0(CO_2) \right] + \frac{kT}{2q} \ln P_{CO_2} + \frac{kT}{4q} \ln P_{O_2} \quad (3.99)$$

Relationship (3.99) for the electromotive force consists of three terms. The first term in the brackets includes thermodynamical information for the gas sensitive layer and the gas under detection, while the two other terms outside the brackets provide the partial pressure dependence of the open circuit voltage from the gas components. Assuming that temperature and oxygen partial pressure are kept constant, expression (3.99) can be written in the form:

$$E = E^0 + \frac{kT}{2q} \ln P_{CO_2} = E^0 + \frac{kT \ln 10}{2q} \log P_{CO_2} \quad (3.100)$$

Where E^0 is constant for a constant temperature. From (3.100) the sensitivity of cell (3.86) may be obtained by derivation:

$$\frac{dE}{d(\log P_{\text{CO}_2})} = \frac{kT \ln 10}{2q} \quad (3.101)$$

Therefore, the open circuit voltage varies linearly with $\log P_{\text{CO}_2}$ with a slope of $\frac{kT \ln 10}{2q}$. In some cases also the slope of open circuit voltage versus $\ln P_{\text{CO}_2}$ may be used, thus proving a slope of $\frac{kT \ln 10}{2q}$. In this work the convention according to

(3.101) has been adopted for the sensitivity thus referred to an emf vs. $\log P_{\text{CO}_2}$ plot.

The sensitivity to the gas species under detection is therefore dependent on the number of electrons incorporated in the galvanic cell reaction, and the temperature. In the above consideration, elemental sodium ($a_{\text{Na}} = 1$) assumed to be reference electrode. Similar treatment holds if a sodium based solid reference electrode with a sodium activity different than unity is employed [69]. An extra term should be considered including the activity of the neutral electroactive species at the reference electrode. The expression for the open circuit voltage may be thus written as:

$$E = -\frac{1}{2q} \left[\Delta G_f^0(\text{Na}_2\text{CO}_3) - \Delta G_f^0(\text{CO}_2) \right] + \frac{kT}{2q} \ln P_{\text{CO}_2} + \frac{kT}{4q} \ln P_{\text{O}_2} + \frac{kT}{q} \ln a_{\text{Na}(\text{ref})} \quad (3.102)$$

From (3.102) it can be deduced that at constant temperature and oxygen partial pressure the sensitivity to the species under detection is the same as the one calculated from equation (3.99) thus independent of the choice of the reference electrode material.

3.7 Phase diagrams

Phase diagrams can be seen as the primary thinking tool for understanding properties of multiphase, multicomponent systems in thermodynamic equilibrium. They provide information regarding how many and which phases exist in thermodynamic equilibrium and the voltages between them. A phase diagram may be thus regarded as a map presenting the domains of stability of phases and their combinations. With respect to the performance of ionic devices, it is important to know the thermodynamic stability of the different phases involved in the electrochemical cell as

electrodes and electrolyte. In this way, the stability ranges of the various phases in a multicomponent system can be recognized and the optimum operating conditions of the device based on material combinations may be revealed. Even if in reality in many cases thermodynamic equilibrium is difficult to achieve due to slow kinetics, it is important to know how many phases exist in ideal equilibrium conditions. A system is considered to be in equilibrium if the chemical potential of a component is the same throughout the system. The general relationship that is the basis for construction of phase diagrams is the Gibbs phase rule. If temperature and total pressure are kept constant it may be written [70] as:

$$P + F = C + 2 \quad (3.103)$$

Where F the degrees of freedom available in the system, P the number of phases, and C the number of components (e.g. elements or electrically neutral entities). While for binary systems the situation is commonly simple, for ternary or quaternary systems it is rather complex since typically many phases are involved. However, ternary compounds are of major importance because they are commonly used as gas sensitive layers for the detection of complex gases in type III sensors. Considering that most electrochemical systems are under operation at or near constant temperatures, two-dimensional figures may be used to describe phase diagrams of ternary electrodes under isobaric and isothermal conditions. For representation of composition, the isothermal Gibbs triangle may be used where the three elements lie at the corners, and the position of each point within the triangle represents a fraction of each of the elements present, thus a fixed composition of the material. In single-phase regions of a ternary phase diagram, two compositional parameters must be fixed if temperature and total pressure are invariant. In two-phase regions of a ternary system one compositional parameter is fixed for temperature and total pressure constant, thus the activity of an electroactive species within a two-phase region may vary. Lines of constant intensive variables such as the potential within the two phase regions of a ternary system, so - called tie lines are approximately parallel and may not cross each other. In reality tie lines within the two-phase regions are not exactly parallel and may be slightly bent but not crossed. Three phase regions in a ternary system are invariant triangles with no degree of freedom representing regions of constant intensive variables. Assuming a hypothetical ternary diagram A - B - C, in any of the three

phase isobaric-isothermal triangles the activities of all components related to each other by the Gibbs-Duhem equation:

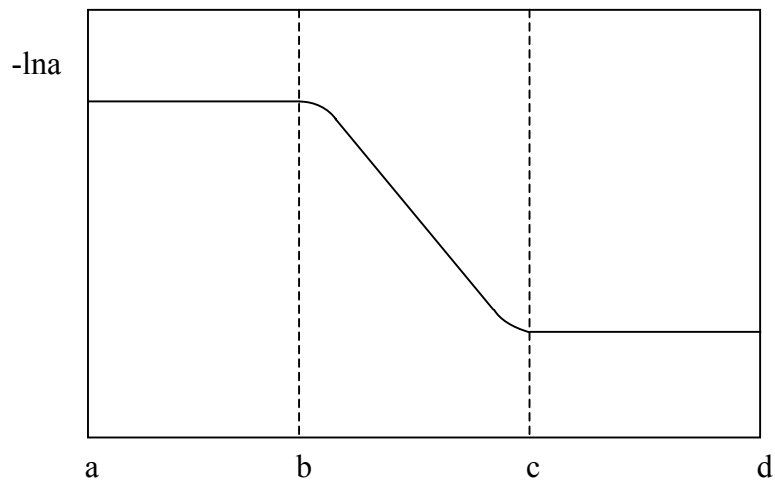
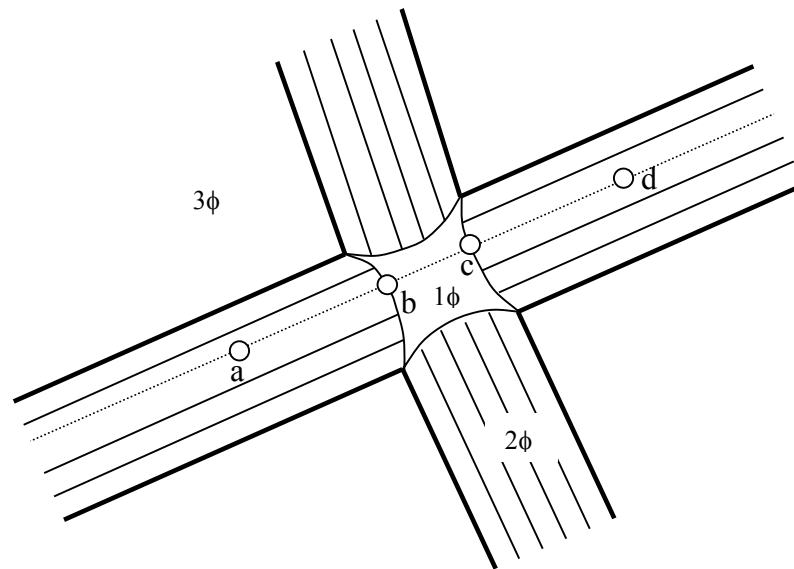


Figure 3.12: a) The region $A_xB_yC_z$ of a hypothetical ternary phase diagram A-B-C is enlargly shown whereas 1ϕ , 2ϕ and 3ϕ indicate one, two or three phase regions, and b) variation in the activity of species i along the path a to b to c to d.

$$\sum_i n_i d\mu_i = 0 \Rightarrow n_A d\mu_A + n_B d\mu_B + n_C d\mu_C = 0 \quad (3.104)$$

where i is A, B and C. Application of Gibbs-Duhem relationship to obtain thermodynamical parameters for electrode materials has been conducted in [71, 72]. Figure 3.12 (a) shows enlarged the single-phase region $A_xB_yC_z$ of a ternary diagram A - B - C. Within this region holds:

$$x d\mu_A + y d\mu_B + z d\mu_C = 0 \quad (3.105)$$

Tie lines such as those from (a) to (b) or from (c) to (d) representing lines of constant potential within the two phase regions are also shown. The variation of the activity of species i along the path (a) \rightarrow (b) \rightarrow (c) \rightarrow (d) is also schematically illustrated. Paths (a) \rightarrow (b) and (c) \rightarrow (d) lying on tie lines of different potentials, within two phase region, while path (b) \rightarrow (c) lies on a single phase region with composition $A_xB_yC_z$. The evaluation of tie triangle equilibrium potentials in ternary systems may be accomplished employing the method of determinants [73] for a three component system A - B - C:

$$E = \frac{1}{2qd} \sum_{i=1}^3 (-1)^i d_{i1} \Delta G_f^0 (A_{\alpha_i} B_{\beta_i} C_{\gamma_i}) \quad (3.106)$$

where q is the elementary charge, ΔG_f^0 the Gibbs energy of formation per mole and d is the determinant formed by the stoichiometric numbers of the three coexisting phases:

$$d = \begin{vmatrix} \alpha_1 & \beta_1 & \gamma_1 \\ \alpha_2 & \beta_2 & \gamma_2 \\ \alpha_3 & \beta_3 & \gamma_3 \end{vmatrix}$$

And d_{i1} is the minor of d , formed by eliminating the first row and the i -th line of the determinant d . Thus knowing the Gibbs energy of formation of the coexisting phases allows the evaluation of tie triangle equilibrium potentials.

3.8 Components of CO₂ sensor

The electrochemical cell based on Na⁺ conductor for possibility of detection of CO₂ is based on three components. As electrolyte NASICON or Na-β"-alumina may be used since they both exhibit high electrical conductivity due to motion of sodium ions. For NASICON the electrical conductivity is 0.2 Ohm⁻¹cm⁻¹ (300 °C) with an activation energy of 0.29 eV while for Na-β"-alumina it is 0.25 Ohm⁻¹cm⁻¹ (300 °C) with an activation energy of 0.16 eV [74]. Since the activation energy for NASICON is higher, its conductivity becomes higher than that of sodium beta alumina as the temperature rises. The other two compartments of the cell are the electrodes, namely sensing and reference electrode. Whereas the property of the electrolyte is to transport sodium ions, at the electrodes there are electrochemical processes involved. Therefore, the two electrode materials sodium carbonate and sodium cobalt oxide will be separately discussed in sections 3.8.1 and 3.8.2.

3.8.1 Na₂CO₃ as gas sensitive compound

Sodium carbonate is the simplest ternary compound that may be used as gas sensitive material in a type III potentiometric sensor for carbon dioxide, based on a sodium ionic conductor. It contains both the mobile species of the electrolyte but also the species under detection as well. Its crystal structure is monoclinic (phase γ) up to 356 °C, from 356 °C to 485 °C monoclinic (phase β) and for higher temperatures up to fusion hexagonal (phase α) [75]. The activation energies are 0.75 eV and 0.56 eV for γ and α phases respectively. The transference number for the sodium ions was found equal to unity [75], thus the electrical conductivity is due to sodium ions migration. At 500 °C the electrical conductivity is 2.2×10⁻⁴ Ohm⁻¹cm⁻¹. Na₂CO₃ may be considered as a single phase region of the ternary system Na - C - O. The phase diagram of the system Na - C - O is illustrated on figure 3.13. Lines represent two phase regions whereas for simplicity tie lines within the two phase regions are omitted. Three phase regions are in between the triangles where the equilibrium voltages within those regions have been calculated from literature data [68] according to the determinant formula (3.106).

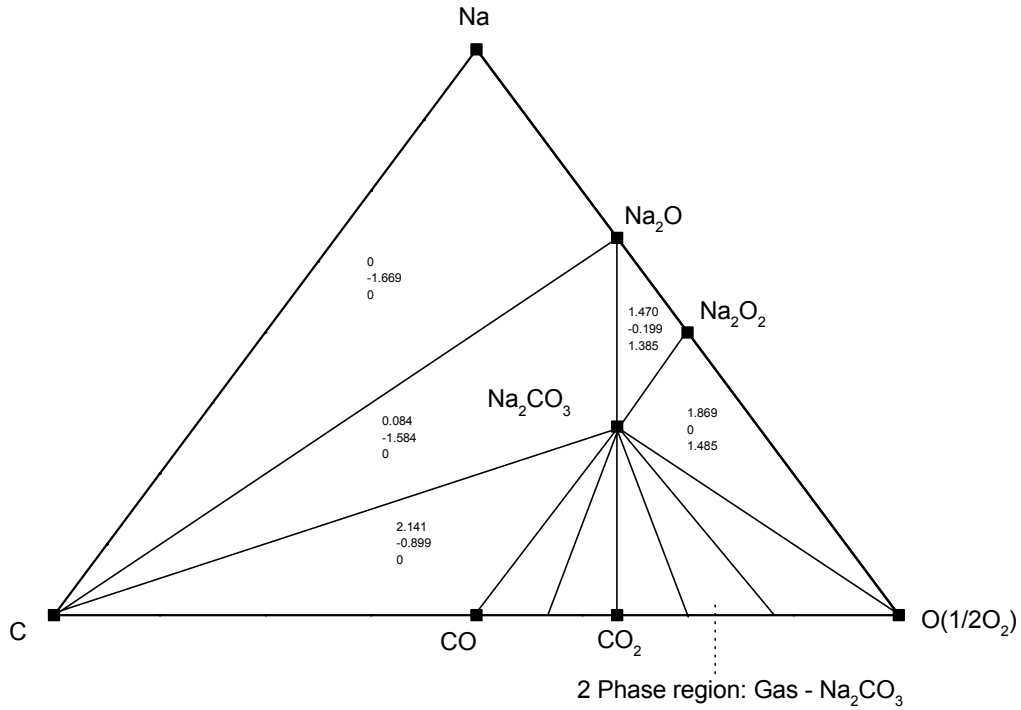


Figure 3.13: Phase diagram of the system Na-C-O from literature data [68] at 427 °C.

Exception is the triangle with Na_2CO_3 , CO, O at the corners representing two phase regions gas - Na_2CO_3 where the lines drawn inside this triangle correspond to different CO/O ratios. The ratio CO/O represents one phase (gas phase), therefore considering the Gibbs phase rule the potential along each of those lines with defined CO/O ratio is constant within the triangle Na_2CO_3 , CO, O. The minimum CO_2 and O_2 partial pressures under which Na_2CO_3 is thermodynamically stable in CO_2 and O_2 atmospheres is obtained assuming the Gibbs energy of the following reactions for the decomposition of Na_2CO_3 , to be zero:



At 427 °C we get: $P_{\text{CO}_2(\text{min})} = 10^{-13.2}$ atm, and $P_{\text{O}_2(\text{min})} = 10^{-80.3}$ atm respectively.

For CO_2 or O_2 partial pressures lower than this value, reactions (3.107) and (3.108) run towards the decomposition of Na_2CO_3 .

3.8.2 Na_xCoO_2 as reference electrode

Reference electrodes in electrochemical sensor cells may be either solid or gas. Generally, in non - aqueous systems the potentials and thermodynamics of electrically neutral species in the electrodes are involved [76], while in liquid electrochemistry ions are measured. Ternary compounds of the type A_xMO_2 where A^+ alkali metal ion may provide suitable phase equilibrium, thus become favorable for use as solid reference electrodes. However, several requirements have to be fulfilled for the applicability in type III electrochemical gas sensors. An essential property of the reference electrode is that its electrical potential should not change if the stoichiometry of the alkali species is slightly changed, increased or decreased. Considering the Gibbs phase rule, the material composition should be selected within a three - phase region, if temperature and total pressure are constant. In case where the ratio of M / O is constant e.g. fixed by preparation, this can be seen as a quasi binary system. In such case, within a two - phase region the degree of freedom is zero, thus the potential will be constant inside a two - phase region. If however by some reason the ratio M / O changes, ternary phase equilibrium should be considered to account. Another requirement for the reference electrode is mixed ionic - electronic conduction allowing fast ion exchange and electron transfer at the interface electrolyte - electrode of the galvanic cell. The electrode reaction should be reversible thus providing a reversible potential. Furthermore the electrode material should be mechanically compatible but also chemically stable with the electrolyte in contact in the galvanic cell. Not only for short times but also for longer periods of time the reference material should not chemically react with the electrolyte even if current is flowing through the cell, at the operating temperature range.

Sodium cobalt oxide belongs to the group of materials A_xMO_2 that have been investigated [77] for use as electrodes in electrochemical systems based on intercalation of alkali ions. These compounds have layer structures in which the lattice is built up by sheets of edge-sharing CoO_6 octahedra between which the alkali ions are intercalated in trigonal prismatic or octahedral sites. In Na_xCoO_2 ($x \leq 1$) four distinct phases exist [78, 79], all with layer structures. The compositions of the various phases are:

(P'3) $0.55 \leq x \leq 0.60$, (P2) $0.64 \leq x \leq 0.74$, (O'3) $x = 0.77$, (O3) $0.8 \leq x \leq 1$.

In the nomenclature used O and P represent octahedral or trigonal prismatic coordination of the sodium ions and 3 or 2 the number of distinguishable sodium layers. In between the $(\text{MO}_2)_n$ layers weak van der Waals type interactions result in high mobility of the alkali ions with $\tilde{D}_{\text{Na}} = 10^{-8} \text{ cm}^2/\text{s}$ [80], in the sodium cobalt oxide, at room temperature. Due to direct overlap of 3d orbitals of cobalt in the layer built of octahedra, cobalt bronze exhibits also electronic conductivity which is several orders of magnitude larger than the ionic one [80]. Coulometric titration of this material has been carried out by Schettler [69] whereas at 470 °C and for x between 0.8-0.93 a two - phase regime (O3-O'3) was observed where the voltage was found to decrease slowly with increasing x.

3.9 Analysis of the kinetic method

As described in section 3.1, potentiometric sensors type I-III measure an equilibrium voltage which is related to the partial pressure of the detecting gas. On the other hand employing kinetic principles several problems of the potentiometric sensors may be overcome. The concept of θ (theta) sensor has been proposed [42] for the detection of gas species based on the application of a periodical with time perturbation to symmetric electrochemical cell. Since the kinetics of the electrochemical system gas-solid ionic conductor is incorporated, this method may allow overcoming problems of cross sensitivity, thus possibility of simultaneous discrimination of different gaseous species, even multicomponent ones with a single electrochemical cell. An additional advantage of this method is that no solid reference electrode is necessary, namely there is no solid-solid interface included in the cell. There is also no requirement for thermodynamic equilibrium since the kinetics are dominant, therefore the response time may be short. Utilizing this principle may allow detection of gaseous species even if not contained as either mobile or immobile species of the solid electrolyte. Several experimental parameters are involved, thus optimization of the cell operating conditions may be feasible.

Figure 3.14 illustrates two types of applied perturbations, sinusoidal and potential step. The corresponding current responses are shown at the right side.

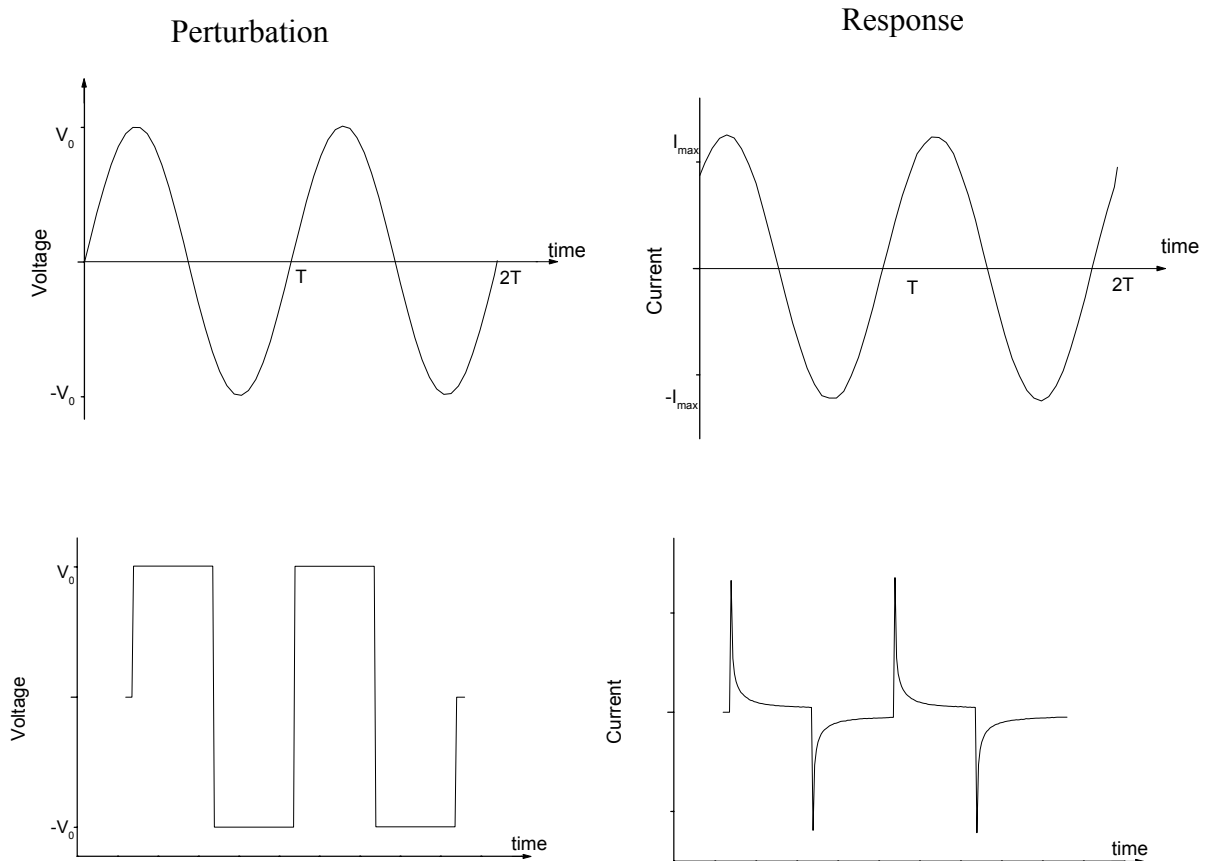


Figure 3.14 Sinusoidal and potential step perturbations with respective responses.

Since this method involve periodical quantities it is advantageous to analyze the response of the system under a periodical perturbation of arbitrary form, in terms of Fourier series development. The only restriction in the following treatment is that the applied perturbation is periodical with time, thus the treatment is of general applicability, independent on the shape of the applied perturbation. Historically, Fourier series named after Joseph Fourier who postulated this representation, playing nowadays an important role in many scientific areas like technical mechanics, mathematics, electrical engineering, etc.

We consider an arbitrary periodical function $f(t)$ with period T . It thus holds:

$$f(t + nT) = f(t) \tag{3.109}$$

For any integer n , Fourier development of the function $f(t)$ is the representation of this function in a form of a series of trigonometric functions [81]:

$$f(t) = \frac{\alpha_0}{2} + \sum_{n=1}^{\infty} [\alpha_n \cos(n\omega t) + b_n \sin(n\omega t)] \quad (3.110)$$

$$\text{where } \omega T = 2\pi \quad (3.111)$$

The expansion (3.110) is also called Fourier series expansion of the function $f(t)$ and α_k and b_k ($k=0, 1, 2, \dots, n$) are called the Fourier coefficients obeying the following relationships:

$$\alpha_k = \frac{2}{T} \int_0^T f(t) \cos(k\omega t) dt \quad (3.112)$$

$$b_k = \frac{2}{T} \int_0^T f(t) \sin(k\omega t) dt \quad (3.113)$$

It is often beneficial to express the Fourier series (3.110) in a complex representation [82]:

$$f(t) = \sum_{k=-\infty}^{\infty} c_k e^{ik\omega t} \quad (3.114)$$

$$\text{where } c_k = \frac{1}{T} \int_0^T f(t) e^{-ik\omega t} dt = \frac{1}{2} (\alpha_k - ib_k), k > 0 \quad (3.115)$$

Thus, the complex Fourier coefficient c_k is related to the Fourier coefficients appearing in (3.110) as:

$$\alpha_0 = 2c_0 \quad (3.116)$$

$$\alpha_k = 2 \operatorname{Re}(c_k) \Rightarrow \operatorname{Re}(c_k) = \frac{1}{2} \alpha_k \quad (3.117)$$

$$b_k = -2 \operatorname{Im}(c_k) \Rightarrow \operatorname{Im}(c_k) = -\frac{1}{2} b_k \quad (3.118)$$

Plotting real versus imaginary part of the complex Fourier coefficients would therefore yield an Argand diagram. This method of analysis provides the possibility to analyze the response of an electrochemical system under a periodical perturbation in terms of the Fourier coefficients and get information on the parameters involved.

References to chapter 3

- 1) W. Weppner, Proc. of the 2nd int. Meeting on chemical sensors, Bordeaux (1986)
- 2) J. Riegel, H. Neumann, H.-M. Wiedenmann, *Solid State Ionics* **152/153**, 783-800 (2002)
- 3) J.S. Lundsgaard, J. Malling, and M.L.S. Birchall, *Solid State Ionics* **7**, 53 (1982)
- 4) S.B. Lyon, D.J. Fray, *Solid State Ionics* **9/10**, 1295 (1983)
- 5) H. Iwahara, H. Uchida, *Anal. Chem. Symp. Ser.* **17**, 227 (1983)
- 6) A. Pelloux, P. Farby, and P. Durante, *Sens. Actuators* **7**, 245 (1985)
- 7) A. Huerland, R. Moos, R. Mueller, C. Plog, U. Simon, *Sensors and Actuators B* **77**, 287-292 (2001)
- 8) W. Weppner, *Ionics* **7**, 404-424 (2001)
- 9) G. Hötzel, Ph.D. Thesis, University of Stuttgart (1986)
- 10) N. Imanaka, Y. Yamaguchi, G. Adachi, and J. Shiokawa, *J. Electrochem. Soc.* **134** [3], 725-728
- 11) M. Gauthier and A. Chamberland, *J. Electrochem. Soc.* **124** [10], 1579-1583
- 12) N. Imanaka, Y. Yamaguschi, G. Adachi, and J. Shiokawa, *J. Electrochem. Soc.* **132** [10], 2519-2520 (1985)
- 13) V. Demuyser, C. W. Bale, *Solid State Ionics* **9/10**, 1285 (1983)
- 14) K. T. Jacob and D. Bhogeswara Rao, *J. Electrochem. Soc.* **126** [11], 1842-1847 (1979)
- 15) M. Gauthier, R. Bellemare, and A. Belanger, *J. Electrochem. Soc.* **128** [2], 371-378 (1981)
- 16) M. Itoh and Z. Kozuka, *J. Electrochem. Soc.* **133** [7], 1512-1517 (1986)
- 17) C. D. Eastman, T. H. Etsell, *Solid State Ionics* **136/137**, 639-645 (2000)
- 18) T. Maruyama, Y. Saito, Y. Matsumoto and Y. Yano, *Solid State Ionics* **17**, 281-286 (1985)
- 19) A. Menne and W. Weppner, *Solid State Ionics* **40/41**, 468-471 (1990)

- 20) R. Cote, C. W. Bale, M. Gauthier, *J. Electrochem. Soc.* **131** [1], 63-67 (1984)
- 21) W. Weppner, *Solid State Ionics* **40/41**, 369-374 (1990)
- 22) W. Weppner, *Materials Science and Engineering B* **15**, 48-55 (1992)
- 23) G. Hötzel and W. Weppner, Proc. Of the 2nd int. Meeting on chemical sensors, Bordeaux, 285-288 (1986)
- 24) G. Hötzel and W. Weppner, *Solid State Ionics* **18/19**, 1223-1227 (1986)
- 25) Y. Yan, N. Miura, N. Yamazoe, *Sensors and Actuators B* **24/25**, 287-290 (1995)
- 26) H. Aono and Y. Sadaoka, *J. Electrochem. Soc.* **147** [11], 4363-4367 (2000)
- 27) J. Liu and W. Weppner, *Solid State Communications* **76** [3], 311-313 (1990)
- 28) J. Liu and W. Weppner, *Solid State Ionics*, Editors: M. Balkanski, T. Takahashi and H. L. Tuller (1992)
- 29) J. Liu and W. Weppner, *Eur. J. Solid State Inorg. Chem.* **Tom 28**, 1151-1160 (1991)
- 30) N. Miura, Y. Yan, S. Nonaka and N. Yamazoe, *J. Mater. Chem.* **5** [9], 1391-1394 (1995)
- 31) Y. C. Zhang, M. Kaneko, K. Uchida, J. Mizusaki, and H. Tagawa, *J. Electrochem. Soc.* **148** [8] H81-H84 (2001)
- 32) N. Miura, S. Yao, Y. Shimizu, and N. Yamazoe, *J. Electrochem. Soc.* **139** [5], 1384-1388 (1992)
- 33) Y. C. Zhang, H. Tagawa, S. Asakura, J. Mizusaki, H. Narita, *J. Electrochem. Soc.* **144** [12], 4345-4350 (1997)
- 34) T. Maruyama, X. Ye and Y. Saito, *Solid State Ionics* **23**, 113-117 (1987)
- 35) Y. Saito and Maruyama, *Solid State Ionics* **28/30**, 1644-1647 (1988)
- 36) E. Steudel, P. Birke and W. Weppner, *Electrochimica Acta* **42** [20-22] 3147-3153 (1997)
- 37) S. Choi, W. Chung, D. Lee, *Sensors and Actuators B* **35/36**, 263-266 (1996)
- 38) Y. Yan, N. Miura, and N. Yamazoe, *J. Electrochem. Soc.* **143** [1], 609-613 (1996)
- 39) B. Y. Liaw and W. Weppner, *J. Electrochem. Soc.* **138** [8], 2478-2483 (1991)
- 40) J. Liu and W. Weppner, *Appl. Phys. A* **52**, 94-99 (1991)
- 41) H. Ullmann, *Keramische Gassensoren*, Akademie Verlag, Berlin (1993)
- 42) J. Liu and W. Weppner, *Appl. Phys. A* **55**, 250-257 (1992)
- 43) H. Rickert in "Electrochemistry of Solids: An Introduction", Springer-Verlag, Berlin-Heidelberg-New York (1982)

- 44) R.A. Huggins, *Ionics* **8**, 300-313 (2002)
- 45) C. Tubandt, *Z. Electrochem.* **26**, 338 (1920)
- 46) W. Weppner, *Solid State Ionics* **32/33**, 466-473 (1989)
- 47) W. Weppner and R.A. Huggins, *J. Electrochem. Soc.* **124** [10], 1569-1578 (1977)
- 48) J. R. Macdonald, "Impedance spectroscopy: emphasizing solid materials and systems", Wiley-Interscience Publication, New York-Chichester-Brisbane-Toronto-Singapore (1987)
- 49) C. M. A. Brett and A. M. O. Brett, "Electrochemistry: Principles, Methods, and Applications", Oxford University Press, Oxford-New York-Tokyo (1993)
- 50) R.D. Shannon, *Acta Cryst. A* **32**, 751-767 (1976)
- 51) Y. W. Hu, Ph.D. thesis, Stanford University (1980)
- 52) A.J. de Bethune, *J. Electrochem. Soc.* **102**, 288 C (1955)
- 53) Atkins, "Physical Chemistry" sixth edition, Oxford University Press, Oxford-Melbourne-Tokyo (1998)
- 54) I. Langmuir, *Journal of the American Chemical Society* **54**, 2798-2832 (1932)
- 55) C. Wagner, *Nachrichten der Akademie der Wissenschaften in Göttingen*, Nr. 3, 1-27 (1973)
- 56) C.H. Hamann, W. Vielstich, "Elektrochemie", Wiley-Vch Verlag, Weinheim-New York-Chichester-Brisbane-Singapore-Toronto (1998)
- 57) A. Fick, *Pogg. Ann.* **94**, 59 (1855)
- 58) J. Crank, "The Mathematics of Diffusion" Second Edition, Oxford University Press (1975)
- 59) A.R. Allnatt and A.B. Lidiard, "Atomic transport in Solids", Cambridge University Press (1993)
- 60) J.E. Bauerle, *J. Phys. Chem. Solids* **30**, 2657-2670 (1969)
- 61) P. Hagemuller, W. Van Gool, "Solid Electrolytes: General Principles, Characterization, Materials, Applications", Academic Press Inc. New York-London (1978)
- 62) C. Ho, Ph.D. Thesis, Stanford University (1980)
- 63) G. Popkurov, *Current Topics in Electrochemistry* **7**, 23-47 (2000)
- 64) J. E. B. Randles, *Discussions of the Faraday Society* **1**, 11-19 (1947)
- 65) C. Ho, I. D. Raistrick, and R. A. Huggins, *J. Electrochem. Soc.* **127** [2], 343-350 (1980)

- 66) D. R. Franceschetti and J. R. Macdonald, *J. Electrochem. Soc.* **129** [8], 1754-1756 (1982)
- 67) R.D. Armstrong, T. Dickinson and J. Turner, *Electroanalytical Chemistry and Interfacial Electrochemistry* **44**,157-167 (1973)
- 68) I. Barin, "Thermochemical Data of Pure Substances", VCH, Weinheim-New York (1993)
- 69) H. Schettler, Ph.D. Thesis, University of Tübingen (1994)
- 70) D.V. Ragone, "Thermodynamics of Materials" Vol. 1, J.Wiley and Sons, New York-Chichester-Brisbane-Toronto-Singapore (1995)
- 71) N.A. Godshall, Ph.D. Thesis, Stanford University (1980)
- 72) N.A. Godshall, I.D. Raistrick, and R.A. Huggins, *J. Electrochem. Soc.* **131** [3], 543-549 (1984)
- 73) L.C. Chen and W. Weppner, *Naturwissenschaften* **65**, 595 (1978)
- 74) J.B. Goodenough, H.Y-P. Hong, and J.A. Kafalas, *Mat. Res. Bull.* **11**, 203-220 (1976)
- 75) P. Cerisier and F. Roux, *Journal of Solid State Chemistry* **22**, 245-251 (1977)
- 76) R.A. Huggins, *Solid State Ionics* **136/137**, 1321-1328 (2000)
- 77) H. Schettler, J. Liu, W. Weppner, R.A. Huggins, *Appl. Phys. A* **57**, 31-35 (1993)
- 78) C. Delmas, J-J Branconnier, C. Fouassier and P. Hagenmuller, *Solid State Ionics* **3/4**, 165-169 (1981)
- 79) L. W. Shacklette, T. R. Jow, and L. Townsend, *J. Electrochem. Soc.* **135** [11], 2669-2674 (1988)
- 80) A. Stoklosa, J. Molenda and D. Than, *Solid State Ionics* **15**, 211-216 (1985)
- 81) G. James "Modern Engineering Mathematics", Third Edition, Pearson Education Limited, Essex (2001)
- 82) Bronstein, Semendjajew, Musiol, Mühlig, "Taschenbuch der Mathematik" Verlag Harri Deutsch, Thun und Frankfurt am Main (2000)

CHAPTER 4

Experimental aspects

This section deals with the experimental details for the preparation of the investigated cells and the measurement apparatus and techniques that have been employed in this work.

4.1 Measuring apparatus (Kiel cell)

For electrochemical measurements at defined temperatures and gas partial pressures or gas mixtures the following apparatus, so - called "Kiel cell" has been used. The apparatus is schematically shown in figure 4.1. It consists of two compartments, a double walled quartz glass cylinder with one end closed and a steel support. These two are binding each other using O-rings. Through its relatively small and defined volume, utilization of this apparatus allows to change relatively fast the gas atmosphere over the sample and thus a reasonable estimation for the response time of the cell under investigation.

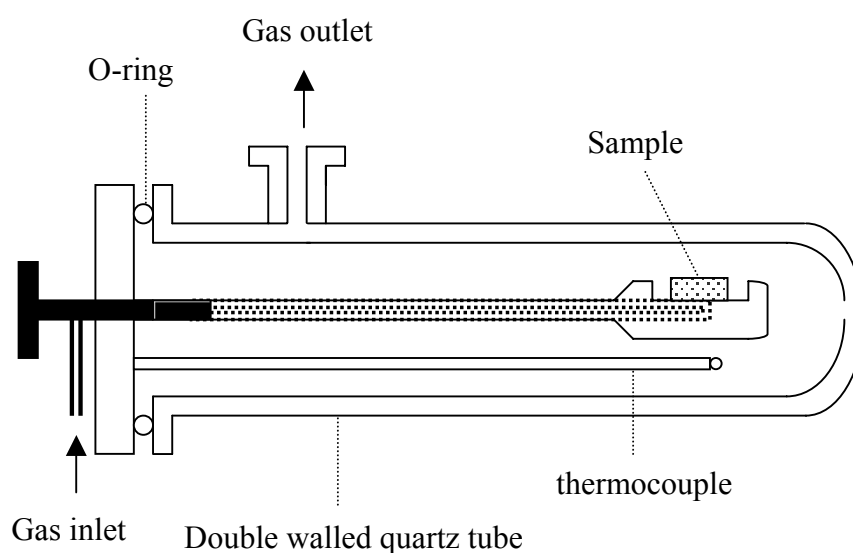


Figure 4.1: Schematic representation of the apparatus for electrochemical measurements under defined temperature and gas mixtures.

It can be used for measurements at temperatures up to 1000 °C, and may accomplish nominal experimental conditions for long term measurements, thus providing suitable experimental conditions for investigations on electrochemical gas sensors. The apparatus was placed and fastened in a tubular furnace with the steel support to be maintained just outside the furnace. The temperature of the furnace was controlled with commercial NiCr / Ni thermocouples allowing the temperature to be maintained constant during the experiment. Furthermore, inside the quartz tube an additional thermocouple (Pt / Pt - 13% Rh or NiCr / Ni) placed near to the sample, for controlling the temperature of the sample or sensor under investigation. Platinum wires inside alumina tubes with small diameter were used to transfer the electrical signal from the electrochemical cell to the steel support base of the apparatus where it was further processed via BNC connectors to the electrical instruments. In the gas outlet a glycerin bubbler has been installed, and each time the apparatus has been assembled for measurements, its gas tightness has been individually checked before inserting the sample.

4.2 Preparation of cells and experimental setup

The details on preparation of individual materials and electrochemical cells as well as the experimental setup conditions for measurements will be presented in this section.

The experimental set up for the investigations on the response time of the oxygen type I sensor consists of the following. As solid electrolyte for oxide ions, two identical 10 mol % yttria stabilized zirconia tubes (Zircoa Corp. of America, Ohio, USA) were used with the flat ends closed. The tubes were 30 cm in length, 10 mm in outer diameter and had a wall thickness of 1.5 mm. Electrodes were made by painting platinum paste (M 8005, Demetron GmbH, Hanau, Germany) inside and outside at the flat closed ends of both tubes. The inside top ends of the tubes were painted with different amounts of platinum and annealed for 2 h at 850 °C in ambient air. Figures 4.2 and 4.3 show scanning electron microscope pictures for the two different platinum coverages of the zirconia electrolyte, thinner platinum film with smaller patches and thicker platinum film with larger patches. The average diameter of the platinum plaques was determined to be 5 µm and 10 µm respectively. The electrical signal was

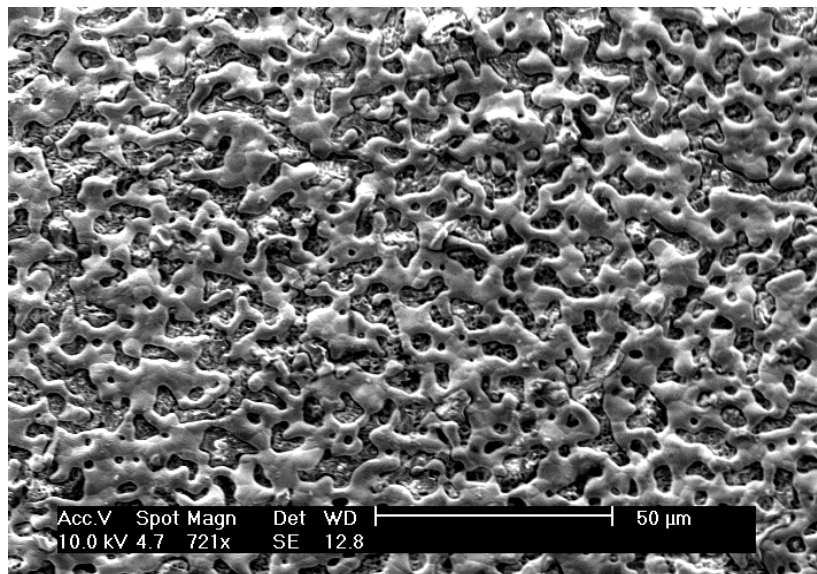


Figure 4.2: Scanning electron micrograph of the thinner platinum electrode on top of the zirconia electrolyte.

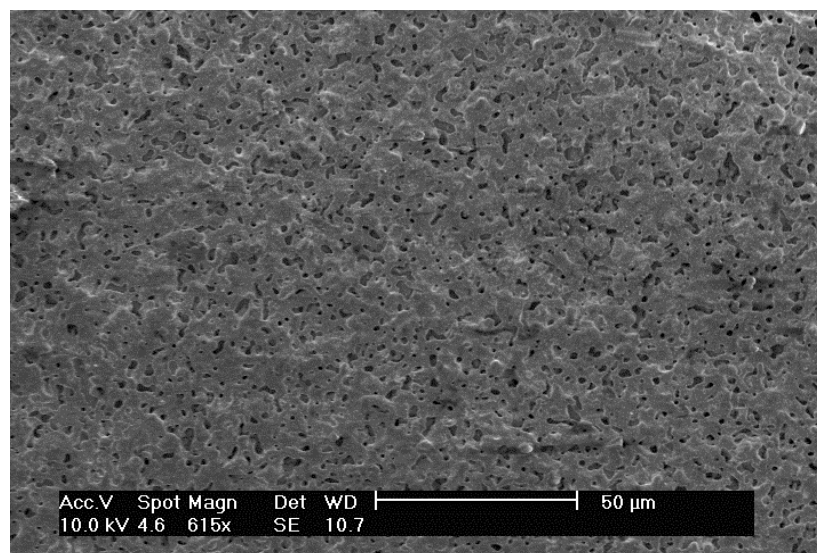


Figure 4.3: Scanning electron micrograph of the thicker platinum electrode on top of the zirconia electrolyte.

carried using platinum wires into small diameter alumina tubes, one inside and one outside of the zirconia tube. The tube was placed into a tubular furnace where a NiCr/Ni thermocouple placed near the flat end of the zirconia tube for measuring the temperature. The oxygen partial pressure was maintained inside the tube by mixing pure oxygen (oxygen 5.5) with argon (argon 5.0) utilizing mass flow controllers (Tylan General FC 280 SA), whereas outside the tube by the oxygen partial pressure of ambient air. Placing the apparatus with the mass flow controllers very close to the furnace in which the zirconia electrolytes were inside, permitted the use of very short connections for the gas mixture from the mass flow controllers to the zirconia tubes, thus making it possible to change the oxygen partial pressure rapidly. The total flow rate for the mixture of oxygen and argon was maintained constant at 20 sccm/min during the experiments with both tubes. The open circuit voltage of the gauges was measured with a high input impedance ($> 10^{14}$ Ohms) electrometer (EM 1.0, Ionic Systems, Germany) and the electrical signal was further proceeded to a chart recorder (Philips PM 8262 Xt) where voltage transients could be registered.

The experimental details on the kinetic investigations on electrochemical type III cells under CO₂ atmospheres, consists of the preparation of individual materials and complete cells. NASICON or Na- β'' -alumina have been employed as solid sodium ionic conductors.

NASICON has the general formula $\text{Na}_{1+x}\text{Zr}_2\text{Si}_x\text{P}_{3-x}\text{O}_{12}$, whereas in this work the composition with $x = 2$ has been prepared according to the sol-gel process [1]. An aqueous solution of NaOH (Merck, 99%) and NH₄H₂PO₄ (Aldrich, 99+%) is heated up to 80 °C and gradually a solution of Zr (C₃H₆OH)₄ (Aldrich, 70%) and Si(C₂H₄OH)₄ (Alfa, 99%) in absolute ethanol (Roth, 99,8+%) was added to it. An extra amount of 10% NaOH was added for compensation of the Na₂O loss during sintering [2]. The forming gel was filtered and the resulting powder collected and dried overnight at 120 °C. The dried powder was then grained in a mortar to obtain fine particles size and calcined by keeping the powder to 400 °C for 1 h and then to 900 °C for 12 h with heating and cooling rates of 2 °C/min. Then the powder was ball milled several times in zirconia cups with isopropanol and dried again at 120 °C overnight. Finally, the powder was pressed isostatically (1 h at 130 KN) to form bars which were then sintered inside platinum containers at 1150 °C for 1 h, with heating

and cooling rate of 2 °C/min. The bars were afterwards cut into discs, which were polished.

Sodium cobalt bronze with the formula Na_xCoO_2 ($x = 0.7, 0.9$) was prepared with solid state reaction [3], by heating appropriate mixtures of the starting materials Na_2O_2 (Merck, 95+%) and Co_3O_4 (Fluka, >71% Co) in Al_2O_3 crucibles at 900 °C for 24 h. The heating and cooling rates were adjusted to 2 °C/min. Before the starting mixture was brought to reaction at a high temperature oven it was grained in a mortar. Alternatively [2], in some cases it was prepared by using as starting materials proper mixtures of Na_2CO_3 (Merck, 99.9+%) and Co_3O_4 (Fluka, >71% Co). The precursors were heated at 850 °C for 24 h with the heating-cooling rate to be adjusted at 1 °C/min. Using these starting materials (Na_2CO_3 and Co_3O_4) the desired phases could be prepared only at or above 850 °C. Extra amounts of 10 wt % Na_2O_2 or Na_2CO_3 respectively were added to compensate loss during sintering [2, 4]. The composition of the sodium cobalt bronze was verified through ICP measurements, by revealing Na/Co ratio. After preparation the material was kept in a silica gel excicator until it has been used in electrochemical cells.

Complete cells with solid reference electrode may be divided into two major cell structures namely those with Na_2CO_3 - Li_2CO_3 - VO_2 sensitive compound and glassy reference electrode and those with Na_2CO_3 sensitive electrode and sodium cobalt oxide reference electrode. For the first category, NASICON has been employed as solid electrolyte for sodium ions in the electrochemical cell schematically shown in figure 4.4. The electrolyte material was typically in form of pellets of 1 - 1.5 mm thickness and 6-10 mm diameter, which were polished at both sides. The reference material consisted of powder of $\text{Na}_{0.9}\text{CoO}_2$ mixed with about 10% glass powder (Schott 8422 glass type). Adding α - terpyneol (Merck-Schuchardt) to the mixture of sodium cobalt bronze and glass powders resulted to a solution which was then painted on the surface of the electrolyte and leftover to dry at 120 °C for several hours. Discs of TZP3Y (3 mol % yttria stabilized tetragonal zirconia polycrystals (Tosoh Corp., Tokyo, Japan) produced by tape casting were sintered at 1450 °C for 2 h in ambient air. Platinum electrodes were painted on both surfaces and short-circuited. Electrodes were afterwards burned at 850-900 °C. The discs were finally brought in contact with

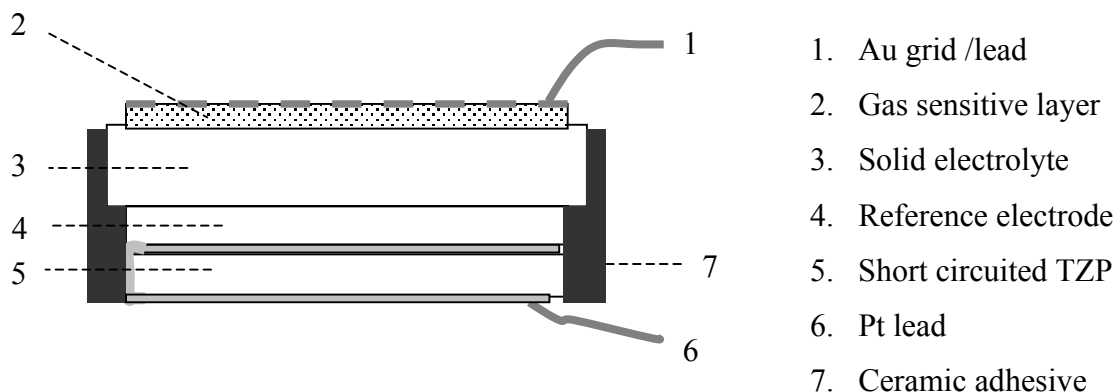


Figure 4.4: Structure of the device under investigation in carbon dioxide atmospheres.

the reference electrode and attached by applying peripherally high temperature ceramic adhesive (940 Cotronics Corp., N.Y.). The sensitive electrode material constituted by mixture of Na_2CO_3 (Merck, 99.9+%), Li_2CO_3 (Fluka, 99+%) and VO_2 (Chempur, 99.5+%) was applied by melting and quenching the material on the surface of the solid electrolyte whereas on the surface of the gas sensitive compound a gold grid was used as metallic conductor. For the second cell category, as shown schematically in figure 4.5, NASICON or $\text{Na} - \beta''$ - alumina electrolytes employed, in contact with sodium cobalt oxide solid reference electrode. As gas sensitive compound pure Na_2CO_3 has been used. The electrolyte disc typically 1-2 mm thick with a diameter of 6-10 mm was polished on both sides. Platinum paste electrodes needed to be heated up to 850-900 °C during preparation because of the necessity to remove organic impurities in the Pt paste electrodes and to ensure adherent films on top of the solid electrolyte. The reference electrode material was in form of pellet, uniaxially pressed with 6-8 mm diameter. The reference and electrolyte discs were brought in contact using a self-made spring loaded accessory and peripherally encircled by a fast cure ceramic adhesive (940 Cotronics Corp., N.Y.) followed up by the utilization of high temperature gas tight ceramic epoxy (Thermeez 7030, Cotronics Corp., N.Y.). The isolation of the reference electrode from the surrounding atmosphere was accomplished by fixing a Macor[®] ceramic disc on top of the

reference electrode. The gas sensitive compound sodium carbonate was applied by either painting a solution of pre-grained sodium carbonate powder (Merck, 99.9+%) with α - terpyneol (Merck - Schuchardt), or by using thermal evaporation technique to create sodium carbonate films on the surface of the electrolyte. For producing sodium carbonate thin films on the electrolyte surface, a thermal evaporation machine Pfeiffer PLS 500 has been employed. The material was pressed isostatically into bars, which were then inserted in a copper crucible in the machine chamber. The cell was attached to a holder inside the chamber, which was evacuated before the evaporation process. Typical experimental parameters for the production of sodium carbonate films involve an evaporation time of 30 min, under a power of 0.19 kW, with a voltage of 9.38 kV and current of 0.011 A, under a total pressure of 2.6×10^{-4} mbar. With the above conditions the evaporation rate of sodium carbonate was approximately 0.4 nm/sec. During the evaporation process CO_2 gas was continuously supplied to the chamber. The thickness of the sodium carbonate films under those parameters was evaluated to be 0.8 μm .

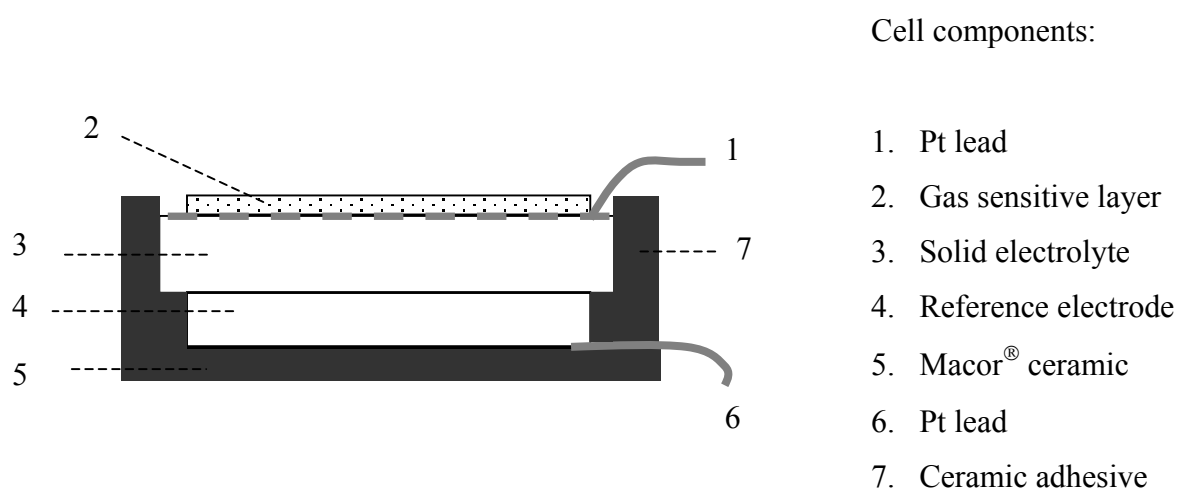


Figure 4.5: Schematic representation of the electrochemical cell under investigation in carbon dioxide atmospheres.

For the investigation on the kinetics of the Na_2CO_3 sensing electrode, experiments in electrochemical cells with elemental sodium as reference electrode were conducted. Metallic sodium is a reversible electrode for sodium ions, establishing sodium activity equal to unity. However, because of its high reactivity the preparation and sealing of the reference electrode were carried out carefully in an argon filled glove box. The schematic structure of the constructed electrochemical cell is shown in figure 4.6. Alumina tubes of about 9 cm length and 16 mm diameter with 2 mm wall thickness employed, whereas at the one end of the tube a sodium beta''-alumina pellet was fixed by using high temperature ceramic seals (940 and Thermeez 7030, Cotronics Corp., N.Y). The tubes were then inserted in a glove box and filled with elemental sodium (Aldrich, 99.95%) whereas the open end was encapsulated by a Macor[®] disc and the same high temperature ceramic seals mentioned above. Each tube left inside the glove box for at least 24 h allowing the seals to dry. While the reference electrode preparation was always identical, the following assemblies were accomplished for the sensing electrode. a) Metallic conductor platinum sputtered and sodium carbonate layer in-situ formed, b) metallic conductor platinum sputtered and porous sodium carbonate painted, and c) metallic conductor platinum paste painted and porous sodium carbonate painted. The in-situ formation of sodium carbonate gas sensitive layer on the surface of the electrolyte was made by passing a current of sodium ions from the reference through the electrolyte and towards the measuring electrode. This was carried out at elevated temperatures (at or above 400 °C) and at high CO_2 partial pressures (at or above 10% CO_2). Platinum films of 50 nm thickness by sputtering were employed when the gas sensitive layer was in-situ formed. Measurements under CO_2 atmospheres were carried out in "Kiel cells" where the temperature was controlled with either Pt/Pt-13% Rh thermocouples connected with THERM 3280-1 temperature controller or with NiCr/Ni thermocouples connected with Eurotherm 91e temperature controller. The desired carbon dioxide partial pressure was maintained by mixing synthetic air (synthetic air 5.5) with either pure CO_2 or diluted CO_2 (carbon dioxide 4.5) using mass flow controllers (Tylan FC-280 and Millipore 2900) with total flow rates between 70 sccm/min or 100 sccm/min, if otherwise not noted. All mass flow controllers used in this work have been calibrated using tables [5] in cases where those are applicable. For special gas mixtures individual calibration (Brooks Vol-U-meter calibrator, Brooks Instrument B.V., The Netherlands) at standard

conditions was performed. Na – β'' – alumina (Ceramatec, Salt Lake City, USA, and Ionotec Ltd, Cheshire, England) used, initially in plate form which was cut in small rectangular shaped pieces. The material was kept in a glove box until it has been used. Metallic electrodes made by gold (Heraeus, Hanau, C5755A) or platinum paste (Heraeus, Hanau, CL11-5100) needed to be heated up to 850-900 °C during preparation because of the necessity to remove organic impurities in the paste electrodes and to ensure adherent films on the surface of the solid electrolyte. Humidified gas mixtures were prepared by passing the gas mixture through distilled water at a certain temperature. Figure 4.7 shows the experimental arrangement for the investigations in CO₂ containing gas including the gas mixing system, tubular furnace for maintaining a certain temperature and instruments for measuring the electrical signal. An additional mass flow controller (IV) could be used for maintaining a desired concentration of an additional gas, thus enabling to check cross sensitivities.

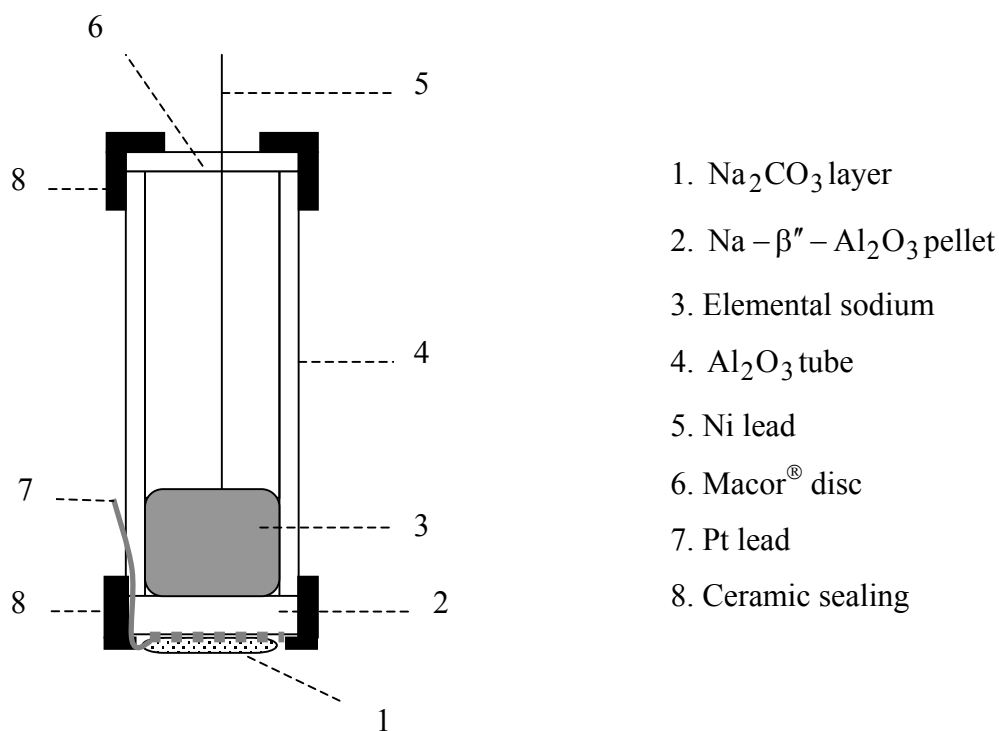


Figure 4.6: Construction of electrochemical cell for the investigation of Na₂CO₃ electrode.

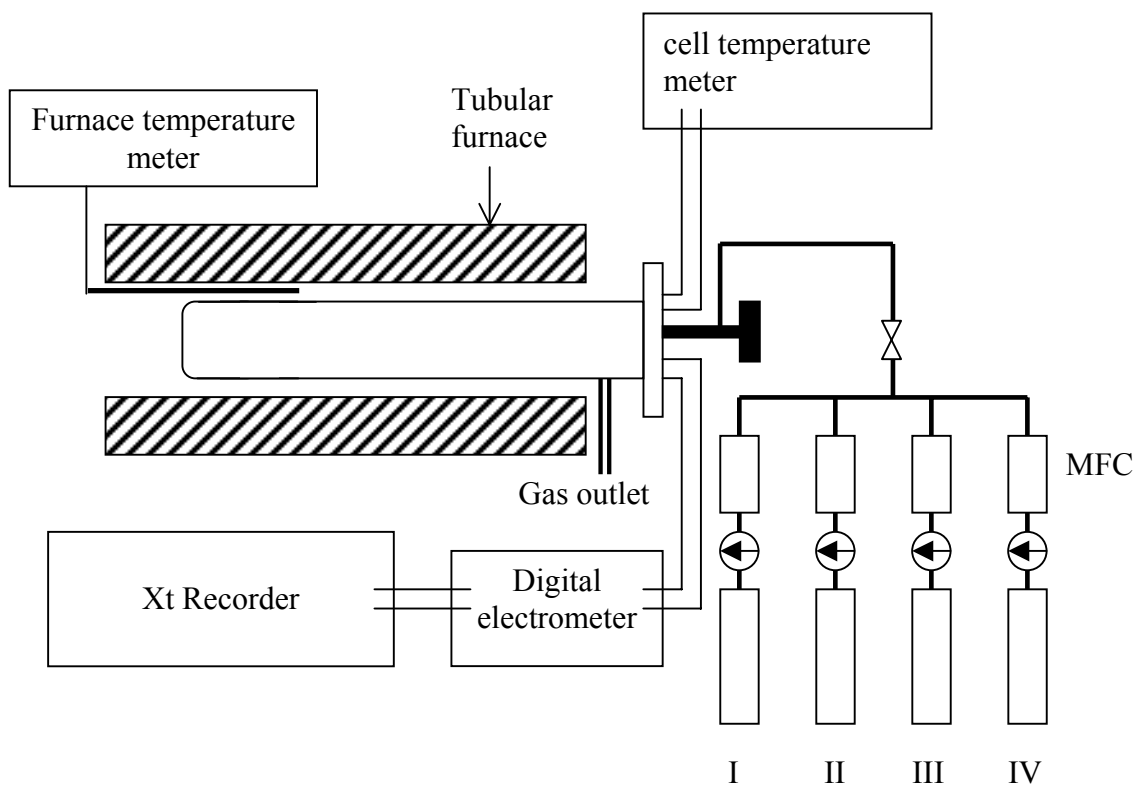


Figure 4.7: Schematic representation of the experimental setup for investigations under carbon dioxide atmospheres.

For investigations on the kinetics of the interface solid-gas in monolithic cells with one or two gaseous species present and by employing dynamic techniques, Na- β'' -alumina electrolytes have been used. The electrolyte was in the shape of rectangular pieces, which were polished at both face areas and afterwards dried at 120 °C for at least one day. Thin platinum electrodes were painted on the surfaces and Pt wires were used for carrying the electrical signal. The cell was heated to 850-900 °C for 2 h to ensure proper adhesion of the Pt films to the electrolyte. The schematic structure of the electrochemical cell exposed to the gas mixture is shown in figure 4.8. The temperature of the sensor was measured with a Pt/Pt - 13% Rh thermocouple inside the "Kiel cell" connected with a temperature controller (Therm 3280-1), and the temperature of the furnace was maintained with a Ni/CrNi thermocouple. Gas mixtures were obtained by mixing argon with sulfur dioxide and

nitrogen dioxide diluted in synthetic air, using mass flow controllers (Tylan FC280 and Millipore FC2900). Cells were heated up to the desired temperature in argon gas. When nitrogen dioxide or sulfur dioxide were present, the oxygen partial pressure was maintained to be 0.205 bar. Short length coaxial wires were used to carry the electrical signal between the cell under investigation and the potentiostat (Potentiostat&Galvanostat PG1.0, Ionic Systems, Germany). An AD-DA card allowed digitalization of the electrical signal, which was registered using Lab-view software while at the same time, the electrical signal could be shown in a chart recorder or an oscilloscope. The electrical perturbation was manually controlled by a function generator (Hewlett-Packard 33120A) connected to the potentiostat.

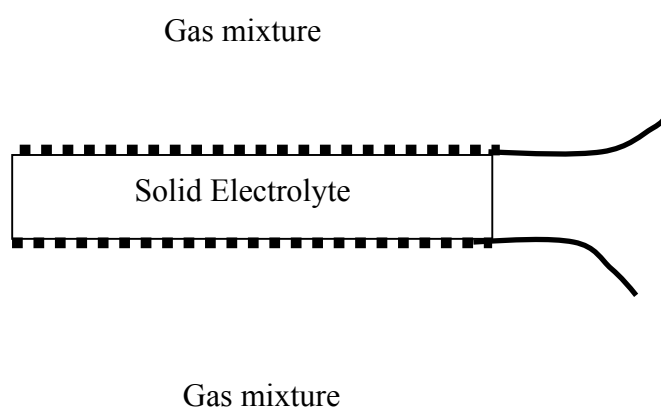


Figure 4.8: Schematic arrangement of the electrochemical cell for kinetic studies.

4.3 Experimental methods

Several experimental methods have been used for this work. A brief survey of impedance spectroscopy, scanning electron microscope, inductive coupling plasma and thermal analysis will be presented in this paragraph.

- Impedance measurements were carried out with two devices. A 4192A LF Hewlett Packard Impedance Analyzer was used for the frequency region 13MHz to 5Hz while for lower frequencies down to 10^{-4} Hz an EIS-6416b impedance spectrometer was utilized, combining a perturbation generator (PG-6416b) with a filter-amplifier

(SR-640, Stanford Research Systems Inc.). The amplitude of the perturbation was in the range 40-100 mV. For electrochemical cells with an open circuit voltage under the experimental conditions when the complex impedance has been measured, compensation of the voltage was performed during the impedance measurements. The impedance devices were placed as close as possible to the experimental setup to minimize inductive or capacitive effects at high frequencies. Impedance measurements were repeated to avoid any stray capacitive effects. The minimum frequency was chosen in order to fulfill the stability criterion for the electrochemical system under investigation.

- Scanning electron microscope (SEM) and energy-dispersive X-ray microanalysis (EDAX) were carried out with a computer controlled Philips XL30 microscope without coating the specimens. This instrument provides the possibility to look at topography of samples-interfaces and simultaneously determine the elemental compositions in distinct regions. The principle of SEM based on the bombardment of a sample with a focused beam of electrons whereas the detected scattered electrons from the surface producing a highly magnified image. As a by-product of the interaction of the electron beam with the atoms in the sample surface x-rays are produced having energies which are characteristic of the atoms that produce them. Thus by attaching an energy-dispersive x-ray detector information for the elemental composition can be obtained.

- A quantitative method of extracting information for the chemical composition of a sample was provided by use of ICP. Inductively coupled plasma (ICP) discharge is a source of atomic emission spectrometry. RF power is applied to a coil causing electric and magnetic fields to be set up in the surrounding area. With argon gas flowing through a spark, electrons are accelerated by the RF fields, causing further ionization and forming a plasma. The sample typically in a solution form, is introduced through the induction region. Quantitative information obtained by comparing the emission spectrum of the sample to a reference one corresponding to a standard solution with known concentrations of the elements of interest. ICP measurements were performed using a computer driven instrument (Optima 3X00, Perkin Elmer Corp., Norwalk, USA).

- Differential thermal analysis (DTA) is a dynamic technique where the temperature difference between the material under investigation and a reference material is

measured as a function of temperature. The sample typically in fine powder form is inserted into a furnace where both substance and reference material are heated up to a certain temperature. Because this is a differential technique sensitive changes can be easily registered. Thermogravimetric analysis (TGA, TG) is a technique in which the mass of a substance is measured as a function of temperature or time while substance and reference material are subjected to a temperature program. For both differential thermal analysis and thermogravimetric analysis the temperature raise is typically linear. The reference substance should show no phase transitions within the measured temperature range, have a similar heat conductivity and heat capacity as the measured one and should not react with the substance under study. A computer controlled thermal analyzer (STA 409 C NETZSCH) was used in this work, where simultaneously DTA and TGA/TG could be performed. The temperature raised with 5 °C/min if not otherwise noted. As reference material Al₂O₃ has been used. The temperature difference of substance and reference material was registered with PtPh10%-Pt (S- type) thermocouples whereas the surrounding atmosphere could be controlled by having a special gas, or left open to air.

For cold pressing of powder to form pellets or bars uniaxially or isostatic techniques have been used. Isostatically, the powder could be pressed to form bars of 6 – 10 mm diameter and up to about 15 mm in length. Uniaxially the powder was pressed to form pellets of 6 - 10mm diameter and 1 – 2 mm in length.

X-ray measurements were conducted with two diffractometers (SEIFERT XRD 3000TT and 3000PTS) where Cu K_α radiation was used. X-ray analysis of the materials used in this work either in powder or in pellet form was performed as a preliminary investigation of the materials used.

Pellets were polished with a polishing machine (Rotopol-V, Struers, Copenhagen, Denmark) using polishing discs of different roughness down to 1 μm.

References to Chapter 4

- 1) V. Leonhard, H. Erdmann, M. Ilgenstein, K. Cammann, J. Krause, *Sensors and Actuators B* **18-19**, 329-332 (1994)
- 2) E. Steudel, Dr.-Ing. Thesis, University of Kiel (1998)
- 3) H. Schettler, J. Liu, W. Weppner, R.A. Huggins, *Appl. Phys. A* **57**, 31-35 (1993)
- 4) H. Schettler, Ph.D. Thesis, University of Tübingen (1994)
- 5) Tylan General Instruction Manual, Mass flow Controllers and Flowmeters

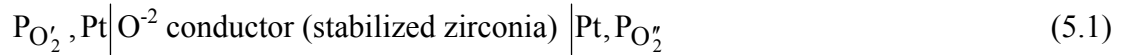
CHAPTER 5

Results and discussion

5.1 Response of O_2 sensors based on ZrO_2

5.1.1 Results

The solid state galvanic cell of the potentiometric oxygen gauge is a concentration cell of the following type:



For the investigation of the response time identical galvanic cells, based on yttria stabilized zirconia tubes with exactly the same composition, preparation and thermal history, except for the amount of platinum applied as electrodes as described in the experimental section, were studied. The experimental conditions for the two gauges were the same. The registered response curves for various changes of the oxygen partial pressure are presented and analyzed as follows.

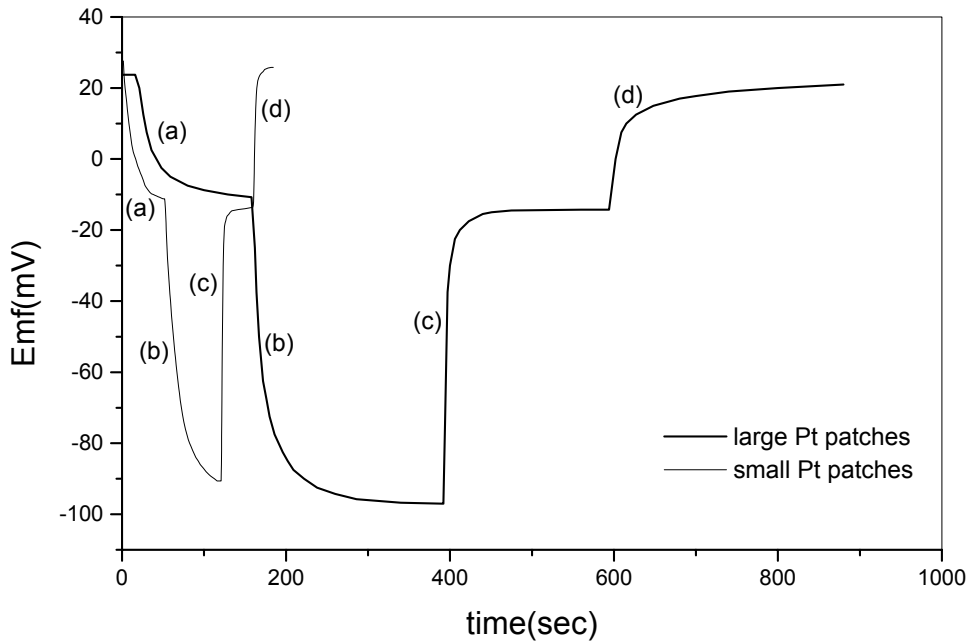


Figure 5.1: Comparison of the response of thin Pt layer electrode and thick Pt electrode for variations of the oxygen partial pressure from pure oxygen to 10% oxygen, from 10% oxygen to pure argon, and vice versa at 550 °C.

Figure 5.1 shows typical experimental results for the response of both gauges at 550 °C where the oxygen partial pressure changed in the following ways: (a) from pure oxygen to 10% oxygen, (b) from 10% oxygen to pure argon, (c) from pure argon to 10% oxygen and (d) from 10% oxygen to pure oxygen. The observed steady state open circuit cell voltages were the same in both sensors [1] and agreed with the value calculated from Nernst's law (3.1). Comparison between the response times of the large and small sized platinum patches upon step variations on the oxygen partial pressure at one side of the gauges showed that the response time depends on the size of the patches. This is clearly illustrated in figure 5.1 with the gauge with small platinum patches showing faster response than the gauge with the large platinum patches.

To further investigate the response time of the two sensors, similar variations of the oxygen partial pressure have been performed at different temperatures. The temperature variation of the response times for the electrode with small sized platinum patches is shown in figure 5.2 for temperatures in the regime 550-800 °C.

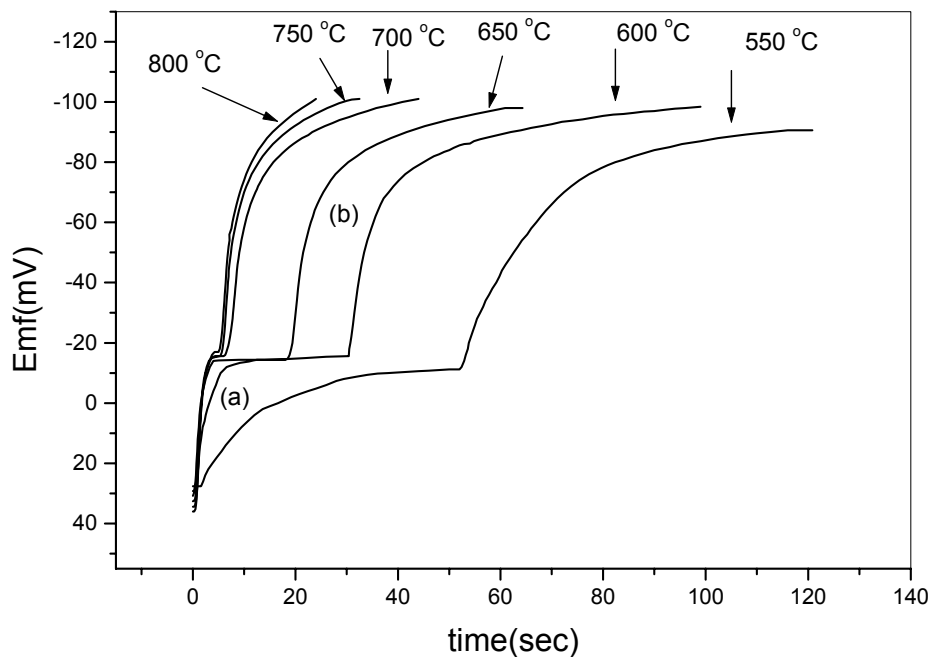


Figure 5.2: Temperature dependence of the response of the thin Pt layer electrode for two step changes in the oxygen partial pressure.

Similar temperature dependence was observed for the gauge with the thin platinum electrode. As a general observation from figure 5.2, the response times upon variations of the oxygen partial pressure increase with decreasing temperature, for both small and large sized platinum patches. The gauge with the smaller patches showed at fixed temperature, faster response times than that with the larger patches.

As discussed in chapter 4, the two different platinum coverages on the two identical ceramic zirconia tubes shown in pictures (4.2) and (4.3) can be represented by platinum patches of different average diameter in each one of the gauges. The above noted as electrode with small sized patches has a smaller average diameter whereas the one noted as electrode with large sized patches has a larger average diameter. In view of the experimental results the derived response curves have been analyzed in order to model the response of the two tubes, in two different ways:

1) From the response curves, it could be seen that the open circuit voltage (emf) follows a square root of time dependence for short periods of time $\tau \ll \frac{L^2}{D}$, for both tubes, where L is the length of the zone over which relaxation occurs and D the rate determining diffusion coefficient, respectively. Typical plot of open circuit voltage versus \sqrt{t} is shown at figure 5.3, for the thin Pt layer electrode tube, where the oxygen partial pressure has stepped down from 1 atm O₂ to 0.1 atm O₂ at 750 °C. The slope of the observed straight line in an open circuit voltage vs. \sqrt{t} plot such as the one indicated in figure 5.3 allows the calculation of the diffusion coefficient of the rate determining species from the solution of Fick's diffusion equation [2] from the formula (5.2):

$$D = \frac{\pi}{4} \left(\frac{FL}{RT} \right)^2 \left(\frac{dE}{d\sqrt{t}} \right)^2 \quad (5.2)$$

Since only the interface between platinum and the electrolyte contribute to the open circuit voltage while the redistribution of oxygen in the bulk of zirconia has no influence, half of the diameter of the Pt plaques was taken to be diffusion length. From the open circuit voltage vs. \sqrt{t} plots at different temperatures, the temperature dependence of the diffusion coefficient of the rate determining species according to equation (5.2) could be determined for both thinner and thicker platinum electrodes.

2) The diffusion coefficient was calculated from the diffusion length according to the formula (5.3) emanating from the diffusion equation equation (3.68) considering the mean square displacement of a particle moving in one direction [3, 4]:

$$D = \frac{L^2}{\tau} \quad (5.3)$$

The oxygen has to diffuse along the boundary between platinum and zirconia, while the equilibration in the bulk of the electrolyte as a result of a change in the oxygen partial pressure does not contribute to the emf. In equation (5.3) τ was taken to be the response time t_{90} .

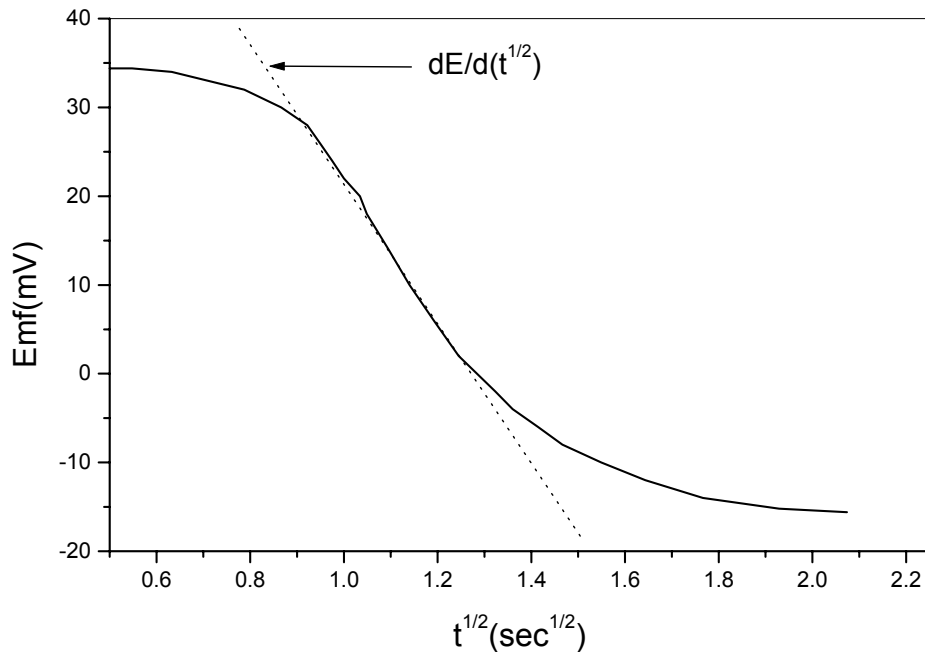


Figure 5.3: Variation of the emf as a function of \sqrt{t} for short times after changing the oxygen partial pressure from pure O_2 to 10% $O_2 + Ar$, for the thin Pt layer electrode at $750^\circ C$. The diffusion coefficient is determined from the slope of the straight line according to the indicated formula.

Figure 5.4 shows results for the diffusion coefficient according to equation (5.3) for both small and large platinum patches electrodes. The results obtained from the response relaxation measurements, and with both types of evaluation of the diffusion

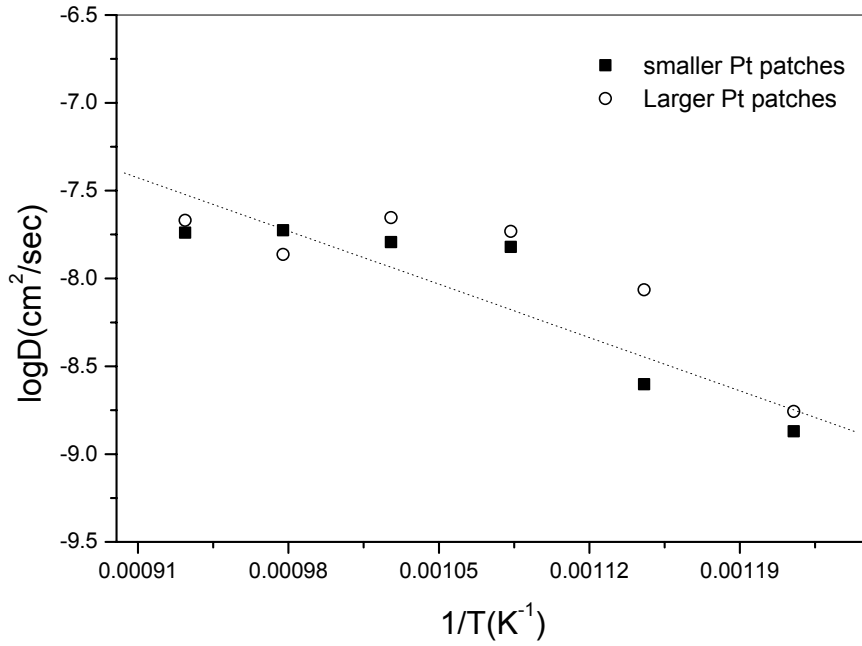


Figure 5.4: Experimental results for the diffusion coefficient of the thin and thick Pt layer electrodes as a result of random walk model at temperatures 550 °C to 800 °C.

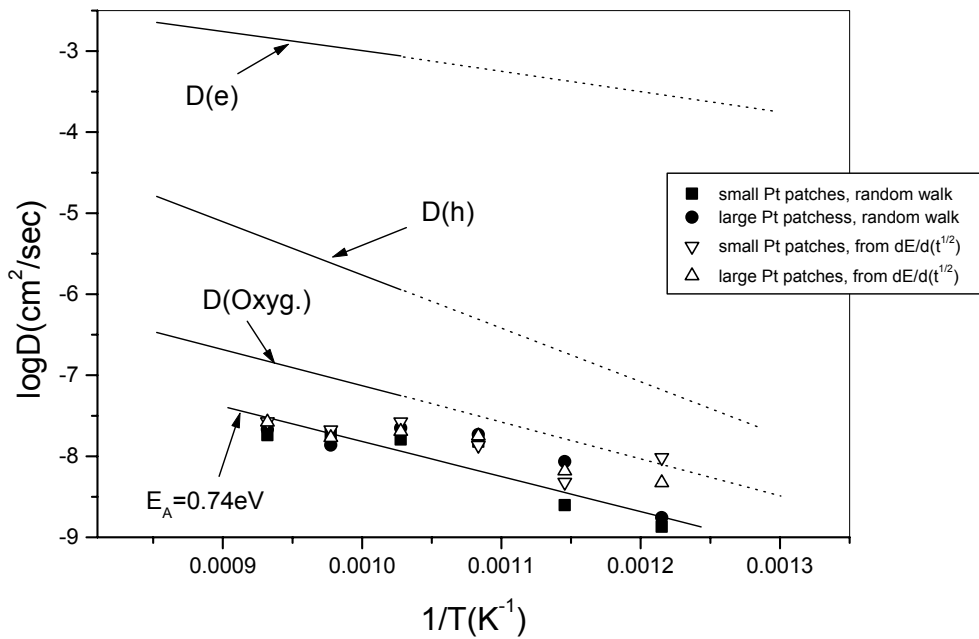


Figure 5.5: Results of the determination of the diffusion coefficient of the rate - determining process for the thin and thick Pt electrodes from the $1/\sqrt{t}$ and L^2/τ relationships in an Arrhenius diagram. For comparison, the diffusion coefficients of electrons, holes and oxide ions are shown.

coefficient are shown in Figure 5.5 where the diffusivities of electrons, holes and oxide ions in stabilized zirconia [2, 5] are plotted for comparison. It can be observed that both types of evaluation according to (5.2) and (5.3) are in agreement with each other within the expected limit of error, and the activation energy is in the range between 0.7 and 0.8 eV.

5.1.2 Discussion

From a microscopic point of view the process of oxygen incorporation from the gas phase into the solid electrolyte is schematically represented in figure 5.6. The patch on the left side represents the thin whereas that on the right side the thick platinum electrode. The process of oxygen incorporation may therefore split into the following steps:

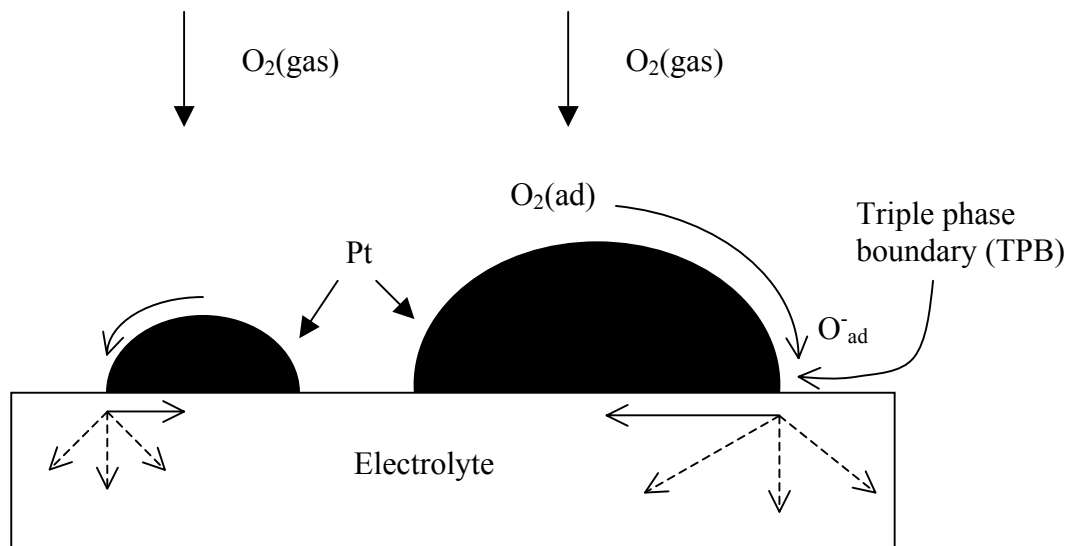


Figure 5.6: Schematic representation of the process of oxygen incorporation from the gas phase into the solid electrolyte.

- Oxygen diffusion in the gas phase and dissociative adsorption of O₂ molecules at the surface of platinum and uncovered surface area of zirconia.
- Diffusion of adsorbed oxygen along the surface of platinum to the triple – phase boundary metal(electronic conductor)-solid electrolyte-gas.
- Transfer of electrons to form O_{ad}⁻ and O⁻² in the zirconia lattice.
- Diffusion of oxygen in the zirconia electrolyte underneath the platinum, within the contact zone platinum-solid electrolyte.

There are several possible reasons causing the delay in the response of the oxygen gauge upon abrupt changes of the oxygen partial pressure:

- The exchange and ionization of oxygen is not occurring according to thermodynamic equilibrium or is delayed, not establishing the redox equilibrium.
- The surface oxygen activity established by the equilibration with the gas is significantly changed by the bulk diffusion of oxygen. As a result of the new concentration gradient established by the change in oxygen activity, oxygen diffuses from the bulk of the solid electrolyte toward or away from the interface.
- At the interface between the platinum electrode and the solid electrolyte electronic equilibrium is not established, or the voltage drop across the interface is locally not uniform along the interface.

The response time upon changes of the oxygen partial pressure in the gas depends strongly on the size of the platinum patches on the surface of the stabilized zirconia solid electrolyte, and accordingly on the size of the common interface. This observation excludes dissociation of oxygen molecules, diffusion along the surface of the platinum patches, ionization equilibria and bulk diffusion of oxygen in the solid electrolyte from being the rate determining processes. Diffusion of oxygen through platinum is ruled out since platinum is essentially impermeable to oxygen even at elevated temperatures [6].

Both with regard to the order of magnitude and activation energy, best agreement for the diffusion coefficient of the rate determining species obtained with the above two evaluation methods from the experimental data, is observed with the diffusivity of oxide ions.

The diffusion coefficients for electrons and holes appearing in figure 5.5 have been taken from literature experimental results [2, 5] involving relaxation measurements

after polarization of zirconia based galvanic cells. The diffusivity of oxide ions (oxygen vacancies) has been calculated from the ionic conductivity and the number of oxygen vacancies. The results indicate that oxide equilibration in zirconia is rate determining. In the case of chemical diffusion it might be expected that hole or electron diffusion are rate determining, but this could be understood by the simultaneous diffusion of electrons within the metal and oxide ions within the electrolyte along the interface between zirconia and platinum. From the results it can be concluded that a diffusional process is rate determining for the speed of response of zirconia based potentiometric oxygen sensors. Similar model has been proposed by Braunshtein et al. [7] to account as rate determining process in $(\text{CeO}_2)_{0.9}(\text{Gd}_2\text{O}_3)_{0.1}$ solid electrolytes. They investigated the observed current limitation under oxygen atmospheres concluding that diffusion of oxygen along the interface electrode-electrolyte is rate determining.

The holes required to diffuse simultaneously with the oxygen in zirconia for charge neutrality, are not considered to be rate determining because electronic charge carriers are readily mobile in the platinum metal. The oxygen which is transferred compensated by holes with the amount of transferred oxygen to be twice the amount of holes which have a concentration of 10^{17} cm^{-3} in the given oxygen partial pressure range at $800 \text{ }^\circ\text{C}$ [5].

This situation can be seen as similar to the diffusion of silver in Ag_2S and the diffusion of electronic species in the metal sheet when sulfidizing silver [8]. While the interfacial region of the contact platinum-electrolyte near the triple phase boundary electronic conductor (platinum) - solid electrolyte - gas has already reached equilibrium with the new oxygen partial pressure, the regime in the center underneath the platinum patch has still the old composition before the partial gas pressure change. In this view, regions of different electrostatic potential drop across the metal patch-electrolyte interface are connected to each other and form an average voltage drop. The response time is given by the time it takes to equilibrate the entire interfacial regime by diffusion of oxygen from the triple phase boundary toward the center of the metal-electrolyte interface. The significance of electrode morphology was pointed out by Kenjo et al. [9] in investigations by means of linear sweep voltammetry in electrochemical cells involving zirconia electrolytes under oxygen atmospheres. They proposed that morphological parameters of the electrode, especially the contact zone

between platinum and the electrolyte should be considered for an adequate description of the electrode kinetics.

From an electrical point of view the equivalent circuit of figure 5.7 may describe the response of the zirconia probes. A Warburg type diffusion is represented by resistances $R_{||}$ and capacitances E_1, E_2, \dots in the transmission line of figure 5.7(b).

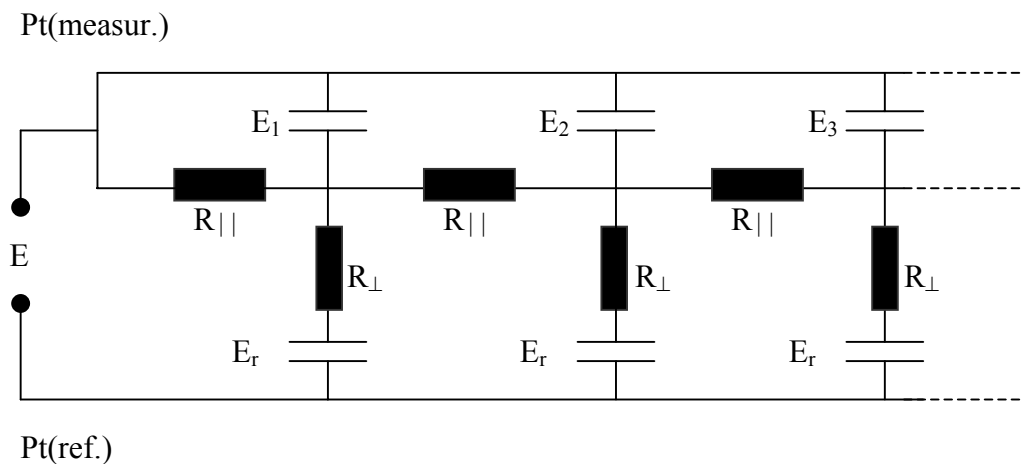
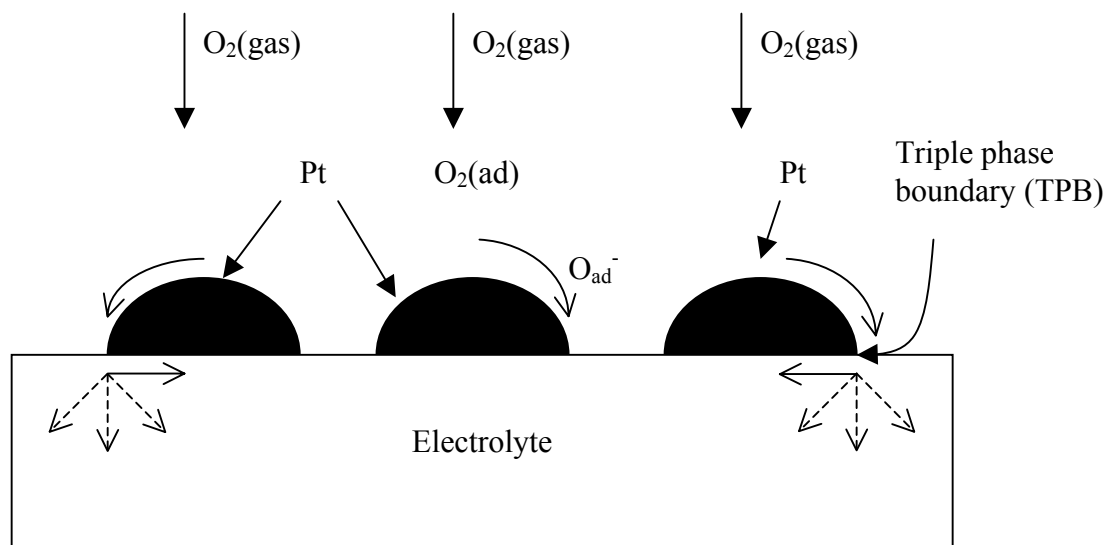


Figure 5.7: Schematic representation of the response of zirconia based oxygen probes and equivalent circuit

This represents the charging of the interface between platinum and the electrolyte and building up the new double layer capacitance and potential drop across the interface according to the new oxygen partial pressure. The adjustment of the new double layer capacitance at the electrode-electrolyte interface after changing the oxygen partial pressure will require a certain time, leading to a delay in the response time of the cell. The resistances R_{\perp} represent the ionic resistance of the electrolyte, which is constant and independent of the oxygen partial pressure. The capacitors E_r indicate the double layers at the reference side, which also remain constant during the experimental investigations. The open circuit voltage (emf) of the oxygen sensor is determined by the potential drops across the capacitors which are charged up by the oxygen diffusing underneath the platinum as represented by the parallel resistances $R_{||}$.

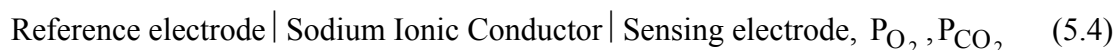
5.2 Potentiometric CO₂ sensor

The electrochemical cell of type III all - solid - state gas sensors consists of an electrolyte sandwiched between two electrodes, reference and sensing. The reference electrode should maintain a constant activity of the electroactive species while at the sensing electrode equilibrium between the gas and the auxiliary phase is accomplished. The whole sensor arrangement includes solid - solid interface between the reference electrode and the electrolyte, solid - solid interface between the electrolyte and the gas sensitive layer, and solid - gas interface between auxiliary phase and the gas under detection. Since the voltage drop according to the discussion in section 3.3 is within a narrow region at the interfaces, the performance of the entire electrochemical cell is directly dependent on the performance of the individual interfaces involved. Therefore in this view, the results will be arranged in sections regarding those for the investigation of the kinetics of complete cells under CO₂ atmospheres followed up by those regarding investigation on the kinetics of the interfaces involved at the reference and sensing electrodes. For results presented in whole section 5.2 unique convention has been adopted, namely the sensing electrode has been connected to the positive pole of the measuring unit.

5.2.1 Cell with glassy reference and complex auxiliary compound

5.2.1.1 Results

This paragraph presents the results on the investigation of the kinetics of type III electrochemical cell with Na₂CO₃-Li₂CO₃-VO₂ auxiliary compound under CO₂ atmospheres. The electrochemical cell under investigation which is schematically shown in figure 4.4 may be written as:



As reference electrode a combination of Na_{0.9}CoO₂ with glass and TZP ceramic was employed. The auxiliary compound, a mixture of Na₂CO₃ – Li₂CO₃ – VO₂ was attached to the electrolyte as described in the experimental section. Transient responses of the cell (5.4) for various changes of the CO₂ partial pressure, at 430 °C are shown in figure 5.8. The CO₂ partial pressure changed accordingly to: (a) from

2×10^{-4} to 5×10^{-4} atm CO₂, (b) from 5×10^{-4} to 10^{-3} atm CO₂, (c) from 10^{-3} to 8×10^{-4} atm CO₂, (d) from 8×10^{-4} to 6×10^{-4} atm CO₂, (e) from 6×10^{-4} to 4×10^{-4} atm CO₂, (f) from 4×10^{-4} to 2×10^{-4} atm CO₂. While varying the carbon dioxide partial pressure, the oxygen partial pressure was maintained to be equal to $P_{O_2} = 0.205$ bar and the total gas mixture flow rate kept constant at 100 sccm/min. The auxiliary phase composition was Na₂CO₃ 52.24 mol %, Li₂CO₃ 26.84 mol %, VO₂ 20.92 mol %. Considering the experimental setup, the gas mixture required to travel a certain distance until reaches the sensor device. The time for providing another gas composition over the cell was evaluated to be 10 min and is included in the transient curves of figure 5.8. Figure 5.9 shows the open circuit voltage of cell (5.4) as a function of the CO₂ partial pressure at 430 °C. The cell voltage varies linear with the logarithm of CO₂ partial pressure, with a standard deviation of the experimental points from the least squares linear fit to be 1.26 mV. The effect of varying the composition of the auxiliary phase and the reproducibility of this fabrication method are shown bellow. Table 5.1 summarizes the investigated compositions of Na₂CO₃ – Li₂CO₃ – VO₂ mixtures and the corresponding sensitivities to CO₂. The preparation technique and all other compartments of the sensor as well as the experimental conditions have been identical for the cells with compositions (A) – (D).

Table.5.1: Compositions of the auxiliary phases and corresponding experimental sensitivity to CO₂ at 430 °C for the cell assembly (5.4).

Composition	Na ₂ CO ₃ (mol %)	Li ₂ CO ₃ (mol %)	VO ₂ (mol %)	Sensitivity (mV/decade)
(A)	32.89	62.92	4.18	61.58
(B)	52.24	26.84	20.92	70.93
(C)	62.21	29.74	8.04	66.29
(D)	64.28	21.5	14.21	60.02

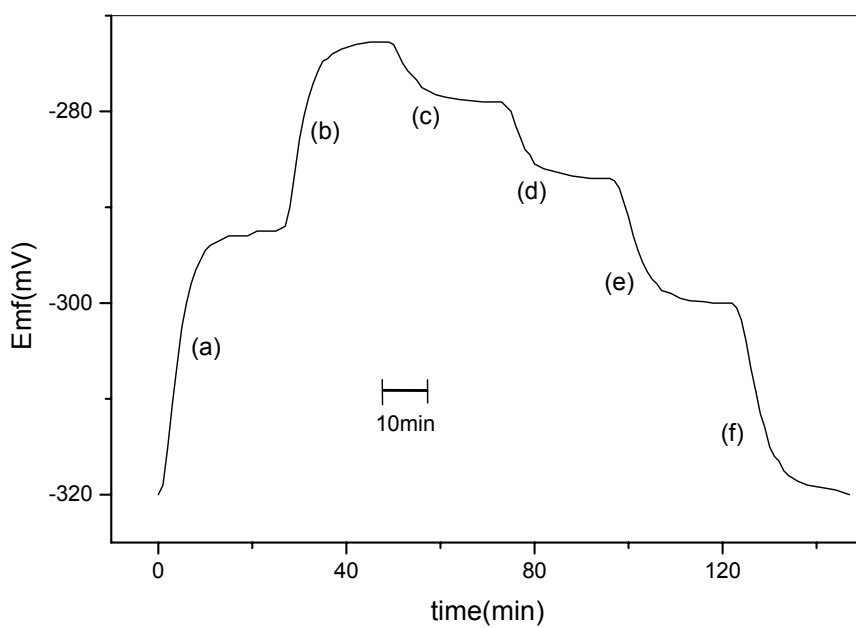


Figure 5.8: Transient responses to the cell (5.4) upon changes to the CO₂ partial pressure at 430 °C.

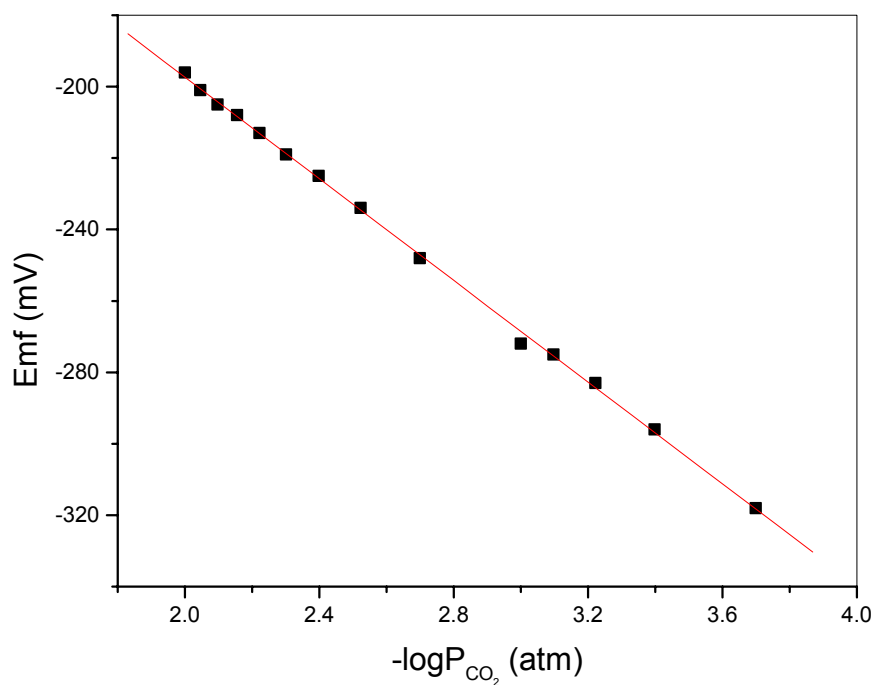


Figure 5.9: Open circuit voltage of cell (5.4) vs. logarithm of CO₂ partial pressure at 430 °C.

Symbols (A), (B), (C) and (D) appearing on table 5.1 correspond to different ratios of $\text{Na}_2\text{CO}_3 : \text{Li}_2\text{CO}_3 : \text{VO}_2$. The reproducibility error for the sensitivity at different sensors with same composition of the auxiliary phase is within 15 %. That is within the agreement between the experimentally determined sensitivity, and the calculated one from Nernst equation for a two-electron process. The reproducibility of the open circuit voltage values at cells with either identical or different compositions of the auxiliary compound, at a fixed CO_2 concentration and temperature is within ± 50 mV.

Variations of both carbon dioxide and oxygen partial pressures in cell (5.4) allowed the evaluation of sensitivities with respect to those two gaseous species. Maintaining the total gas flow rate at 20 sccm/min and employing auxiliary phase of composition (B), open circuit voltage measurements were conducted at different oxygen and carbon dioxide partial pressures. For oxygen partial pressures 0.1 - 0.5 atm the sensitivity to carbon dioxide evaluated to be 50.2-56.9 mV/dec at 390 °C whereas for carbon dioxide partial pressures in the range of 1.66×10^{-4} - 6.6×10^{-4} atm the sensitivity to oxygen evaluated to be 40.1-45.3 mV/dec at the same temperature.

The long term stability test of several cells showed after aging of the sensors, further shift of the open circuit voltage absolute value between 1 – 4 mV per month independently on the composition employed for the auxiliary compound.

The effect of flow rate change on the open circuit voltage was investigated by varying the total gas flow rate from 25 - 100 sccm/min at 440 °C in cell type (5.4) with composition of auxiliary phase (B). At carbon dioxide partial pressures 2×10^{-4} – 10^{-3} atm a variation of the open circuit steady state voltage within 2 mV was observed. Figure 5.10 shows the temperature dependence of the sensitivity of cell (5.4) in comparison to the calculated one from Nernst equation for a two-electron process. The experimental evaluation of the sensitivity carried out from the open circuit voltage vs. $\log P_{\text{CO}_2}$ curves at different temperatures in the range from 10^{-4} – 10^{-3} atm CO_2 employing composition (B) of the auxiliary phase. Figure 5.11 shows the effect of presence of other gases and moisture in addition to carbon dioxide, to the open circuit voltage of cell (5.4) with composition B at 430 °C at CO_2 partial pressure of 2×10^{-4} atm.

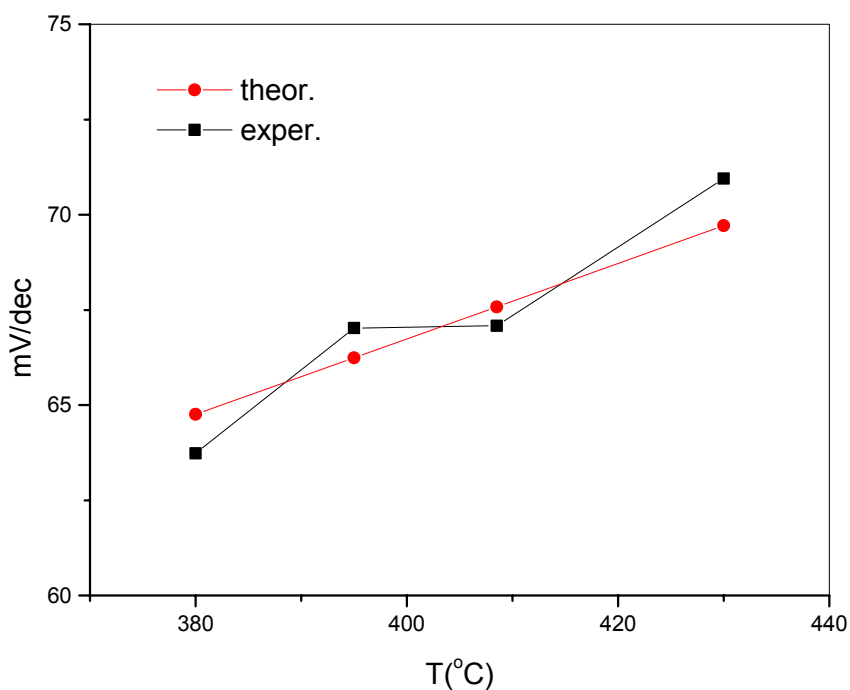


Figure 5.10: Temperature dependence of the experimental sensitivity of cell (5.4) to carbon dioxide, in comparison to the calculated one.

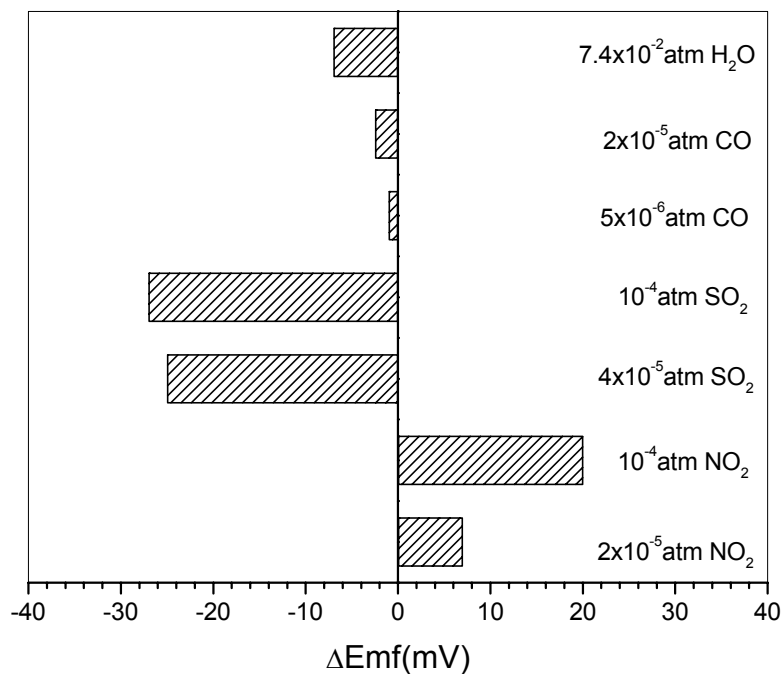


Figure 5.11: Cross sensitivities of cell (5.4) to various gases at 2×10^{-4} atm CO₂ at 430 °C.

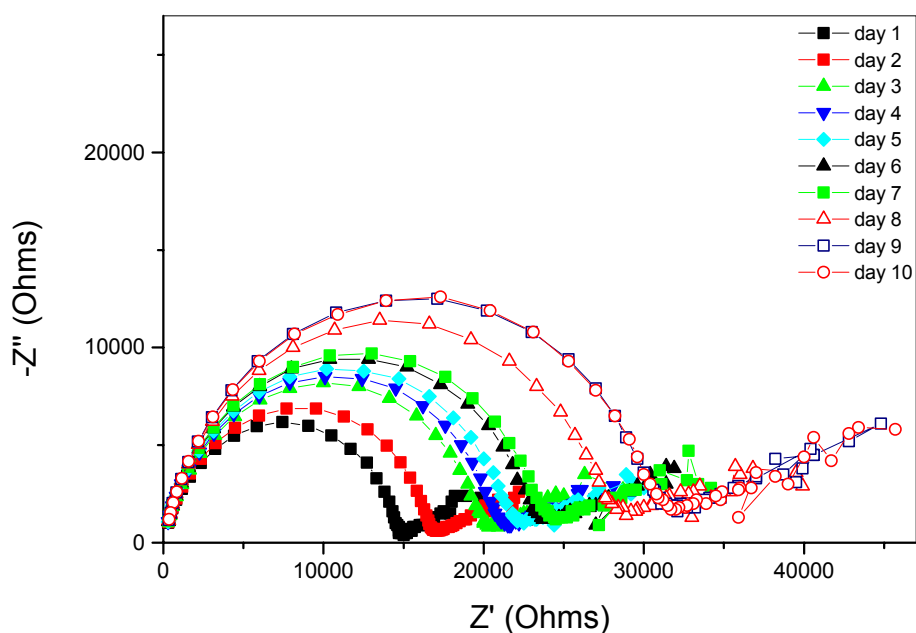


Figure 5.12: Complex plane impedance plots of the cell (5.4) during aging time at 430 °C.

Addition of small amounts of SO₂ or NO₂ influences the cell voltage in a higher degree than addition of CO or moisture. Under the presence of 7.4×10^{-2} atm H₂O the sensitivity to CO₂ at 430 °C was lowered to 45.67 mV/dec while withdrawal of moisture provided the original sensitivity before moisturing the cell.

To investigate the kinetic processes taking place at the interfaces during aging of the sensor, resulting to a voltage shift during the first days of operating the cell at elevated temperatures, impedance spectroscopy was applied. Figure 5.12 shows complex plane impedance plots of a freshly prepared sensor with composition of auxiliary phase (B), during aging time. The complex impedance was measured in the frequency range from 5 Hz to 13 MHz employing a sinusoidal perturbation with 100 mV amplitude under 10^{-2} atm CO₂. The frequency dispersion in the impedance plots consists of a semicircle with its value on the real axis to be increasing with time during aging towards higher Z' values. At lower frequencies the frequency dispersion follows up a straight line inclined about 20° to the real axis. The complex impedance plane plot curve stabilizes after aging as shown in figure 5.12 where for

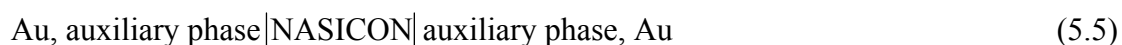
comparison the measurement points corresponding to day 10 are shown, overlapping those of day 9.

Energy dispersive analysis (EDAX) has been used to identify regional compositions of the individual sensor materials as well as analyzing the interfacial region between the electrolyte and the sensitive material. Cells of type (5.4) which have been heated at about 400 °C for a couple of days and exposed to CO₂ atmospheres, were fractured into two pieces and the cell cross section has been subjected to EDAX analysis. The results of qualitative elemental composition at different regions of the cell are summarized on table 5.2. Three main regions can be distinguished namely NASICON bulk, auxiliary phase bulk and an interfacial region between the electrolyte and the sensing electrode. Whereas at the electrolyte and the sensing electrode no foreign element could be identified, at the interfacial region between the electrolyte and the auxiliary compound a blending of elements originating from NASICON (Na, O, Si, P, Zr) and from the sensing electrode (Na, O, V) was found.

Table 5.2: Summary of the EDAX analysis on cross section of cell (5.4).

Region	Elements present
NASICON bulk	O, Na, Si, P, Zr
Interfacial region	O, Na, Si, P, Zr, V
Auxiliary phase bulk	C, O, Na, V.

To further investigate the characteristics of the interface NASICON-auxiliary phase symmetrical cells with planar structure of the following type have been constructed:



The auxiliary phase material in the symmetrical cell (5.5) was identical in composition and preparation on both face areas, whereas composition (B) of table 5.1 has been employed. In ambient air, at temperatures bellow 200 °C the open circuit voltage of freshly prepared cells of type (5.5) was within 1 mV, while for temperatures 300-430 °C the open circuit voltage raised up to 90 mV.

In Figure 5.13 scanning electron micrograph pictures of the auxiliary phase on top of the electrolyte is shown just after preparation (a), and after long-term measurements at 400-440 °C under CO₂ atmospheres (b). The electrode surface found to be relatively uniform and dense with needle formation typical for alkali carbonates. After long term operation at high temperatures chaps appeared at the electrode surface as shown in figure 5.13 (b).

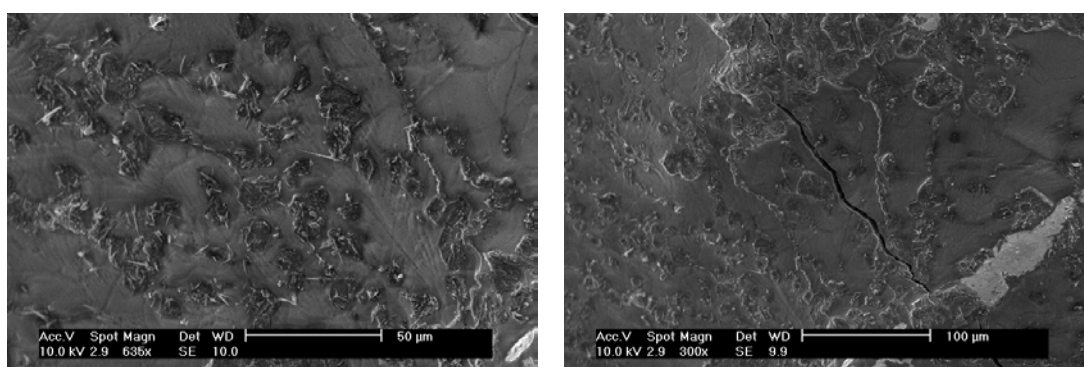


Figure 5.13: Scanning electron micrograph of the sensing electrode before (left) and after (right) long term operation of the cell.

The electrical conductivity of this auxiliary compound was revealed by means of impedance spectroscopy to be $8.4 \times 10^{-4} \Omega^{-1} \text{cm}^{-1}$ at 400 °C with an activation energy of 0.98 eV in the temperature range 250 - 440 °C.

5.2.1.2 Discussion:

Utilization of the Na₂CO₃ - Li₂CO₃ - VO₂ auxiliary compound has several features. Addition of Li₂CO₃ to Na₂CO₃ lowers significantly the melting point [10], thus allowing the preparation of the sensor at lower temperatures than by using pure Na₂CO₃. Small extra amounts of electronically conducting VO₂ [11] enhance the electrical conductivity of the auxiliary compound thus would permit faster equilibration. It also creates as shown at the SEM images a dense coverage of the electrolyte in contrast to pure Na₂CO₃ which is porous thus allowing gas to penetrate through. However on the other hand, because of the lower melting point of this

auxiliary phase the maximum operating temperature of the cell is limited. The sensitivity of cell fabrication (5.4) agrees within the experimental error with the calculated one from Nernst equation for a two-electron process, within the sensor's operating temperature regime. The sensitivity to CO₂ translated to the number of electrons involved in the galvanic cell reaction, provides a value between 1.9 - 2.3 which is well compared to the expected value $z = 2$. Within the range of the compositions for the gas sensitive layer that have been investigated, the sensitivity is practically independent from the composition used. The small uncertainty in the reproducibility of the sensitivity to carbon dioxide observed in experiments with individual cells, is within the agreement between the experimental and the calculated sensitivity.

The experimental observations derived from EDAX, impedance spectroscopy and open circuit voltage measurements suggest the growth of a complex compound at the interface NASICON - gas sensitive layer. Qualitative elemental investigation at the interfacial region showed that the product formation involves elements from the electrolyte and from the electrode. The interfacial compound formation is assumed to be the origin of the unexpected oxygen dependence of the cell (5.4) that has been experimentally observed. The growth of such a compound, which may act as a capacitor at the interface electrolyte-electrode, is assumed to be responsible for the poor reproducibility of the open circuit voltage at individual sensors and the long-term voltage shift with time. From the experiment on symmetrical cell it may be deduced that the reaction leading to the formation of interfacial compound is enhanced as soon as the sensor is heated up. Yamazoe [12] found the formation of a corrosion layer between NASICON and binary carbonate electrodes when the cell with binary carbonate electrode as sensitive compound was heated for measurements. They observed an agreement between the measured and the calculated sensitivity above 400 °C, but a poor reproducibility of the absolute open circuit voltage in different cells, attributed to the formation of the interfacial compound. Guth [13] observed the formation of a reactive layer at the interface electrolyte-electrode after long times using alkali metal carbonates, and Fabry [14] insisted partial decomposition of binary carbonate mixtures (Na₂CO₃ – BaCO₃, Na₂CO₃ – SrCO₃) in contact with NASICON electrolytes at elevated temperatures.

From a thermodynamic point of view, there are various compounds involving alkali cations and Si, P, Zr or V showing higher stability, namely lower ΔG_f^0 value than Na_2CO_3 [15], thus the formation of such a compound at the interface electrolyte-sensing electrode, involving those elements would be favorable at elevated temperatures. In addition to the formation of interfacial compound the long term performance of the cell is influenced by possible parasitic reactions with gas components. Since chaps appeared at the surface of the electrode after long term operation of the sensor, the electrolyte is directly exposed to oxygen from the gas phase. Thus, the kinetically favorable [16, 17] formation of sodium oxides at the measuring electrode which would result to voltage decrease, cannot be excluded with respect to the long term sensor performance.

5.2.2 Cell with Na_xCoO_2 reference and Na_2CO_3 auxiliary compound

5.2.2.1 Results

The results of investigation in electrochemical cells with $\text{Na}_{0.9}\text{CoO}_2$ reference electrode and pure Na_2CO_3 as auxiliary compound under CO_2 atmospheres are presented in this paragraph. The cell assembly and its individual components which are shown in figure 4.5 in the experimental section, may be represented as:



where $\text{Na} - \beta''$ – alumina or NASICON have been used as electrolyte for sodium ions, and the gas sensitive compound Na_2CO_3 was either painted or thermally evaporated on the surface of the electrolyte. According to the discussion in paragraph 3.6 the sensing characteristics of cell (5.6) in thermodynamic equilibrium may be evaluated by considering equation (3.102). Thus, knowledge of thermodynamic data for the auxiliary compound and the gases involved in the galvanic cell reactions as well as the sodium activity at the reference electrode is required. The potential of the prepared $\text{Na}_{0.9}\text{CoO}_2$ reference material showed in open circuit voltage measurements against elemental sodium and by employing $\text{Na} - \beta''$ – alumina electrolytes, the following temperature dependence:

$$E_{\text{Na}_{0.9}\text{CoO}_2 - \text{Na}} [\text{V}] = 2.9806 - 0.0012 \cdot T [\text{K}] \quad (5.7)$$

with the standard deviation from linear fitting to be $\sigma = 0.0125$ V. Figure 5.14 shows the open circuit voltage of cell (5.6) versus CO_2 partial pressures at 400°C where the oxygen partial pressure was 0.205 bar and the total gas mixture flow rate kept at 70 sccm/min. $\text{Na}_{0.9}\text{CoO}_2$ reference electrode has been used and $\text{Na} - \beta''$ -alumina as solid electrolyte. The auxiliary compound Na_2CO_3 was painted on the surface of the electrolyte. For comparison the calculated emf vs. CO_2 partial pressure from equations (3.102) and (5.7) is also shown. The experimental sensitivity evaluated to be 59.8 mV/dec (theoretical value is 66.7 mV/dec at 400°C) which corresponds to $z = 2.2$ for the number of electrons involved in the galvanic cell reaction. The magnitude of the experimentally measured voltage is lower for about 0.25 V to the theoretical one. The absolute voltage values to a fixed CO_2 concentration were not well reproducible for individual cells with same fabrication, shifting up and down and were not long term stable. Electrochemical cells of the type (5.6) with NASICON electrolytes showed similar behavior with even lower voltage absolute values which were also not reproducible and found to be unstable for long term measurements (> 1 week).

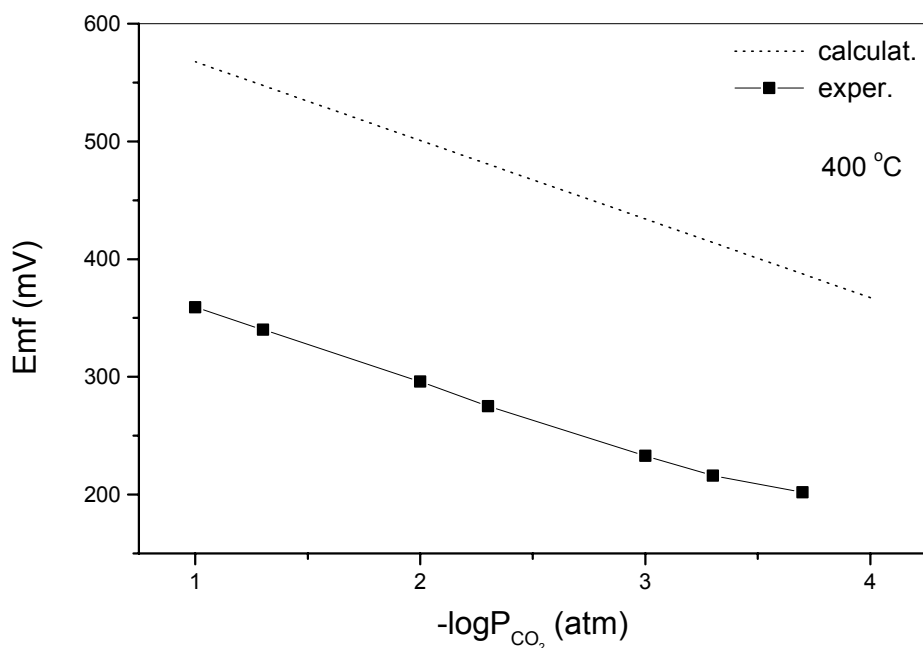


Figure 5.14: Electromotive force of cell (5.6) as a function of CO_2 partial pressures at 400°C . For comparison the theoretical emf is also plotted.

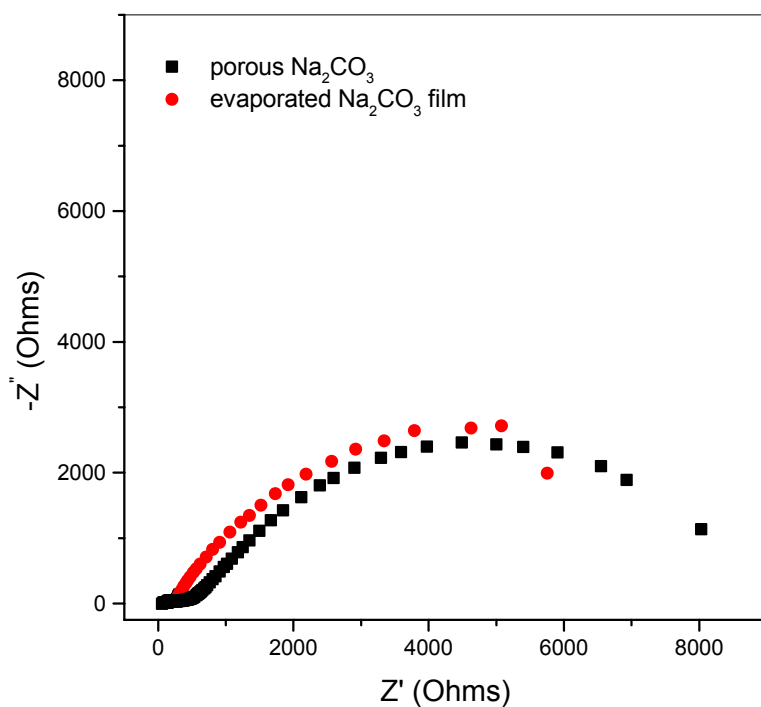


Figure 5.15: Complex plane impedance plots for cells of type (5.6) at 450 °C whereas the auxiliary compound Na_2CO_3 was either porous painted or thin film by thermal evaporation technique.

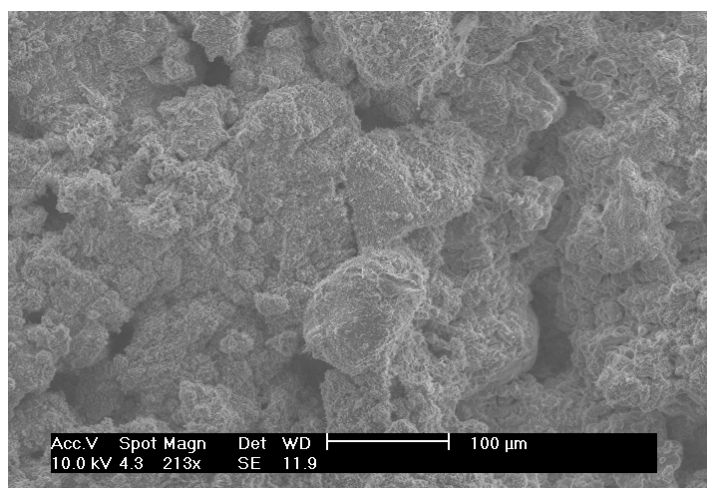
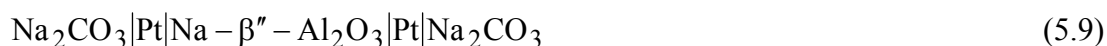
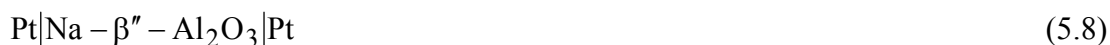


Figure 5.16: Scanning electron microscope image of porous Na_2CO_3 electrode on the electrolyte surface.

Alternatively, thermal evaporation technique has been utilized for generating Na_2CO_3 films on the surface of NASICON in cells of structure (5.6). With this method, a sensitivity of 66.6 mV/dec at 450 °C was evaluated (theoretically 71.7 mV/dec at 450 °C). However, for longer times (> 4days) the sensitivity decreased to 2 mV/dec, therefore the cell became practically not sensitive to CO_2 .

Complex plane impedance plots for the cell type (5.6) with $\text{Na}-\beta''$ -alumina electrolytes with two different preparation techniques of the sensing electrode are shown in figure 5.15. Na_2CO_3 was either applied as porous painted layer or as thermally evaporated film on the electrolyte surface. Complex impedance was measured in ambient air with perturbation amplitude of 100 mV whereas the frequency varied from 3 mHz to 13 MHz. The corresponding interfacial capacitances as evaluated from the complex impedance plots were 973 μF for the evaporated electrode and 480 μF for the painted electrode.

In symmetrical cells of the type:



the observed voltage at 400 °C in ambient air was between 0 - 2 mV.

5.2.2.2 Discussion

Regarding the performance of cell (5.6) in CO_2 atmospheres, two main aspects could be distinguished. First, the open circuit voltage of cell (5.9) is lower in magnitude than the calculated one using thermodynamic properties of the measuring and reference electrode. Second, the sensitivity, that is the slope of the straight line in an emf vs. $\log P_{\text{CO}_2}$ plot agrees reasonably well to the expected one for a two-electron process, providing an experimental value of $z = 2.2$.

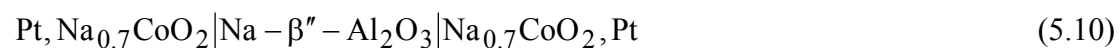
The calculation of the cell voltage as function of the CO_2 partial pressure involves thermodynamic data for the gas sensitive Na_2CO_3 compound and the reference electrode $\text{Na}_{0.9}\text{CoO}_2$. The thermodynamic data of the Na_2CO_3 sensing electrode will be discussed apart in section 5.2.4. Equation (5.7) for the potential of the reference electrode vs. elemental sodium is in good agreement with literature results [18]. Furthermore the reproducibility of the sensor fabrication found to be poor, with the

absolute voltage value at fixed CO₂ and O₂ partial pressures and temperature to be shifting up and down in experiments with distinct cells. This observation is consistent with other experimental results reported [19-21]. Kinetically driven parasitic reactions such as the formation of sodium oxide or peroxide would influence the voltage and the sensing characteristics in the long term run. This effect was clear when a porous film of sodium carbonate by thermal evaporation has been employed. In contrast such behavior was not observed when a dense electrode not allowed gas penetration to the surface of the electrolyte was employed as discussed in section 5.2.1. However in both cases voltage shifts were observed for long times. At both sides of the electrochemical cell (5.6) there are undergoing electrochemical processes. The overall cell electrochemical performance is a combination of processes at the reference and measuring electrode. For proper characterization of the cell kinetics the interfaces reference electrode – electrolyte and sensing electrode – electrolyte are separately investigated and discussed in the following sections. The total resistance of cell (5.6) with sensitive layer sodium carbonate evaporated or painted on the surface of the electrolyte found to be large even at elevated temperatures. The evaluated capacitances are in the range of micro - Farad, typical for double layer capacitances. Thus the impedance at low frequencies may be attributed to the double layer between the solid electrolyte and the gas sensitive sodium carbonate electrode.

5.2.3 Investigation of the reference side

5.2.3.1 Results

For the investigation of the interface between sodium cobalt oxide reference electrode and the electrolyte under real sensor conditions the following symmetrical cell has been built up:



The cell was heated at 460 °C in ambient air and small amounts of current from 20 - 100 μA passed through it moving sodium back and forth, from left to the right side and vice versa. The electroneutrality condition for zero total net charge has been taken into consideration, namely:

$$\int_{t=t_1}^{t=t_2} Idt = 0 \quad (5.11)$$

In between the experiment the cell was short-circuited to avoid any influence of stray capacitances. The observed open circuit voltage was 16 mV before drawing current through the cell (5.10). This value was reproducible within 4 mV after current was passed through the cell satisfying the condition (5.11). Figure 5.17 shows complex plane impedance plots of the symmetrical cell (5.10) at different times. The complex impedance measured with amplitude of 40 mV in the frequency range 5 Hz-13 MHz. Days 1 - 7 as shown in figure 5.17, correspond to times where current passed through the cell while days 8 - 12 to times where the cell remained under open circuit voltage conditions.

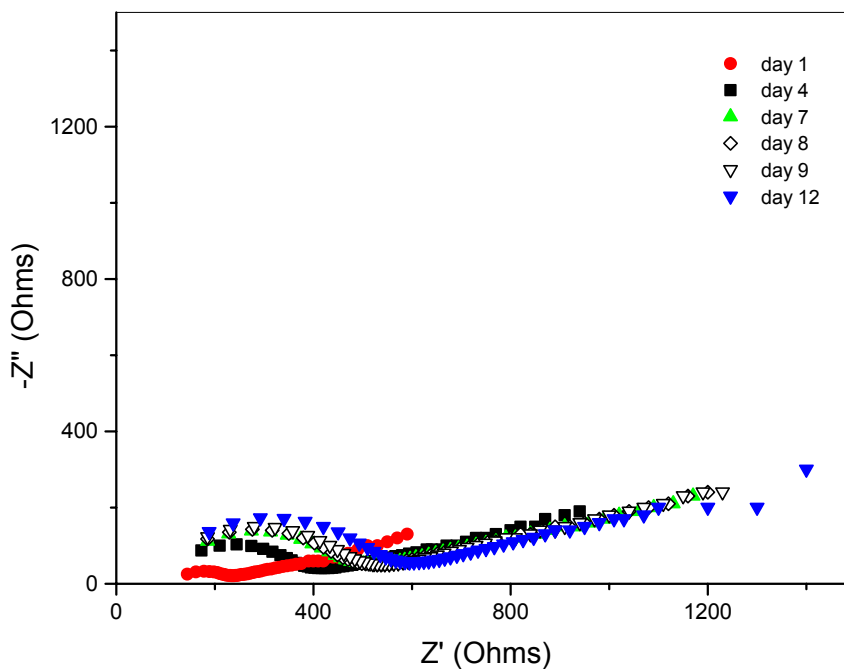


Figure 5.17: Complex plane impedance plots for the symmetrical cell (5.10) at different times.

To further investigate the contact zone between the reference electrode and the solid electrolyte under real conditions in a sensor system, SEM and EDAX were used to identify the interfacial microstructure and topographic composition. The electrochemical cell of type (5.6) with Na – β'' – alumina electrolyte and Na_{0.9}CoO₂ reference electrode de-assembled into its individual components, after it was exposed to CO₂ at 540 °C for 8 days whereas current has been drawn through it in order to form Na₂CO₃ in situ.

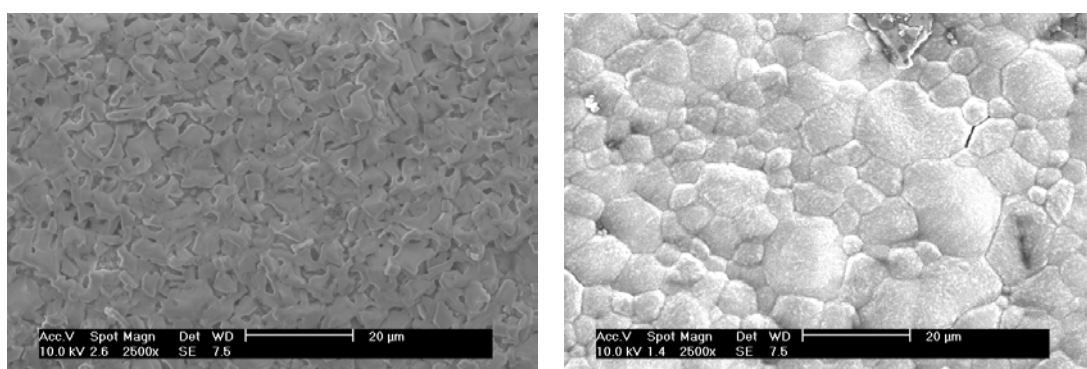


Figure 5.18: SEM images of the reference electrode before and after contact with beta alumina.

Figure 5.18 shows scanning electron microscope images for the reference electrode material as-prepared (left side) and after cell de-assembly (right side). The as-prepared material showed a uniform distribution of small sized particles while the other one non-uniform distribution of larger particles. Simultaneously, the EDAX analysis on the regions shown at the left and right side pictures of figure 5.18 showed the presence of O, Na, Co for the left and O, Na for the right side.

5.2.3.2 Discussion

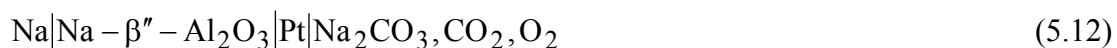
The results of both impedance and SEM-EDAX investigations suggest a reaction between sodium cobalt bronze and the electrolyte Na – β'' – alumina at elevated

temperatures. This reaction develops with time dependent on the operating temperature and may be accelerated if current is drawn through the cell. That is proposed to explain the discrepancy between calculated and observed values from complete cell measurements presented in section 5.2.2. The formation of a new blocking phase in between the reference electrode and the electrolyte introduces new conditions for the interface, which is therefore not well defined thus not capable to establish a constant potential. Reaction between sodium cobalt oxide and NASICON or sodium beta" - alumina was observed also by Schettler [18] by means of XRD patterns on mixtures of electrolyte and electrode material at elevated temperatures for shorter times or slightly lower temperatures and longer times. Steudel [22] found reaction between NASICON and sodium cobalt oxide by means of DTA at about 700 °C for short times. In any of those two cases either at longer times or at higher temperatures the reference material reacts with the electrolyte forming a new phase. According to the results of the compositional analysis on the interface reference electrode-electrolyte the formation of Na₂O₂ (or Na₂O) indicated to be the new phase. Since current was passed through the cell it may be expected that this reaction at the interface reference electrode-electrolyte is kinetically accelerated thus enhanced to occur at shorter times than observed by Schettler. Similar observations are reported in type III cells for possibility of CO₂ detection by employing Li⁺ conductor in contact with LiCoO₂ reference at 400 °C [23]. The lithium activity at the interface reference electrode - solid electrolyte was found unstable with time evolution. As a result the open circuit voltage in the galvanic cell employed under CO₂ atmospheres decreased significantly with time.

5.2.4 Investigation of the measuring side

5.2.4.1 Results

For the investigation of the kinetics and equilibration at the interface sodium carbonate sensing electrode - sodium ion conductor, elemental sodium has been used as reference electrode providing sodium activity equal to unity. The electrochemical cell may be written as:



The cell has been heated up to the desired temperature with low heating rate (1 °C/min). The sodium carbonate sensing electrode was adjusted either by porous painted or in-situ formed Na₂CO₃ film on the surface of the electrolyte, by passing current through the cell. Before measurements were carried out, the cell was heated to 500 °C for short time to ensure adequate adhesion of sensing electrode to the electrolyte. The desired carbon dioxide concentration was maintained by mixing pure or diluted carbon dioxide with synthetic air. The oxygen partial pressure was constant at 0.205 bar and the total gas mixture flow rate kept at 70 sccm/min. The dependence of the electromotive force of the cell (5.12) with porous Na₂CO₃ on the CO₂ partial pressure is shown in figure (5.19), at 450 °C and 500 °C. For temperatures above 500 °C the sealing of elemental sodium reference was found to be inappropriate not allowing electrochemical measurements at higher temperatures. The open circuit voltage varies linear with the logarithm of CO₂ concentration, and increases with increasing CO₂ partial pressure at constant temperature, while it decreases with increasing temperature at fixed CO₂ partial pressure. The response time is 15 - 20 min at temperatures above 400 °C, while for temperatures below 300 °C the response becomes sluggish requiring up to several hours to respond to changes in the carbon dioxide partial pressure. The reproducibility of the open circuit voltage for individual cells prepared with the Na₂CO₃ electrode to be either porous painted or in-situ formed was within ± 12.5 mV. The temperature variation of the sensitivity of cell (5.12) to CO₂ is shown in figure (5.20). The experimental points evaluated from measurements of steady state open circuit voltage vs. log P_{CO₂} curves at different temperatures where the CO₂ partial pressure has been varied between 10⁻⁴ - 10⁻¹ atm. For comparison, the corresponding sensitivity according to Nernst equation for a two-electron process is also shown. The sensitivity is lower than the calculated one at lower temperatures, whereas as the temperature rises it approaches the calculated one. Figure 5.21 shows the effect of the simultaneous presence of other gases to the cell electromotive force at 0.1 atm CO₂. The temperature was maintained at 400 °C and the total gas mixture flow rate equal to 70 sccm/min. Addition of small amounts of Cl₂ and SO₂ shows a strong influence while for CO and NO₂ the effect is smaller. Insertion and withdrawal of CO, NO₂ and Cl₂ required relatively short times, while for SO₂ longer times in the order of hours were necessary to reach steady state. The cell performance was also investigated under the presence of humidity. The sensitivity to

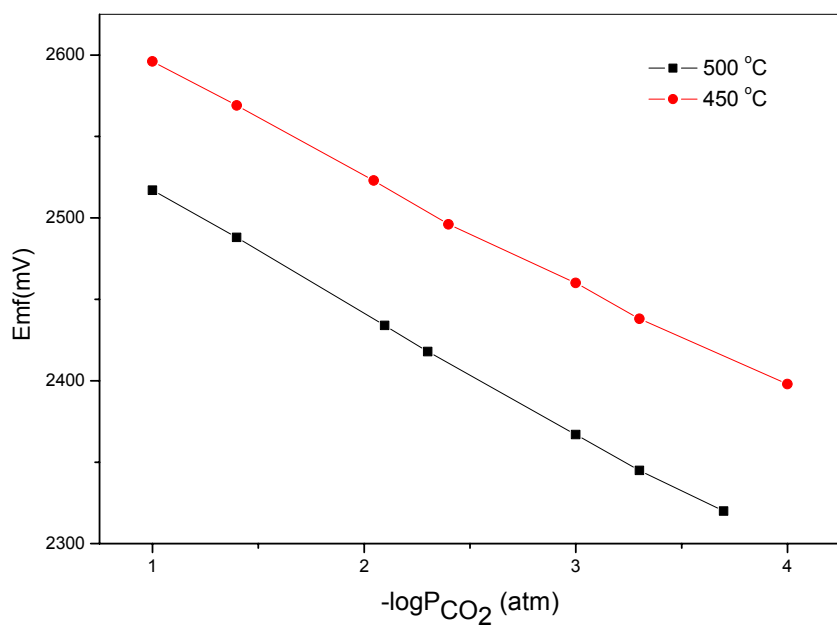


Figure 5.19: Open circuit voltage of the electrochemical cell for investigation of the measuring electrode, at 450, 500 °C where porous Na_2CO_3 has been applied.

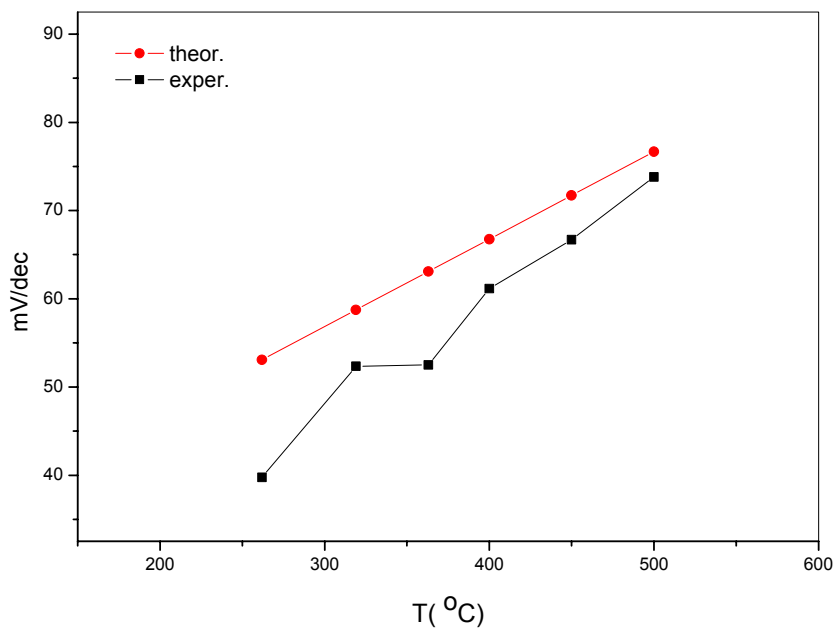


Figure 5.20: Temperature dependence of the sensitivity of cell (5.12) to CO_2 . The calculated values for a two - electron process are plotted for comparison.

CO₂ decreased from 61.14 mV/dec under dried CO₂ atmospheres to 12.36 mV/dec under wet CO₂ gas mixtures, at 400 °C. The response to CO₂ under the presence of moisture was faster requiring 5 - 10 min for steady state. Switching back to dry gas after 2 days of continuously moisturizing the cell, resulted to gradual increase of the sensitivity which finally stabilized at 58.42 mV/dec, which is slightly lower in comparison to the one before introducing moisture over the cell. Complex plane impedance plot of the electrochemical cell (5.12) with elemental sodium reference electrode, before and after moisturizing at 400 °C is shown in figure 5.22. Impedance measurements were carried out with a perturbation amplitude of 100 mV in the frequency range 3 mHz to 13 MHz under carbon dioxide partial pressure of 0.1 atm. The evaluated capacities for the interface sodium carbonate – sodium beta" - alumina are 66.70 μF under dry gas and 2.64x10⁻⁴ F under moisturized gas mixture.

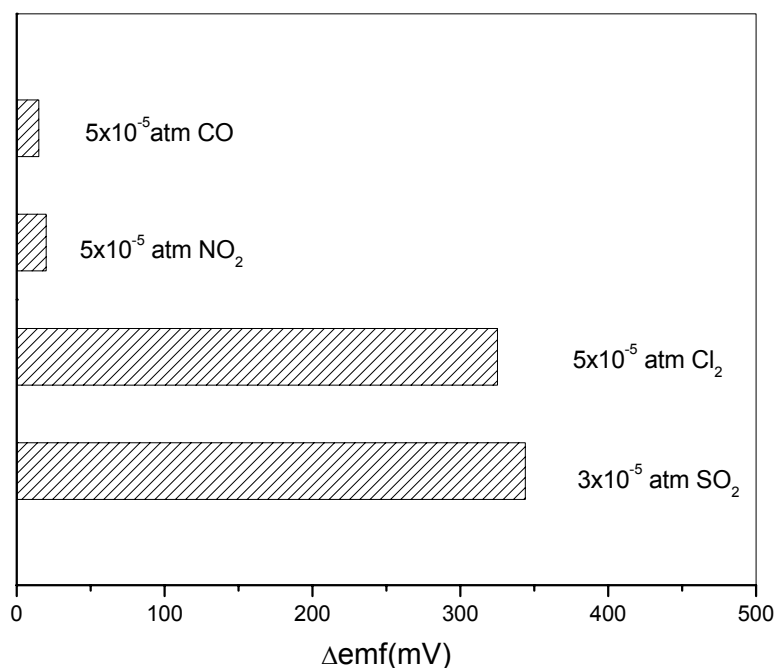


Figure 5.21: Cross sensitivities of the cell (5.12) to various gases in 0.1 atm CO₂ at 400 °C.

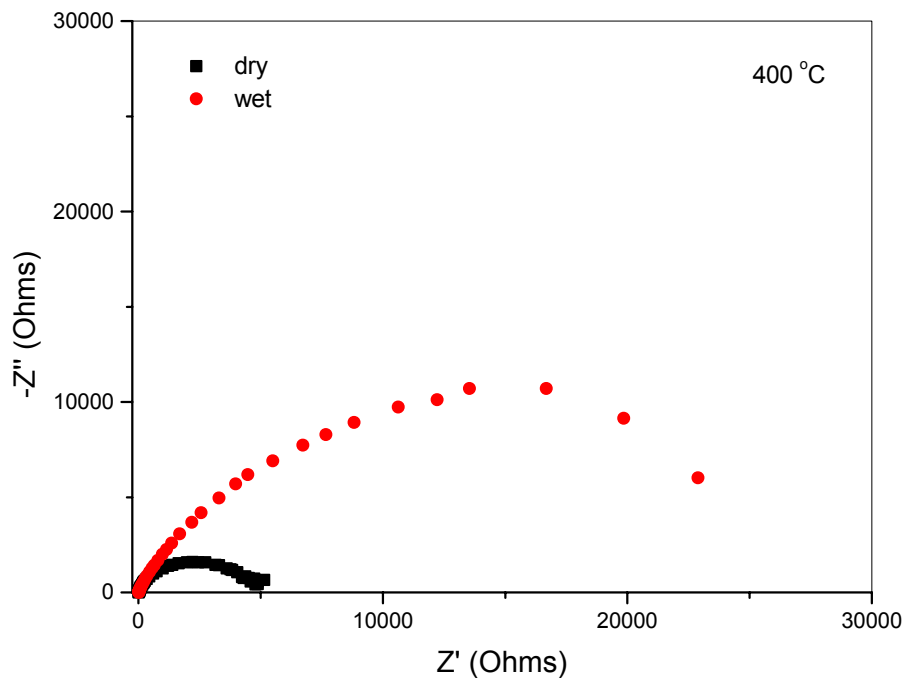


Figure 5.22: Complex plane impedance plot of cell (5.12) under dried and wet gas mixture at 400 °C.

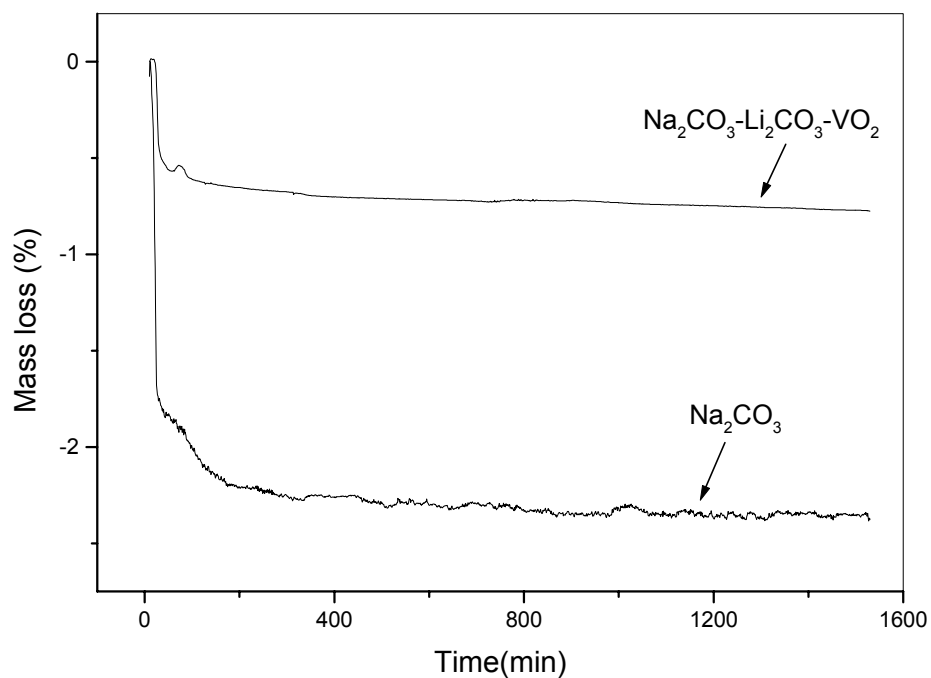


Figure 5.23: Isothermal TG of pure Na_2CO_3 and $\text{Na}_2\text{CO}_3 - \text{Li}_2\text{CO}_3 - \text{VO}_2$ mixture in 10^{-2} atm CO_2 .

Re - drying the cell after introduction of humidifying gas mixture for 2 days did not result to any change in the complex plane impedance plot. Rather the frequency dispersion remained the same the one corresponding to wet gas mixture in figure 5.22. Figure 5.23 shows isothermal TG measurements at Na_2CO_3 and $\text{Na}_2\text{CO}_3\text{-Li}_2\text{CO}_3\text{-VO}_2$ with composition (B) at $430\text{ }^\circ\text{C}$ under 10^{-2} atm CO_2 simulating real conditions of sensor operation. Since both materials are introduced in the thermal analyzer at room temperature, figure 5.23 contains also the heating part until constant temperature has been reached, corresponding to times 0 – 60 min. For times > 60 min isothermal conditions at $430\text{ }^\circ\text{C}$ are fulfilled.

5.2.4.2 Discussion

The results suggest a slow equilibration at the interface sodium beta" alumina- gas sensitive compound Na_2CO_3 . The gaseous species have to equilibrate with the solid electrolyte through the sodium carbonate auxiliary phase which is a poor electrical conductor for sodium ions and with negligible electronic conductivity [24]. Therefore, as indicated by the long times required for equilibration even at elevated temperatures the kinetics of the electrode reaction involving sodium ions, electrons and the gaseous species oxygen and carbon dioxide are slow. Assuming a diffusion process and the sodium diffusion coefficient in sodium carbonate we get an estimation for the diffusion length:

$$L = \sqrt{D\tau} \quad (5.13)$$

where τ is the response time. Application of (5.13) provides at $450\text{ }^\circ\text{C}$ diffusion length of about 0.5 mm corresponding to the estimated thickness of the Na_2CO_3 layer applied on the electrolyte surface.

Figure 5.19 shows the final steady state voltage vs. CO_2 partial pressures. An aging has been observed, typically for some days whereas the voltage increases until reaches a steady state. Accordingly, thermodynamic equilibrium at the sensing electrode is not achieved instantaneously even at higher temperatures. The sensing electrode reaction (3.87) requires the reaction of sodium ions from the electrolyte, electrons from the electronic lead, carbon dioxide from the gas phase and oxygen from a dissociated oxygen molecule in the gas phase, in a single reaction step [25]. At lower temperatures this reaction is not kinetically favorable and intermediate products are

formed. Only the reaction step that involves electrons from the metallic conductor contributes to cell voltage. Purely chemical reactions do not contribute directly but play an important role with regard to the kinetics of the galvanic cell reaction. This can be also seen from the sluggish response times especially at lower temperatures, where the formation of sodium carbonate is hindered by slow electrode kinetics. The sensitivity to carbon dioxide increased gradually with temperature suggesting that the formation of sodium carbonate is kinetically favorable only at high temperatures [16] whereas at intermediate or low temperatures the metastable compounds sodium oxide or peroxide are formed at the measuring side:



However, by raising the temperature Na_2O or Na_2O_2 would further react with CO_2 to form Na_2CO_3 as shown by the slow voltage drift. The observed final voltage values however, including consideration of the reproducibility error, are slightly lower than those calculated from Barin's literature data [15]. Other calorimetrically determined data [26] for the Gibbs free energy of formation of sodium carbonate are cited in JANAF thermochemical tables [27]. Comparison of those data at higher temperatures (700 K) where thermodynamic equilibrium is more likely provides:

$-933.861 \frac{\text{kJ}}{\text{mol}}$ for [15], and $-923.979 \frac{\text{kJ}}{\text{mol}}$ for [27]. The evaluation of data of this

work from electrochemical measurements, under the assumption of full thermodynamic equilibrium, yields the value of $-920.307 \pm 2.412 \frac{\text{kJ}}{\text{mol}}$ at the same

temperature, whereas linear interpolation between closest neighbors has been adopted.

The uncertainty in the experimental value corresponds to the reproducibility error of the open circuit voltage. To see whether or not the temperature measurement error have an effect on this discrepancy we may compare the variations of Gibbs energy of

formation with temperature. Such a comparison yields: $0.275 \frac{\text{kJ}}{\text{Kmol}}$ for [15],

$0.257 \frac{\text{kJ}}{\text{Kmol}}$ for [27], and $0.258 \frac{\text{kJ}}{\text{Kmol}}$ for this work. The corresponding uncertainty

in the temperature would be about 30 K. It may thus not be ruled out that the

controversy in the above comparison may emanate except due to incomplete equilibration at the sensing electrode, from temperature uncertainties.

As illustrated in figure 5.21 major cross sensitivities observed even for small amounts of chlorine and sulfur dioxide in spite of the fact that carbon dioxide was simultaneously present in the gas phase at much higher partial pressures. The cell voltage increase in both cases indicates the formation of a compound with higher stability than Na_2CO_3 . When chlorine or sulfur dioxide are present the formation of NaCl or Na_2SO_4 is assumed to occur according to:

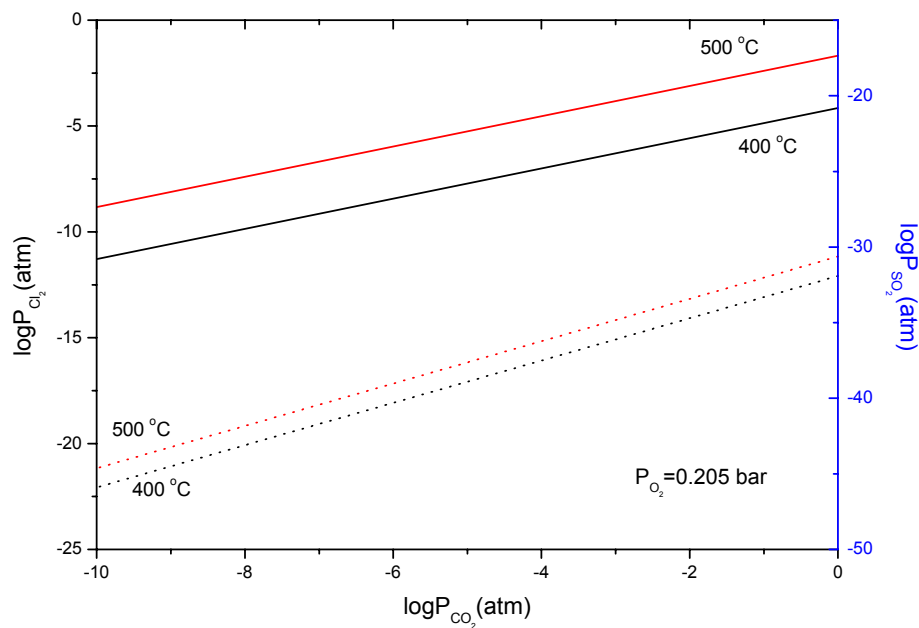


Figure 5.24: Cross sensitivities for the Na_2CO_3 electrode expected from literature data [15].

In terms of thermodynamic data the cross sensitivities may be understood by looking at the stability ranges of Na_2CO_3 in comparison with that of NaCl or Na_2SO_4 as shown in figure (5.24) at 400 °C and 500 °C. Dotted lines correspond to the stability of Na_2CO_3 in comparison to NaCl while solid lines to the stability of Na_2CO_3 with respect to Na_2SO_4 , whereas the oxygen partial pressure assumed to be 0.205 bar. Above the lines NaCl or Na_2SO_4 respectively are more stable than Na_2CO_3 . Thus, even at small Cl_2 or SO_2 partial pressures, cross sensitivities are expected from a thermodynamic point of view, in agreement with the experimental observation.

The complex plane impedance plots in figure 5.22 showed high interfacial impedance at the interface electrolyte - sensing electrode hindering the electrode reaction. The electrolyte bulk resistance and the interfacial impedance sodium beta" - alumina - elemental sodium are negligible at these temperatures [28, 29]. Thus practically only the interfacial impedance of the sensing electrode - electrolyte contributes to the overall impedance. Under humid atmospheres the interfacial resistance becomes higher followed by an increase of the interfacial capacitance due to adsorption of water molecules and formation of a surface layer. Bates [30] observed the formation of a surface layer of NaHCO_3 or hydrated Na_2CO_3 when sodium-beta alumina exposed to $\text{CO}_2 - \text{H}_2\text{O}$ mixtures. The change of complex plane impedance plot when sodium -beta" - alumina exposed to humidity is verified by Butchereit et al. [28].

5.3 Kinetic measurements

In this part of the work, results on the investigation of the kinetics of solid-gas interface with respect to the possibility of selective detection of various gas species simultaneously will be presented. The fundamental background of the kinetic method in monolithic systems has been analyzed in section 3.9. The method is based on the application of a periodical electrical signal, either voltage or current to the electrodes. The system under investigation consists of a solid electrolyte sandwiched between two identically prepared electrodes with same porosity and thickness.

5.3.1 Results

With a small deviation from the thermodynamic equilibrium it has been investigated how different gases respond using a single sensor element. The response when more than one gas species are present has been modeled according to the discussion in 3.9. A sinusoidal voltage perturbation has been applied to the electrodes of the electrochemical cell:

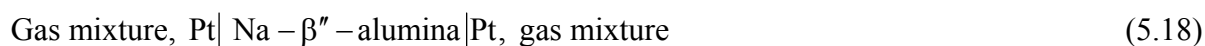


Figure 5.25 illustrates the characteristic response curves for different concentrations of gas species. A sinusoidal perturbation with 90 mV amplitude and 50 mHz frequency has been applied at 550 °C. Curve (a) corresponds to 900 ppm nitrogen dioxide, curve (b) to 500 ppm sulfur dioxide and 900 ppm nitrogen dioxide, and curve (c) to 700 ppm sulfur dioxide and 900 ppm nitrogen dioxide. The I - V characteristic for nitrogen dioxide, namely curve (a) is an ellipsoidal shaped curve, while by additional flux of sulfur dioxide curves (b) and (c) are characteristic of the specific concentration of the sulfur dioxide present in the gas phase. Changing the nitrogen dioxide partial pressure required about 10 min to reach a steady state whereas when both nitrogen dioxide and sulfur dioxide were present in the gas phase, change of the sulfur dioxide partial pressure required times in the order of 1 h for steady state. Complete withdrawal of sulfur dioxide from the gas phase resulted to the original I - V curve (a) corresponding to nitrogen dioxide only after about a day, whereas the cell has been exposed to argon and back to nitrogen dioxide atmospheres.

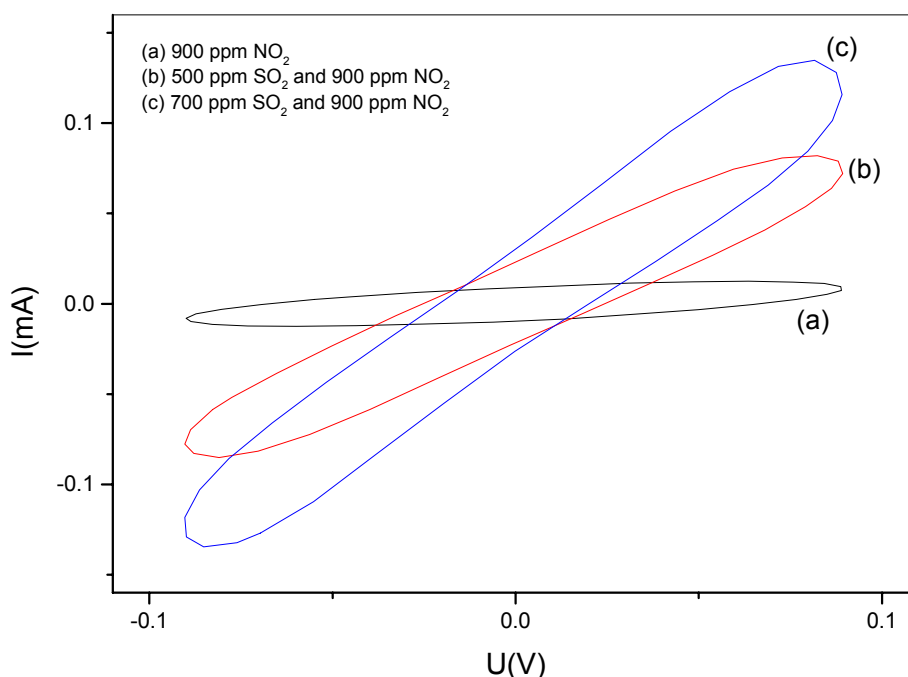


Figure 5.25: I - V plot of cell (5.18) subjected to a sinusoidal perturbation with 90 mV amplitude, 50 mHz frequency, for (a) 900 ppm NO₂, (b) 500 ppm SO₂ and 900 ppm NO₂, (c) 700 ppm SO₂ and 900 ppm NO₂.

The resulting current is, as the applied voltage, periodic function of time. Since its shape is dependent on the specific presence of either nitrogen dioxide or sulfur dioxide in the gas phase, usage of Fourier analysis according to the kinetic method proposed in 3.9 is advantageous, considering that we are dealing with periodic functions. The current response of the electrochemical system under the periodical voltage perturbation has been expressed as a sum of trigonometric functions in accordance with (3.110), composing a Fourier series. For each specific gas partial pressure of either nitrogen dioxide or sulfur dioxide, a Fourier development of the current response has been carried out, allowing to identify the dependence of the Fourier coefficients on the specific gas partial pressure. Figure 5.26 shows the variation of the Fourier coefficient α_1 versus $\ln P_{\text{NO}_2}$ at 550 °C whereas a linear relationship is observed. The line shown in this figure represents linear fitting of these data from least square method. The Fourier coefficient b_1 shows a similar behavior, thus varying also linearly with $\ln P_{\text{NO}_2}$. According to these observations, the response of the

electrochemical system under the presence of nitrogen dioxide may be formulated in terms of the Fourier coefficients as follows.

For NO_2 response:

$$\alpha_1(\text{NO}_2) = A_{\text{NO}_2} + A'_{\text{NO}_2} \ln P_{\text{NO}_2} \quad (5.19)$$

$$b_1(\text{NO}_2) = B_{\text{NO}_2} + B'_{\text{NO}_2} \ln P_{\text{NO}_2} \quad (5.20)$$

Combination of (5.19) and (5.20) results to:

$$b_1(\text{NO}_2) = \left(B_{\text{NO}_2} - \frac{B'_{\text{NO}_2}}{A'_{\text{NO}_2}} A_{\text{NO}_2} \right) + \frac{B'_{\text{NO}_2}}{A'_{\text{NO}_2}} \alpha_1(\text{NO}_2) \quad (5.21)$$

Where $\alpha_1(\text{NO}_2)$ and $b_1(\text{NO}_2)$ are the first order Fourier coefficients corresponding to the presence of only nitrogen dioxide in the gas phase, and A_{NO_2} , A'_{NO_2} , B_{NO_2} , B'_{NO_2} are specific constants derived from plots of $\alpha_1(\text{NO}_2)$ and $b_1(\text{NO}_2)$ vs. $\ln P_{\text{NO}_2}$. From (5.21) a linear relationship between $\alpha_1(\text{NO}_2)$ and $b_1(\text{NO}_2)$ is revealed, thus a function of the characteristic constants A_x, A'_x, B_x, B'_x , $x = \text{NO}_2$.

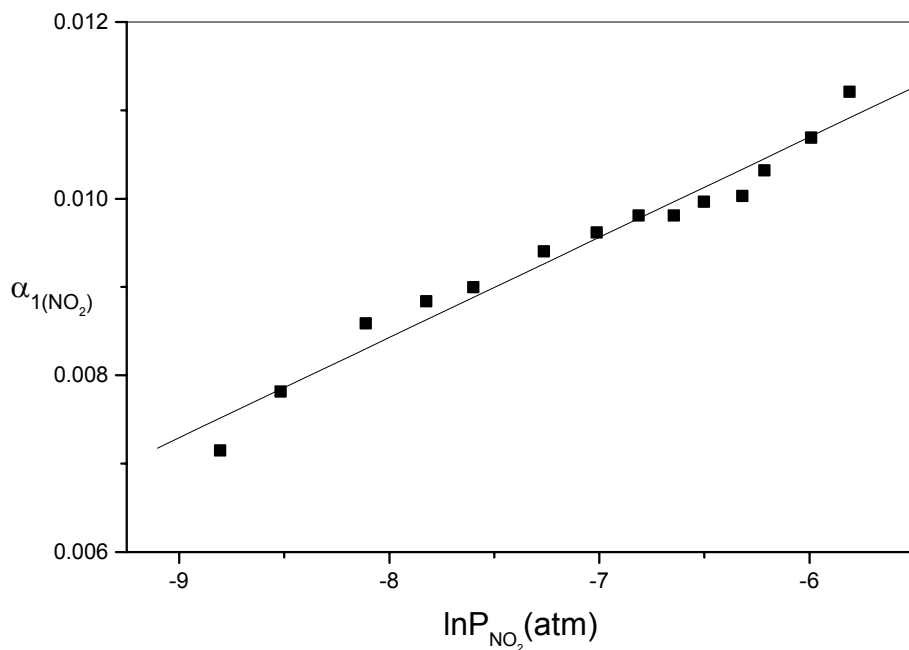


Figure 5.26: Variation of the Fourier coefficient α_1 versus $\ln P_{\text{NO}_2}$ for the response in presence of NO_2 for an applied sinusoidal voltage perturbation with 90 mV magnitude and 50 mHz frequency, at 550 °C.

The change of the Fourier coefficient α_1 when 900 ppm nitrogen dioxide and simultaneously sulfur dioxide of variable partial pressure are present at 550 °C is shown in figure 5.27. The Fourier coefficient α_1 varies linearly with the sulfur dioxide partial pressure, and crosses zero in α_1 vs. P_{SO_2} plot, whereas same behavior was also observed for the Fourier coefficient b_1 . The response for sulfur dioxide under the simultaneous presence of 900 ppm nitrogen dioxide may thus be expressed in terms of the Fourier coefficients as follows.

For SO_2 response in presence of 900 ppm NO_2 :

$$\alpha_1(\text{SO}_2) = A_{\text{SO}_2} + A'_{\text{SO}_2} P_{\text{SO}_2} = A'_{\text{SO}_2} P_{\text{SO}_2} \quad (5.22)$$

$$b_1(\text{SO}_2) = B_{\text{SO}_2} + B'_{\text{SO}_2} P_{\text{SO}_2} = B'_{\text{SO}_2} P_{\text{SO}_2} \quad (5.23)$$

From (5.22) and (5.23) it follows:

$$b_1(\text{SO}_2) = \left(B_{\text{SO}_2} - \frac{A_{\text{SO}_2}}{A'_{\text{SO}_2}} B'_{\text{SO}_2} \right) + \frac{B'_{\text{SO}_2}}{A'_{\text{SO}_2}} \alpha_1(\text{SO}_2) = \frac{B'_{\text{SO}_2}}{A'_{\text{SO}_2}} \alpha_1(\text{SO}_2) \quad (5.24)$$

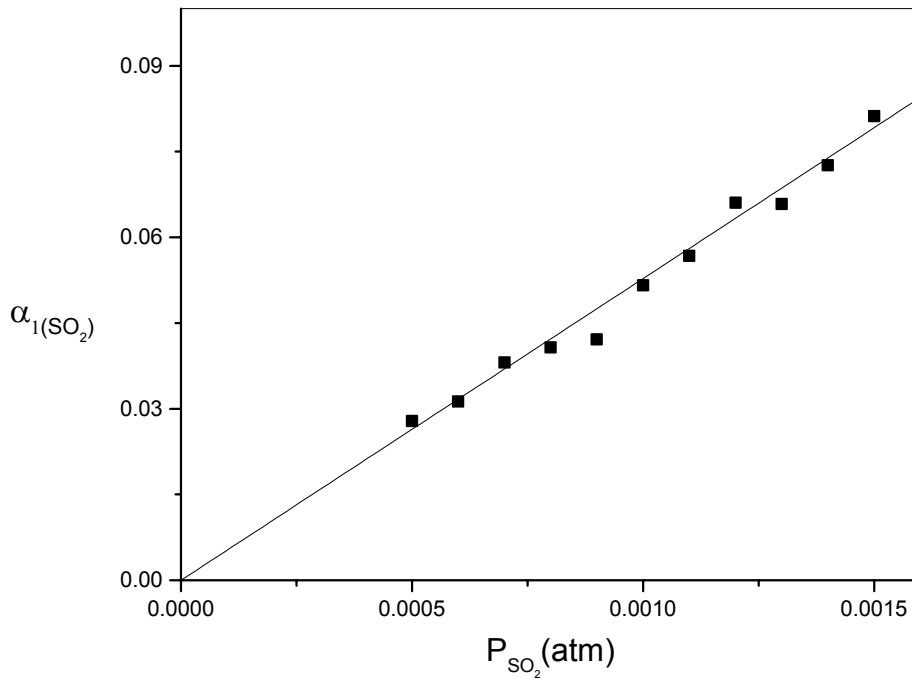


Figure 5.27: Fourier coefficient α_1 versus P_{SO_2} for the SO_2 response in presence of 900 ppm NO_2 for a sinusoidal applied voltage perturbation with 90 mV amplitude and 50 mHz frequency, at 550 °C.

where $\alpha_{1(\text{SO}_2)}$ and $b_{1(\text{SO}_2)}$ are the first order Fourier coefficients corresponding to response to sulfur dioxide under simultaneous presence of 900 ppm nitrogen dioxide and sulfur dioxide. A_{SO_2} , A'_{SO_2} , B_{SO_2} , B'_{SO_2} are specific constants derived from plots of $\alpha_{1(\text{SO}_2)}$ and $b_{1(\text{SO}_2)}$ vs. $\ln P_{\text{NO}_2}$. According to (5.22) and (5.23) the specific constants A_{SO_2} and B_{SO_2} vanish.

Considering relation (5.24) the first order Fourier coefficient $b_{1(\text{SO}_2)}$ is linearly dependent on $\alpha_{1(\text{SO}_2)}$ and is well defined if the constants A'_{SO_2} and B'_{SO_2} are known.

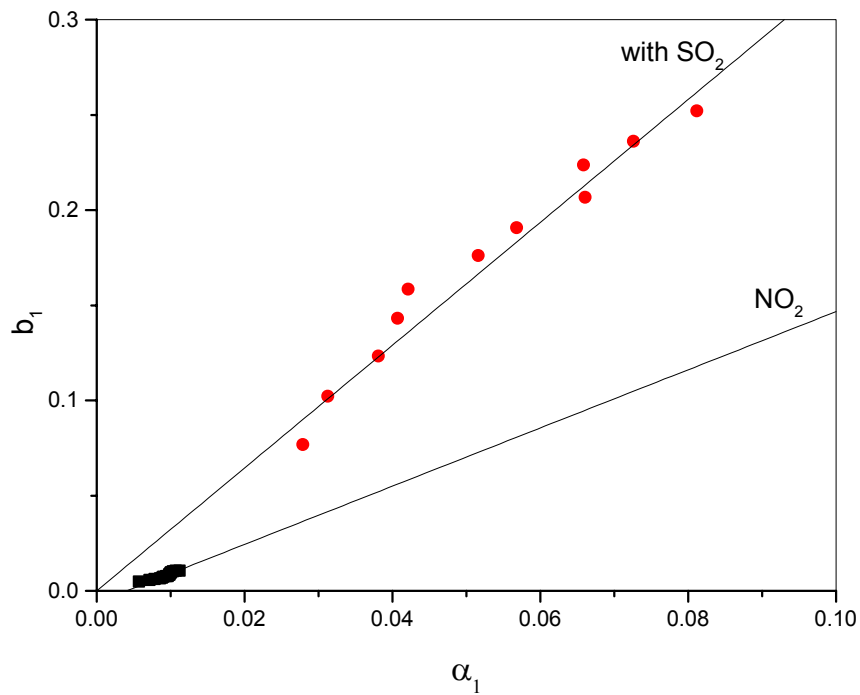


Figure 5.28: Plane plot for the Fourier coefficients b_1 vs. α_1 under the presence of nitrogen dioxide and sulfur dioxide for sinusoidal perturbation of 90 mV amplitude, 50mHz frequency at 550 °C.

Figure 5.28 shows a plot of the first order Fourier coefficients $b_{1(x)}$ against $\alpha_{1(x)}$ where $x = \text{NO}_2, \text{SO}_2$, corresponding to presence of only nitrogen dioxide or simultaneously 900 ppm nitrogen dioxide and variable sulfur dioxide partial pressure in the gas phase. This

plot can be regarded as an Argand diagram since in the complex representation α_k and b_k are linearly related to the real and imaginary part of the complex Fourier coefficient, respectively with the same proportionality constant in accordance to (3.117) and (3.118). The straight lines shown in figure 5.28 represent linear fitting of the data from (5.21) and (5.24) with least square method, within the measured partial pressure range. Since both $\left(\frac{B'_{NO_2}}{A'_{NO_2}}\right)$ and $\left(\frac{B'_{SO_2}}{A'_{SO_2}}\right)$ are positive, the gas partial pressure increases towards the direction yielding higher α_1 and b_1 values, that is towards the right side of α_1 axis and upwards on axis b_1 as shown in figure 5.28.

Figure 5.29 shows the long - term behavior of the cell (5.18) at 550 °C under a sinusoidal perturbation of 90 mV amplitude and 50 mHz frequency, at 900 ppm nitrogen dioxide. It can be seen that the maximum current decreases with time within the measured time interval for about 30% of its initial value.

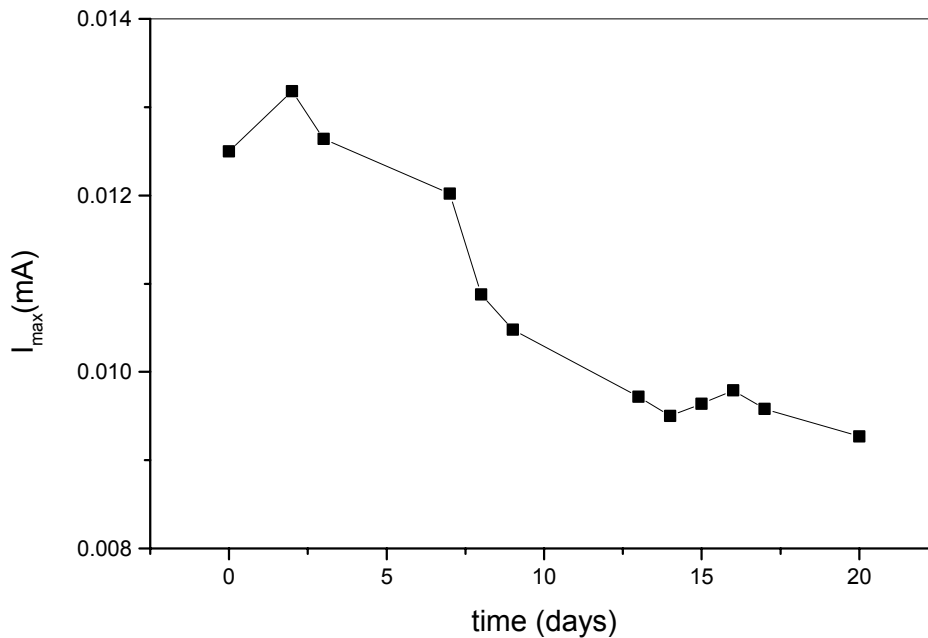


Figure 5.29: Long term decrease of the maximum current of cell (5.18) under 900 ppm NO_2 and sinusoidal perturbation of 90 mV amplitude, 50 mHz frequency at 550 °C.

Rather than applying a sinusoidal perturbation to the electrodes, an arbitrary periodical with time perturbation may be also employed. Figure 5.30 shows the current against square root of time plot for a modulated step voltage waveform. The frequency was adjusted to 50 mHz and the concentration of nitrogen dioxide was 900 ppm, at temperature of 550 °C. The resulting current responding to the voltage perturbation applied to the system, is periodical with time, and its maximum value increases with increasing perturbation amplitude. For short times $t \ll T$, where T the modulation period, the current varies linearly with the reciprocal of square root of time as shown at the left side in figure 5.30. The slope $\frac{dI}{d\left(\frac{1}{\sqrt{t}}\right)}$ in this plot is dependent on the magnitude of the applied voltage amplitude as illustrated at the right in figure 5.30.

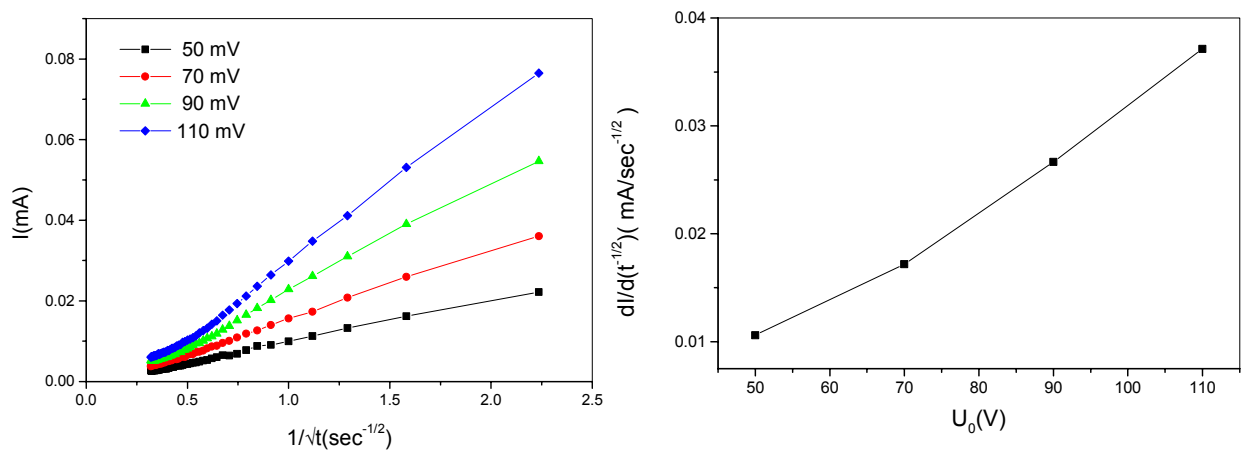


Figure 5.30: Current versus $1/\sqrt{t}$ for step voltage waveform perturbation. The corresponding slopes for short periods of time as a function of magnitude of the applied voltage are shown at the right hand side.

5.3.2 Discussion

Electrochemical cell (5.18) consists of a solid electrolyte sandwiched between two identical electrodes exposed to the gas mixture. Therefore, the same three - phase boundary interface solid electrolyte - electronic conductor - gas is twice included in the cell. The

interfacial kinetics under periodical perturbation are generally of complex nature involving several consecutive processes. The change of the shape of $I - U$ plots as demonstrated in figure 5.25 when one or two gaseous species are present permit the application of the kinetic method proposed in this work. From the evaluation of experimental data it could be seen that the Fourier coefficients of first order vary with the logarithm of nitrogen dioxide partial pressure whereas when sulfur dioxide was also present with the partial pressure of sulfur dioxide. The plot of figure 5.28 which may be regarded as a complex plane plot constitute a two dimensional matrix where the gaseous component partial pressure is given by the Cartesian or Polar coordinates. For further understanding of the various electrode processes from a microscopic point of view, a model has been developed and presented including adsorption of gaseous components at the electrode, charge transfer across interface and diffusion at the electrode. The model describes the kinetic processes occurring at the interface when the system is subjected to a periodical perturbation with one or two gas species present, in a phenomenological manner. Governing equations and accomplishment of the model for the kinetic processes allows comprehensively analyzing the electrode kinetics and direct comparison to experimental data. This may permit determination of the kinetic process that is the most significant among a series of consecutive ones and optimization of the cell operating conditions.

- *Adsorption*

Adsorption studies of nitrogen dioxide [31] and sulfur dioxide [32 - 34] have shown dissociative adsorption for both gaseous species on Pt at elevated temperatures. Mathematical treatment of adsorption under triangular sweep voltage transient was conducted in [35, 36]. Since the derivative of voltage with respect to time doesn't contain time dependent functions, equations simplify.

For an applied sinusoidal potential perturbation the situation is different because of the incorporation of trigonometric functions. The analysis presented here assumes an applied voltage perturbation of the form:

$$U = U_0 \sin(\omega t) \quad (5.25)$$

The assumption being made is that the deviation from equilibrium caused by the application of a small voltage is small, thus the following expression for dissociative Langmuir adsorption as presented in section 3.4.1 is valid:

$$\frac{\theta^2}{(1-\theta)^2} = \exp\left(\frac{zFU}{RT}\right) \quad (5.26)$$

Solving equation (5.26) for the surface coverage θ yields:

$$\theta = \frac{\exp\left(\frac{zFU}{2RT}\right)}{1 + \exp\left(\frac{zFU}{2RT}\right)} \quad (5.27)$$

Thus, according to equation (5.27) the surface coverage changes with time since U is a time dependent function. For the variation of the applied perturbation with time at constant frequency holds:

$$\frac{dU}{dt} = \omega U_0 \cos(\omega t) \quad (5.28)$$

Differentiation of (5.27) with respect to time and considering (5.28) yields:

$$\frac{d\theta}{dt} = \frac{d}{dt} \left[\frac{\exp\left(\frac{zFU}{2RT}\right)}{1 + \exp\left(\frac{zFU}{2RT}\right)} \right] = \frac{zF\omega U_0}{2RT} \cdot \frac{\exp\left(-\frac{zFU_0 \sin(\omega t)}{2RT}\right) \cdot \cos(\omega t)}{\left(1 + \exp\left(-\frac{zFU_0 \sin(\omega t)}{2RT}\right)\right)^2} \quad (5.29)$$

Therefore the current is given by:

$$I_{ad} = Q \frac{d\theta}{dt} = \frac{zF\omega U_0 Q}{2RT} \cdot \frac{\exp\left(-\frac{zFU_0 \sin(\omega t)}{2RT}\right) \cdot \cos(\omega t)}{\left(1 + \exp\left(-\frac{zFU_0 \sin(\omega t)}{2RT}\right)\right)^2} \quad (5.30)$$

where Q is the amount of charge required to form a monolayer of adsorbed intermediates.

The adsorption current may thus expressed as function of perturbation variables:

$$I_{ad} = \frac{zF\omega U_0 Q}{2RT} \cdot \frac{\exp\left(-\frac{zFU_0 \sin(\omega t)}{2RT}\right) \cdot \cos(\omega t)}{\left(1 + \exp\left(-\frac{zFU_0 \sin(\omega t)}{2RT}\right)\right)^2} \quad (5.31)$$

thus providing the dependence of the adsorption current from the magnitude of the perturbation amplitude U_0 .

- Charge transfer

The treatment in this paragraph is for an electrode with kinetic behavior determined by charge transfer. The modulation is assumed small enough to ensure symmetric electrode reaction. Under charge transfer control equation (3.60) relates the current to the applied voltage. Typically the value of the transfer coefficient for a reversible reaction is $\alpha = 0.5$.

Thus, under the sinusoidal voltage modulation (5.25), the relationship between current and voltage can be written [37] as:

$$I_{\text{ch-tr}} = AJ_0 \left[\exp\left(\frac{zFU_0 \sin(\omega t)}{2RT}\right) - \exp\left(-\frac{zFU_0 \sin(\omega t)}{2RT}\right) \right] \quad (5.32)$$

where A the electrode area and J_0 the exchange current density. Equation (5.30) may be written in the final form:

$$I_{\text{ch-tr}} = 2AJ_0 \sinh\left(\frac{zFU_0 \sin(\omega t)}{2RT}\right) \quad (5.33)$$

- Diffusion

The problem of diffusion under overvoltage transient conditions has been treated by Cottrell [38] and Stefan [39]. Analytical solution of this problem under semi-infinite conditions is given by Vetter [40]. The corresponding solution for one type of diffusing species is:

$$I_{\text{diff}} = zFA \sqrt{\frac{D}{\pi t}} c \left[\exp\left(\frac{zFU}{RT}\right) - 1 \right] \quad (5.34)$$

Under the sinusoidal voltage perturbation (5.25), equation (5.34) may be written as:

$$I_{\text{diff}} = zFA \sqrt{\frac{D}{\pi t}} c \left[\exp\left(\frac{zFU_0 \sin(\omega t)}{RT}\right) - 1 \right] \quad (5.35)$$

Diffusing species may be either gaseous components diffusing at the electrode, sodium ions or electrons.

The phenomenological description of the electrode kinetics including adsorption, charge transfer and diffusion processes in terms of mathematical equations allows the comparison of the possible determining steps with experimental data. Table 5.3 shows the comparison by fitting curves of maximum current against amplitude of the applied potential perturbation. First column on the left side indicates the considered mechanism, while in the other two columns the mean error by fitting simulated curves for each individual process to the experimental data is shown. The mean error considering experimental data when nitrogen dioxide is present (900 ppm NO_2) is denoted as σ_{NO_2} while the respective one considering data for sulfur dioxide presence (300 ppm SO_2) is denoted as σ_{SO_2} . The applied voltage perturbation was sinusoidal in form with frequency 50 mHz, at 550 °C. According to table 5.3 best agreement between experimental and simulated data is observed for a charge

transfer process when nitrogen dioxide is present while under the presence of sulfur dioxide for a diffusional process. It may thus be proposed that the characteristic shape in I - V curves but also the diversity of the response to the two gaseous species under investigation in terms of the Fourier coefficients, reflects into two distinguished prevailing processes responsible for the response behavior.

Table 5.3: Mean error for comparison of the various possible determining steps through the simulation to the experimental data.

Process	σ_{NO_2}	σ_{SO_2}
Adsorption	0.111	0.433
Charge-transfer	0.030	0.339
Diffusion	0.241	0.084

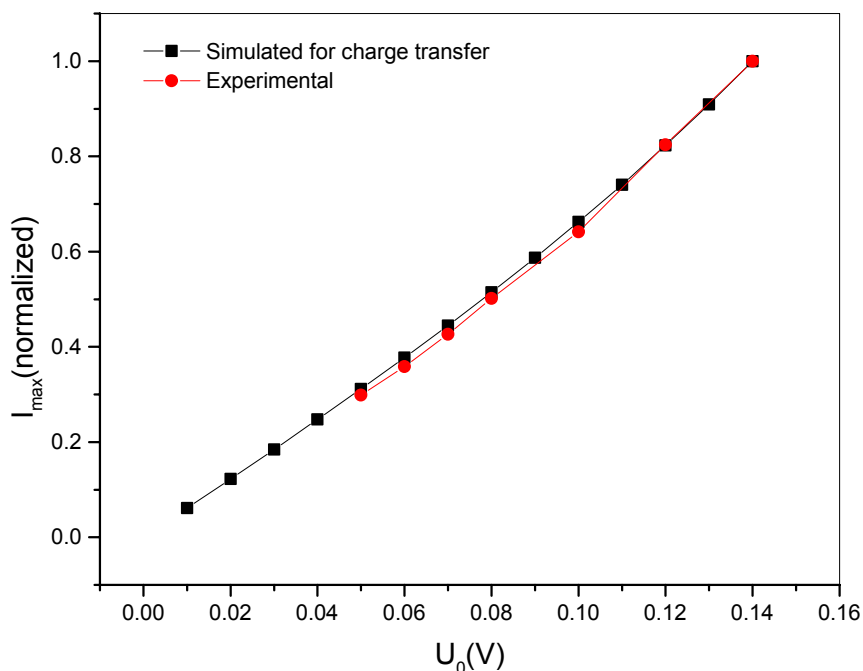


Figure 5.31: Simulated maximum current assuming charge transfer against amplitude of the applied voltage in comparison to the experimental for 900 ppm NO_2 , upon an applied sinusoidal voltage perturbation with 50 mHz frequency at 550 °C.

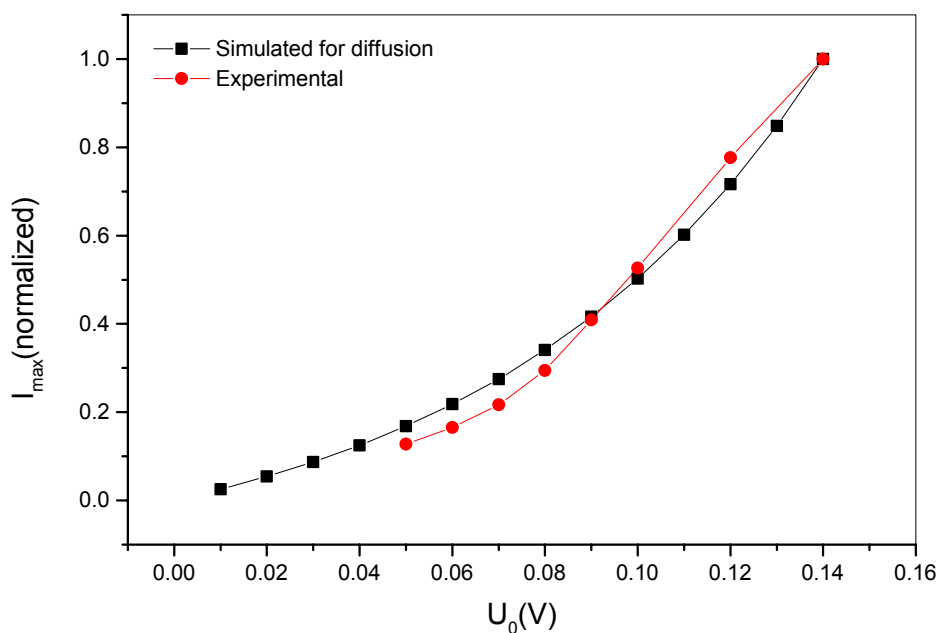


Figure 5.32: Simulated curves assuming diffusion for maximum current against perturbation amplitude in comparison to experimental data in 300 ppm SO_2 , for an applied sinusoidal voltage perturbation with 50 mHz frequency at 550 °C.

Figure 5.31 shows the maximum current against amplitude of the applied voltage when 900 ppm nitrogen dioxide was present in the gas phase, at 550 °C and a perturbation frequency of 50 mHz. The simulated curve for charge transfer as dominant is also shown for comparison. The maximum current against amplitude of the applied voltage when 300 ppm sulfur dioxide was present, in comparison to the simulated one assuming diffusion as rate determining, is shown in figure 5.32. The perturbation frequency was 50 mHz and the temperature 550 °C. Simulating maximum currents have been normalized to unity, and time t was taken within the interval $[0, T]$. The long-term performance of the cell under periodical perturbation as shown in figure 5.29 is governed by gradual coverage of the electrode surface by the gas species. Thus the number of electrode active sites is reduced resulting to a continuous decrease of the maximum current as shown in 5.29.

References to chapter 5

- 1) E.D. Tsagarakis and W. Weppner, Solid State Ionic Devices II Ceramic Sensors, pp. 285-297, Proceedings of the 198th Electrochemical Society Meeting, Phoenix, Arizona, USA (2000)
- 2) W. Weppner, *Z. Naturforsch.* **31a**, 1336-1343 (1976)
- 3) H. Rickert, *Electrochemistry of Solids, An Introduction*, Springer-Verlag, Berlin, Heidelberg, New York (1982)
- 4) J. Crank, "The Mathematics of Diffusion", Second Edition, Oxford University Press Inc., New York (1975)
- 5) W. Weppner, *Electrochimica Acta* **22**, 721-727 (1977)
- 6) P. T. Moseley, J. O. W. Norris and D. E. Williams, Editors: "Techniques and Mechanisms in Gas Sensing", The Adam Hilger Series on Sensors, IOP Publishing Ltd (1991)
- 7) D. Braunshtein, D.S. Tannhauser, and I. Riess, *J. Electrochem. Soc.* **128** [1], 82-89 (1981)
- 8) C. Wagner, Proceedings of the 7th Meeting of the International Committee on Electrochemical Thermodynamics and Kinetics, Lindau, pp. 361-377 (1955)
- 9) T. Kenjo, Y. Yamakoshi, and K. Wada, *J. Electrochem. Soc.* **140** [8], 2151-2157 (1993)
- 10) E.M. Levin, C.R. Robbins, and H.F. McMurdie, "Phase diagrams for Ceramists" Vol. 1, The American Ceramic Society, Ohio (1964)
- 11) J.B. Goodenough, *Progress in Solid State Chemistry* **5**, 145-399 (1971)
- 12) T. Kida, H. Kawate, K. Shimano, N. Miura, N. Yamazoe, *Solid State Ionics* **136/137** 647-653 (2000)
- 13) T. Widmer, V. Brüser, O. Schäf and U. Guth, *Ionics* **5**, 86-90 (1999)
- 14) J. Ramirez-Salgado, P. Fabry, *Solid State Ionics* **158**, 297-308 (2003)
- 15) I. Barin, "Thermochemical Data of Pure Substances", VCH, Weinheim-New York (1993)
- 16) J. Liu and W. Weppner, *Solid State Communications*, **76**, [3], 311-313 (1990)
- 17) H. Aono, Y. Sadaoka, L. Montanaro, E. Bartolomeo and E. Traversa, *J. Am. Ceram. Soc.* **85** [3], 585-589 (2002)
- 18) H. Schettler, Ph.D. Thesis, University of Tübingen (1994)
- 19) T. Maruyama, S. Sasaki and Y. Saito, *Solid State Ionics* **23**, 107-112 (1987)
- 20) N. Miura, S. Yao, Y. Shimizu, and N. Yamazoe, *J. Electrochem. Soc.* **139** [5], 1384-1388 (1992)

- 21) E. Steudel and W. Weppner, Proceedings of the 195th Meeting of the Electrochemical Society, Seattle, Solid State Ionic Devices (1999)
- 22) E. Steudel, Dr.-Ing. Thesis, University of Kiel (1998)
- 23) Y.C. Zhang, H. Tagawa, S. Asakura, J. Mizusaki, H. Narita, *J. Electrochem. Soc.* **144** [12], 4345-4350 (1997)
- 24) P. Cerisier and F. Roux, *Journal of Solid State Chemistry* **22**, 245-251 (1977)
- 25) E.D. Tsagarakis, W. Chu, T. Metzger and W. Weppner, Solid State Ionic Devices II Ceramic Sensors, pp. 270-284, Proceedings of the 198th Electrochemical Society Meeting, Phoenix, Arizona, USA (2000)
- 26) G.J. Janz, E. Neuenschwander and F.J. Kelly, *Trans. Faraday Soc.* **59**, 841 (1963)
- 27) JANAF Thermochemical Tables, Third Edition, D.R. Lide, Jr., Editor, J. Phys. Chem. Ref. Data **14** [1] (1985)
- 28) E. Butcherit, M. Schreiber, J. Schoonman, *Solid State Ionics* **69**, 1-12 (1994)
- 29) R.D. Armstrong, T. Dickinson and J. Turner, *Electroanalytical Chemistry and Interfacial Electrochemistry* **44**, 157-167 (1973)
- 30) J.B. Bates and R.L. Anderson, *Solid State Ionics* **18/19**, 682-686 (1986)
- 31) W. Huang, Z. Jiang, J. Jiao, D. Tan, R. Zhai, X. Bao, *Surface Science* **506**, L287-L292 (2002)
- 32) U. Köhler and H.-W. Wassmuth, *Surface Science* **126**, 448-454 (1983)
- 33) Y.-M. Sun, D. Sloan, D. J. Alberas, M. Kovar, Z.-J. Sun, J. M. White, *Surface Science* **319**, 34-44 (1994)
- 34) J. Haase, *J. Phys.: Condens. Matter* **9**, 3647-3670 (1997)
- 35) S. Srinivasan and E. Gileadi, *Electrochimica Acta* **11**, 321-335 (1966)
- 36) J.O'M. Bockris and S.U.M. Khan, "Surface Electrochemistry. A Molecular level approach", Plenum Press, New York (1993)
- 37) U. Bertocci, *Corrosion* **35** [5], 211-215 (1979)
- 38) F.G. Cottrell, *Z. Physik. Chem.* **42**, 385 (1903)
- 39) Stefan, *Wiener Sitzungsber.* **79 II**, 161 (1879)
- 40) K. J. Vetter, "Elektrochemische Kinetik", Springer-Verlag, Berlin, Göttingen, Heidelberg (1961)

CHAPTER 6

Summary and Outlook

6.1 Summary

The technology of all - solid - state electrochemical sensors requires combinations of materials with appropriate electrical properties. Electrolytes with predominantly ionic conductivity and electrodes with mixed ionic - electronic conductivity form junctions generating strong electrical fields at the interface. The potential drop is within a narrow regime at the interfaces where both ions and electrons are equilibrating. Thus the performance of electrochemical gas sensors depends on the engineering of appropriate interfaces. The electrode reaction resulting in gas detection is based on the interaction of species from the galvanic cell and the gas phase. Under equilibrium conditions, thermodynamic laws provide the sensing properties of the sensor device. During the transition from one to another equilibrium state the kinetics of the interface solid - gas controls or limits the performance of the sensor.

The equilibration of the interface between platinum and zirconia plays a major role in the response behavior of zirconia based potentiometric oxygen sensors. Upon rapid changes of the oxygen partial pressure, delay in the response is observed. Through systematic studies of the response time it is concluded that diffusion of oxygen along the phase boundary between the metallic electrode and the ionically conducting solid is rate - determining. The response time is correlated with the oxide ion diffusion in yttria stabilized zirconia. Oxide ions move within the solid electrolyte while charge compensating electrons move through the metal according to the model proposed to explain the response of zirconia based potentiometric oxygen sensors.

While stabilized zirconia oxygen sensors are based on the formation of an electronic junction, the situation is complex in type III all - solid state sensors for the detection of multicomponent gases. The electrochemical cell consists of materials combination with different electrical properties. In addition, different types of interfaces (solid - gas and solid - solid) exist within the entire cell. The engineering of junction formation and the electrode kinetics with respect to gas sensing has been investigated in electrochemical cells based on NASICON or sodium beta" - alumina electrolytes for the possibility of CO₂ detection. The overall cell performance is a combination of processes occurring at the sensing and the reference side. It was

shown that the kinetics of the redox processes at the interface between the gas and solid ionic conductor and the sensing electrode morphology play a major role with respect to the sensing characteristics under CO₂ atmospheres. Furthermore, the formation of interfacial compounds at both sensing and reference sides result in sluggish response times, deviations from the equilibrium cell voltage and voltage shifts with time.

Common characteristics of potentiometric sensors is the cross - sensitivity to other gas species than the detected ones. The kinetics of the interface solid electrolyte - gas in monolithic system under periodical perturbation according to the θ - sensor concept provides the possibility for selective detection of multiple gas species by a single electrochemical cell. Information from I – V plots using the kinetic method proposed in this work under the presence of nitrogen dioxide and sulfur dioxide in the gas phase, translated to generate a complex plane plot for the Fourier coefficients which includes the concentration dependence from the gaseous species. The developed model for the cell response under periodical perturbation is based on the phenomenological description of the electrochemical kinetics including adsorption, charge transfer and diffusion processes. The kinetic method is an alternative sensing principle, which may be applied to other electrochemical systems for the identification of gaseous species.

6.2 Outlook

It has been shown that the kinetics of the interface solid – gas has a significant influence on the performance of all – solid state electrochemical gas sensors. In type III electrochemical gas sensors multiple gaseous components are incorporating in the galvanic cell reaction. Furthermore, multicomponent solid electrolytes which contain many elements show reactions with the cell electrodes where also a variety of other elements is present. Interfacial compounds are thus formed in-between the electrolyte and the electrodes. In this view thermodynamically stable interfaces are difficult to achieve especially for long terms. A way to overcome this problem may be the discovery and employment of binary solid electrolytes of the type AX where A is the mobile species, and use of electrodes which are stable at the activities where the device is being operated. Additionally, the kinetics of solid – gas interfaces should be considered for the choice of appropriate materials combination. The kinetic method

contributes as an alternative sensing principle, which may be extended to other electrochemical systems by appropriate choice of experimental parameters. Raising the magnitude of the applied voltage perturbation might allow the simultaneous recognition of several gaseous components. However, the stability of this device appears to be rather low in the long term run, but this may be improved by using appropriate electrode materials.